STRUCTURAL AND FUNCTIONAL BASIS OF GLUTAMINASE AS A NOVEL TARGET FOR ARRESTING CANCER CELLS METABOLISM

THANGAVELU KALIYAPPAN

NATIONAL UNIVERSITY OF SINGAPORE

2012

STRUCTURAL AND FUNCTIONAL BASIS OF GLUTAMINASE AS A NOVEL TARGET FOR ARRESTING CANCER CELLS METABOLISM

THANGAVELU KALIYAPPAN

(M.Tech)

A THESIS SUBMITTED FOR THE DEGREE OF DOCTOR OF PHILOSOPHY

DEPARTMENT OF BIOLOGICAL SCIENCES,

FACULTY OF SCIENCE,

NATIONAL UNIVERSITY OF SINGAPORE

2012

Copyrights © 2013 by Thangavelu Kaliyappan

The contents of this document are the exclusive property of *The National University of Singapore*. It may not be used by anyone other than *The National University of Singapore*, nor may it be copied in any way, without the expressed permission of *The National University of Singapore*. If you wish to use this document in any way, please contact the author

Acknowledgements

I am most grateful to my supervisor Associate Professor J. Sivaraman for his generosity, patience, encouragement, advice and guidance throughout my study at the NUS. His vast experience in the field of structural biology, particularly, the cancer targets and drug development projects has inspired me to work on human glutaminase which is one of the key cancer targets.

I would like to wish my deepest gratitude and thanks to A/P Low boon Chun, for his expert ideas, guidance, encouragements, discussions and collaboration with cell biology studies helped for the completion of this project. I am extremely grateful to Dr. Catherine, for her major contribution for my projects and invaluable assistance. I really enjoyed and learnt many techniques through her.

I greatly appreciate A/P Valiyaveettil Suresh, Dr. Tobias Karlberg, Dr. Ganapathy Balaji, and Dr. Mahesh Uttamchandani for their generous support and contribution to the projects. I am also indebted to A/P K Swaminathan, for his discussions on crystallography related to this project and all members of Structural Biology Lab 4, Shiva, Kuntal, Pankaj, Maduri, Kanmani, Anu, Deepthi, and Pavithra. I am thankful to Roopa and Dr. Mallika for proofreadings this thesis.

My special thanks to Ms. Lissa Joseph and Tzer fong who initially trained me in conducting protein expression and molecular biology experiments. I would like to thank Dr. Sundramurthy Kumar, Dr. Jobichen Chacko, Dr. Tang Xuhua and Dr. Jeremy for their help in running structure-related programmes. I wish to thank Dr J Seetharaman who helped me with the data

collection at Brookhaven National Laboratory (BNL, USA). I would also like to extend my appreciation to Girish, Karthik, Shenebamoorthy, Vivek, Vijay, Vinod Roy, Sunil Tewary, Smarajit risi and Ashok for their advices and supports in my research.

I would like to thank to all my past and present members Rajesh shenoy, Cherlyn, Veeru, Nilofer, Priyanka, Sarath, Digant and Rajesh for their kind help and support. Thanks to everyone in the structural biology corridor including Jack, Tan, Sang, for their support and help. I want to thank my closest friends Abilash, Manjeet, and Umar for being there all the times, lunches and dinners, sharing worries and frustration, funs and all the memorable times in Singapore. I offer my special thanks to my parents and brothers, who constantly encouraged me to go forward in studies and served as torch throughout my life.

I also thank NUS for providing me the great opportunity to pursue my PhD. with a research scholarship

TABLE OF CONTENTS

Summary

In recent years, various enzymes involved in cancer cell metabolism are getting a lot of interest as potential targets for the small molecule development towards cancer therapy. Glutaminase is the key enzyme responsible for catalysing the conversion of glutamine to glutamate, and represents the first step in glutamine metabolism (glutaminolysis). This process provides the cancer cell with high energy requirements to meet their accelerated growth and proliferation. In humans, two major glutaminase isoforms - KGA (Kidney-type glutaminase) and LGA (Liver-type glutaminase) have been reported. The KGA isoform is over expressed in several tumour types such as lymphoma, prostate, brain and kidney cancers, and it has become an attractive cancer target for small molecules. However, the structural and molecular basis of KGA inhibition and how the function of KGA is regulated in the cancer cells are still not clearly understood. In this thesis we report our structural and functional studies on KGA and its implications in cancer cell metabolism.

Chapter I provides a general introduction based on the detailed literature survey on cancer cell metabolism and a key metabolic enzyme, glutaminase. In the chapter II we report the allosteric inhibition mechanism of KGA by a small molecule inhibitor BPTES [bis-2-(5-phenylacetamido-1,2,4-thiadiazol-2-yl) ethyl sulfide] and further we identified Raf-Mek-Erk signaling pathway as the regulator of KGA. On the basis of crystal structures, we reveal that BPTES binds to an allosteric pocket at the dimer interface of KGA, triggering a dramatic conformational change of the

key loop (Glu312-Pro329) near the catalytic site and rendering it inactive. The binding mode of BPTES on the hydrophobic pocket explains its specificity to KGA. Interestingly, KGA activity in cells is stimulated by EGF, and KGA associates with all three kinase components of the Raf-1/Mek2/Erk signaling module. However, the enhanced activity is abrogated by kinase-dead, dominant negative mutants of Raf-1 (Raf-1-K375M) andMek2 (Mek2-K101A), protein phosphatase PP2A, and Mek-inhibitor U0126, indicative of phosphorylation-dependent regulation. Furthermore, treating cells that coexpressed Mek2- K101A and KGA with suboptimal level of BPTES leads to synergistic inhibition on cell proliferation. Consequently, mutating the crucial hydrophobic residues at this key loop abrogates KGA activity and cell proliferation, despite the binding of constitutive active Mek2-S222/226D. These studies therefore offer insights into (i) allosteric inhibition of KGA by BPTES, revealing the dynamic nature of KGA's active and inhibitory sites, and (ii) cross-talk and regulation of KGA activities by EGF-mediated Raf-Mek-Erk signaling. Chapter III of this thesis reports the crystal structure of catalytic domain of KGA in complex with DON (6-Diazo-5-oxo-L-norlucine), an active site inhibitor. The complex structure revealed the DON binding pocket of KGA that form a covalent bond with active site residue Ser286 of KGA. Further we performed site-directed mutagenesis to validate the importance of key residues from the active site to understand the active site inhibition mechanism of KGA. The overall conclusion and future directions are provided in Chapter IV.

List of Tables

List of Figures

List of Abbreviations

Å	Angstrom (10^{-10}m)
ADP	Adenosine diphosphate
ATP	Adenosine triphosphate
(APC/C)	Anaphase-promoting complex/cyclosome
BCH	BNIP-2 and Cdc42GAP Homology
BNIP-2	BCL2/adenovirus E1B 19kD Interacting Protein 2
BINP-H	BNIP Homology
BPTES	Bis-2-(5-phenylacetamido-1,2,4-thiadiazol-2-yl) ethyl sulfide
cAMP	Cyclic Adenosine monophosphate
CNS	Crystallography and NMR system
CCD	Charged coupled device
CK	L-2-amino-4-oxo-5-chloropentanoic acid
Cdc42	Cell division cycle 42
CT	Computed tomography
DCA	Dicholoro acetate
DLS	Dynamic light scattering
DON	6-Diazo-5-oxo-l-norlucine
DMSO	Dimethyl sulfoxide
DNA	Deoxyribonucleic acid
DTT	Dithiothreitol

E.coli	Escherichia coli
EC	Enzyme Commission
EDTA	Ethylenediamine tetraacetic acid
EGF	Epidermal growth factor
EGFR	Epidermal growth factor receptor
ERK	Extracellular signal-regulated kinase
FDG	Fludeoxyglucose
FPLC	Fast performance liquied chromatography gel electrophoresis
FGF	Fibroblast growth factor
GAP	GTPase-activating protein
GDP	Guanosine diphosphate
GIP	Glutaminase interaction protein
GTP	Guanosine triphosphate
HAD	HIV-Associated Dementia
HEPES	4-(2-hydroxyethyl)-1-piperazineethanesulfonic acid inhibitor-1
HEK	Human Embryonic Kidney cells
HG	Hydroxyglutatarate
HIF	Hypoxia inducible factor
IPTG	Isopropyl thio-galactoside
JAK	Janus kinase
IDH1	Isocitrate dehydrogenase 1
kDa	Kilo Dalton
KGA	Kidney type glutminas

LB	Lactate dehydrogenase
LDH	Lactate dehydrogenase
LGA	Liver type glutaminase
LPA	Lysophosphatidic acid
MAPK	Mitogen-activated protein kinase
MCF 7	Human mammary carcinoma epithelial cell line
MEK	MAP kinase/ERK kinase
MES	2-(N-morpholino)ethanesulfonic acid
MS	Mass Spectrometry
Myc	Myelocytomatosis oncogene cellular homolog
NADH	Nicotinamide adenine dinucleotide
NADPH	Nicotinamide adenine dinucleotide phosphate
NF-kB	Nuclear factor κ B
Ni-NTA	Nickel nitrilo-triacetic acid.
NMDAR	N-methyl-D-aspartate receptor
NMR	Nuclear Magnetic Resonance
OAA	Oxaloacetate
OD	Optical Density
PCR	Polymerase chain reaction
PAGE	Polyacrylamide Gel Electrophoresis
PDB	Protein Data Bank
PDGF	Platelet derived growth factor
PDH	Pyruvate Dehydrogenase

PDZ	Psd-95, Dlg and ZO1
PET	Positron Emission Topography
PK	Pyruvate Kinase
PKM1	Pyruvate Kinase M1 isoform
PKM2	Pyruvate Kinase M2 isoform
PP2A	Phospho-protein phosphatase 2A
PSTI	Pancreatic Secretory Trypsin Inhibitor
RMSD	Root-Mean Square Deviation
RTK	Receptor Tyrosine Kinase
SAPK	Stress-Activated Protein Kinase
SDS	Sodium Dodecyl Sulfate
Si RNA	Small interfering RNAs
SNT	Alpha-1-syntrophin
STAT	Signal transducer and activator of transcription
TCA	Tricarboxylic acid cycle
TEV	Tobacco Etch Virus
TGF	Transforming Growth Factor
Tris	Tris (hydroymethyl)-aminomethane
WHO	World Health Organization
WT	Wild Type

Amino Acids

Ala (A)	alanine
Arg (R)	arginine
Asn (N)	asparagine
Asp (D)	aspartic acid
Cys (C)	cysteine
Gln (Q)	glutamine
Glu (E)	glutamic acid
Gly (G)	glycine
His (H)	histidine
Ile (I)	isoleucine
Leu (L)	leucine
Lys (K)	lysine
Met (M)	methionine
Phe (F)	phenylalanine
Pro (P)	proline
Ser (S)	serine
Thr (T)	threonine
Trp (W)	tryptophan
Tyr (Y)	tyrosine
Val (V)	valine

Publications

1. Structural basis for the allosteric inhibitory mechanism of human kidney-type glutaminase (KGA) and its regulation by Raf-Mek-Erk signaling in cancer cell metabolism.

   Thangavelu, K., Pan, C.Q., Karlberg, T., Balaji, G., Uttamchandani, M., Suresh, V., Schüler, H., Low, B.C., and Sivaraman, J. (2012).

   Proc Natl Acad Sci U S A 109, 7705-7710.

2. Structural basis of the active site inhibition mechanism of human kidney type glutaminase

   Thangavelu, K.., and Sivaraman, J. (Manuscript under preparation)

Chapter I

General Introduction

1.1 Cancer

Among the top killer diseases, cancer is a leading cause of death and it continues to be a major public health problem around the world. According to World Health Organization (WHO) statistics, cancer caused 7.6 million deaths (13% of all deaths) in 2008, and by 2030, it is expected to increase to 13.1 million deaths worldwide (estimated by WHO) (Boyle P, 2008). Cancer is the term for complex diseases characterized by many physiological changes that lead to uncontrolled cell growth. Cells are basic unit of life; they grow and divide to produce more healthy cells in a controlled manner (e.g. by growth factor control). However, sometimes, cells do not function normally; they keep dividing and produce more cells in an uncontrolled manner (abnormal growth), which also invades surrounding tissues. This unregulated growth of cells ultimately leads to form a clump of tissue called a tumor. The processes by which normal cells are transformed into cancer cells are still not well understood and has remained as a key biological question yet to be answered (Anand et al., 2008; Seyfried and Shelton, 2010).

1.1.1 The Hallmark of Cancers

In a recent review, Hanahan and Weinberg proposed six common hallmark features that can underlie the transformation of normal cells to cancer cells (Hanahan and Weinberg, 2000, 2011). These six hallmark features are believed to be shared by most cancers (Figure 1). It includes followings:

(1) Cancer cells stimulate their self-growth signals (uncontrolled proliferation)
(2) Resistance towards antigrowth signals

(3) Resistance towards apoptosis (programmed cell death)

(4) Promoting angiogenesis

(5) Limitless multiplication potential

(6) Tissue invasion and spread to distant sites (metastasis)

Apart from these six common features of cancer, Warburg effect or aerobic glycolysis is also now recognized as a hallmark of most cancer cells (Gatenby and Gillies, 2004; Seyfried et al., 2008).

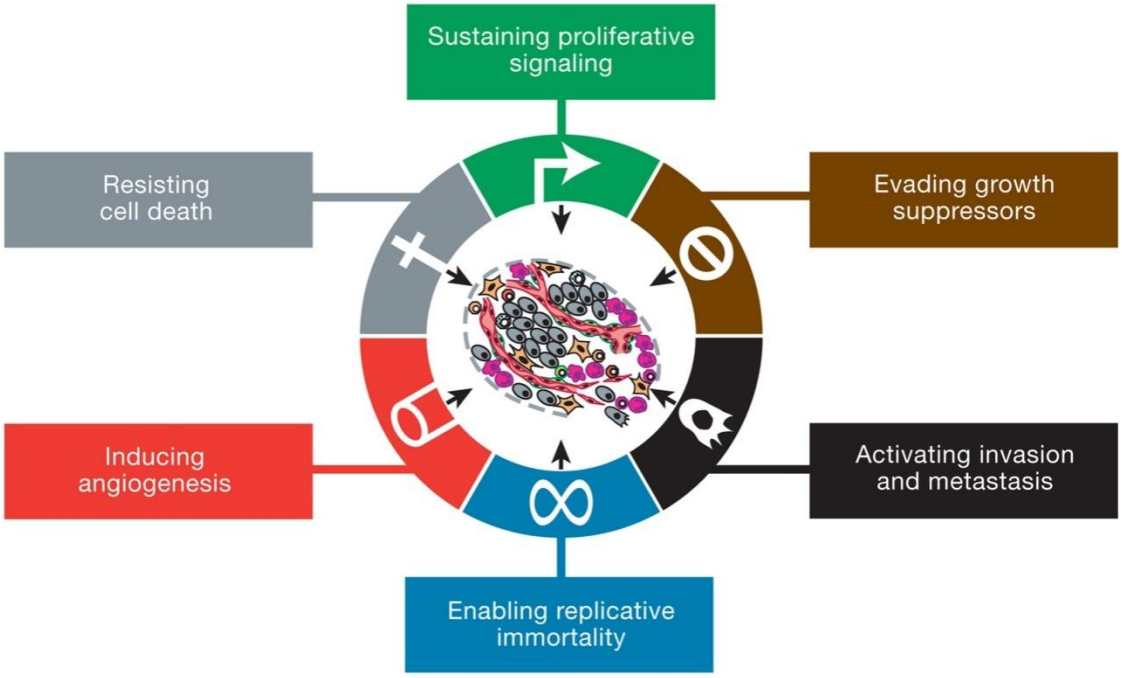

Figure 1: The hallmark features of cancer cells. This figure is adapted from (Hanahan and Weinberg, 2011).

1.2 Cancer Cell Metabolism

In the 1920s, Otto Warburg first observed that the cancer cells metabolize glucose in a way different from normal cells (Warburg et al., 1927). He demonstrated that cancer cells exhibit increased uptake of glucose in which glucose is converted to lactate, even in the presence of oxygen, termed as the "Warburg Effect" (Brahimi-Horn et al., 2007; WARBURG, 1956a; Warburg, 1956b; Warburg et al., 1960a; WARBURG et al., 1960b)Otto Warburg received Nobel Prize of Physiology or Medicine in 1931 for his discovery of "altered metabolism in cancer". The Warburg Effect is a unique metabolism that is observed in most cancer cells and not found in normal cells (Vander Heiden et al., 2009). The phenomenon of Warburg effect is now broadly accepted, which formed a basis for the recent research on the cancer cell metabolism. The metabolic alteration is essential to facilitate the incorporation of nutrients into bioenergetics and biosynthetic requirements of cell survival and metabolism (Bauer et al., 2005; Locasale and Cantley, 2010; Vander Heiden, 2011). Figure 2 emphasizes the timeline in the development of cancer metabolism.

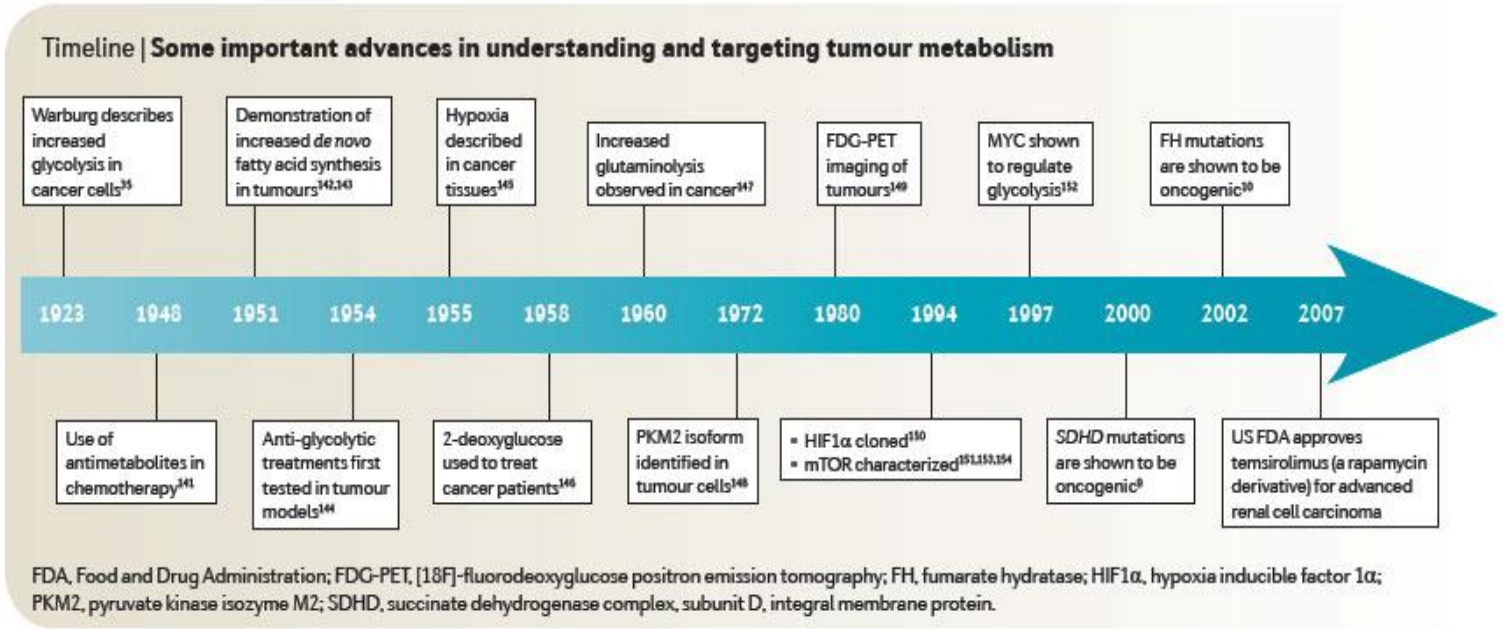

Figure 2: Diagram showing the time line and the development of cancer metabolism. This figure is adapted from (Tennant et al., 2010).

1.2.1 Glucose Metabolism in Normal cells

In normal cells, glucose is completely metabolized by the following linked metabolic pathways:

a) Glycolysis

b) Tricarboxylic acid (TCA) cycle

c) Oxidative phosphorylation

Glucose is initially metabolized through glycolysis that takes place in the cytoplasm of a cell. This process involves a series of enzymatic reactions which ultimately produces two molecules of pyruvate and two ATPs from one glucose molecule (Figure 3). The generated pyruvate enters mitochondria and is converted to acetyl CoA by the action of pyruvate dehydrogenase (PDH). Condensation of acetyl CoA with oxaloacetate (OAA) is catalyzed by the enzyme citrate synthetase to form citrate in the TCA (tricarboxylic acid) cycle. Citrate is further completely oxidized in mitochondria to produce a variety of six- and three-carbon intermediates, and results in production of thirty-six ATPs molecules at the end of oxidative phosphorylation (Lehninger, 1945). Thus, in total thirty-eight ATPs are produced from a single molecule of glucose, when oxygen is present. By this process, glucose satisfies the cells with most energy (90%) requirements (Vander Heiden et al., 2009**)**. On the other hand, the series of reactions involved in the conversion of glucose to lactate in the absence of oxygen, is called anaerobic respiration or fermentative glycolysis, which produces only 2 ATPs (Figure 3).

1.2.2 Altered Glucose metabolism in Cancer cells (Warburg effect)

In order to satisfy the cellular energy demands in the normal cells, the end product of glycolysis, pyruvate enters into mitochondria to generate ATP through the TCA cycle. However, in cancer cells, the pyruvate has shown to be directed away from the TCA cycle and is converted to lactate by the enzyme lactate dehydrogenase (LDH). In a typical cell, this lactate production only happens in anaerobic conditions, but, cancer cells are able to produce lactate even when oxygen is available, a process termed "aerobic glycolysis" or the Warburg Effect (WARBURG, 1956a) (Figure 3). The importance of Warburg effect is experimentally validated in most of the cancer cells, where increased glucose uptake is found, which thereby promotes the formation of tumors (Altenberg and Greulich, 2004; Kroemer and Pouyssegur, 2008; Ortega et al., 2009; Schnelzer et al., 2000).

According to Otto Warburg, most cancer cells are highly reliant on aerobic glycolysis and not on the mitochondrial function (citric acid cycle and oxidative phosphorylation) for their energy needs. Since the cancer cells depend on less efficient glycolysis which serves only 2 ATP molecules (Figure 3), they require additional glucose to satisfy their increased cellular energy demands. Hence, in contrast to normal cells (which produces 38 ATP molecules), cancer cells need to use 19 more glucose molecules to generate (2 ATP X 19 glucose=38 ATP) equivalent 38ATP molecules. The enhanced glucose uptake of cancer cells or the Warburg effect is experimentally proved through the recent imaging studies called positron emission topography (PET) imaging. The PET imaging is very sensitive to radio-active molecules.

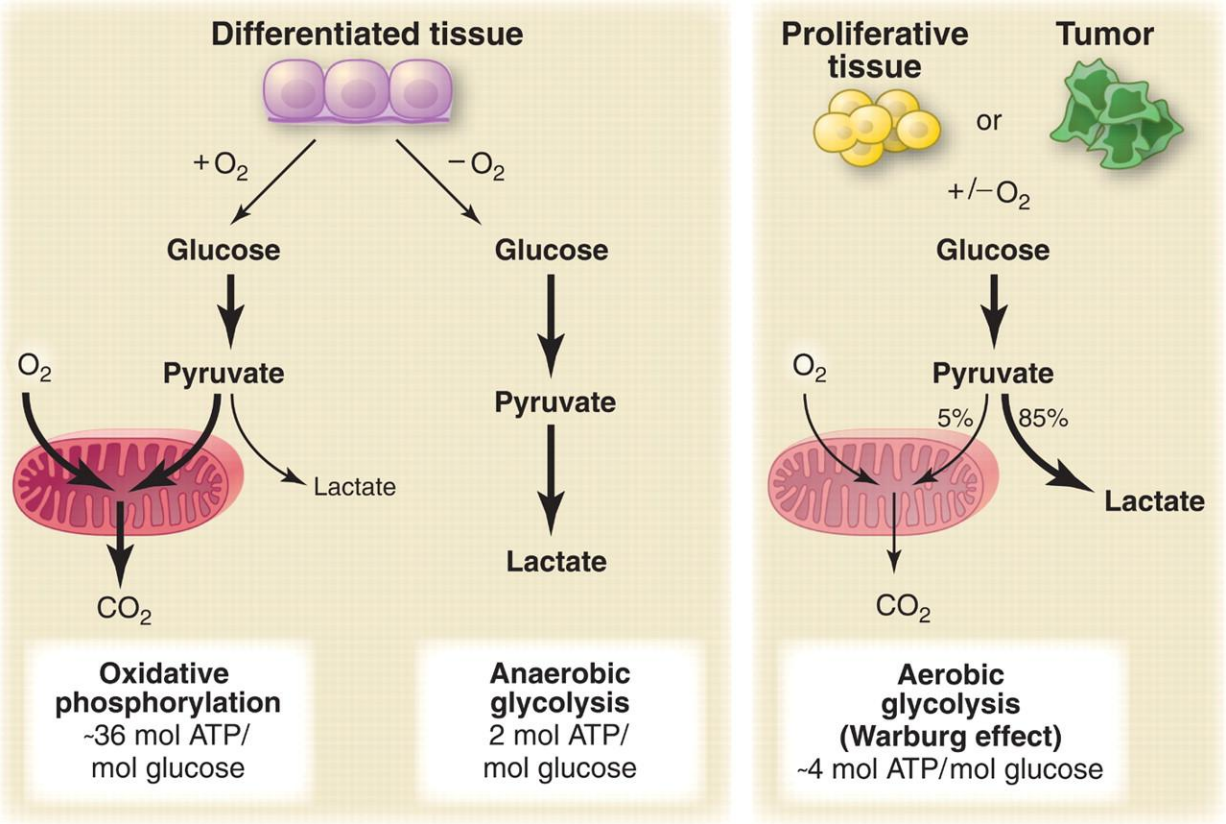

Figure 3: Modes of glucose metabolism in normal and cancer cells. In the presence of oxygen, a normal cell (differentiated) metabolizes glucose via glycolysis, TCA and oxidative phosphorylation to generate ATP. Cancer cells (proliferative) tend to convert most glucose to lactate, even in the presence of oxygen (aerobic glycolysis). This figure is adapted from (Vander Heiden et al., 2009).

To assess the glucose intake of tumors, a radio-active glucose analogue, 18F-FDG (2-dexoy-2-(18F) fluoro-D-glucose, is injected into patients and a PET scanner is used to image the distribution of FDG around the body (Ben-Haim and Ell, 2009; Mankoff et al., 2007). The imaging technique is currently being used not only in diagnosis of human tumors but also in staging and monitoring growth of tumors (López-Ríos et al., 2007).

The Warburg effect in cancer cells is backed by various explanations. One possible explanation is that the abnormal activity of metabolism-related enzymes from different

signaling pathways is responsible for promoting the Warburg effect (Teicher et al., 2012). For example, the activity of the enzyme pyruvate kinase that converts phosphoenolpyruvate into pyruvate in the glycolytic pathway was found to be different in many cancer cells (Christofk et al., 2008a). Two different isoforms of Pyruvate kinase (PK) have been known; PKM1 and PKM2. The PKM2 isoform is specifically up-regulated in most cancer cells, but not in the normal cells (Mazurek et al., 2005). Interestingly, pyruvate kinase (PKM2) was suggested to bypass the pyruvate into lactate production pathway or alternative glycolytic pathway (Figure 4) (Christofk et al., 2008b; Hitosugi et al., 2009). To accommodate this alternative glycolytic pathway, the cancer cells appear to adopt increased rates of glutamine metabolism not only to produce ATP but also for the synthesis of macromolecular precursors such as nucleotides, certain amino acids, and fatty acids, and to generate energetic biomass (DeBerardinis et al., 2008; DeBerardinis et al., 2007).

1.2.3 Glutamine Metabolism in Cancer Cells (Glutaminolysis)

Glutamine is the second major energy source for many cancer cells (Lu et al., 2010). Cancer cells are highly dependent on alternative glycolysis (pyruvate to lactate), and therefore only less pyruvate is processed to generate ATP through mitochondrial TCA cycle (truncated TCA cycle in cancer cells), and results in impaired mitochondrial function. Since TCA cycle is crucial for generating energy intermediates, the cancer cells must find an alternative mechanism to replenish this cycle. Accordingly, many cancer cells utilize the glutamine metabolism (known as glutaminolysis) as a new energy source. Once glutamine is taken by the cell, mitochondrial glutaminase converts glutamine into

glutamate (Figure 4 and Figure 5). Glutamate is then converted into α-ketoglutarate through deamination process catalyzed by the enzyme glutamate dehydrogenase.

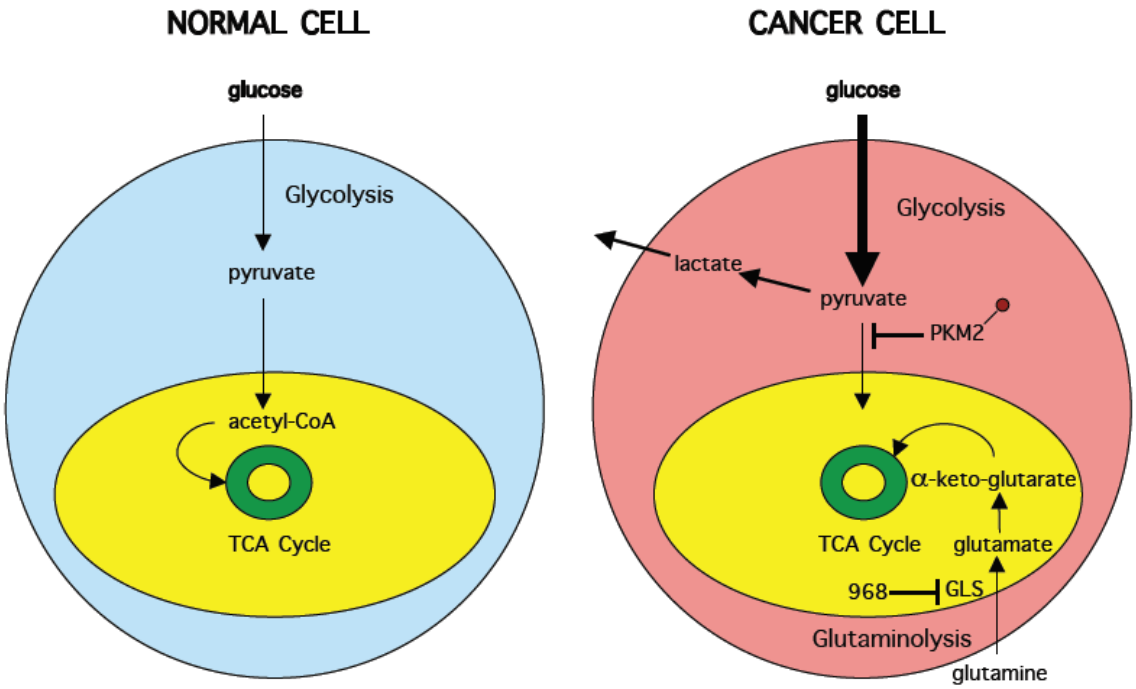

Figure 4: Metabolic differences observed between normal cells and cancer cells. In normal cells, glucose is concerted to acetyl CoA (yellow) and is further metabolized *via* TCA cycle (green). In cancer cells, pyruvate is primarily used to generate lactate. The pyruvate kinase M2 isoform (PKM2, tumor specific isoform) prevents the pyruvate entry to mitochondria. To accommodate this, cancer cells utilize a process called glutaminolysis, as an alternate source to replenishing the TCA cycle and energy synthesis. Glutaminase is the key enzyme, which converts glutamine to glutamate and opens up the glutaminolysis process. This figure is adapted from (Erickson and Cerione, 2010).

This α-ketoglutarate in turn enters the TCA cycle and is eventually metabolized to produce oxaloacetate, which condenses with acetyl-coA (generated from glucolysis) to generate citrate. In effect, the glutamine metabolism acts as new energy producing pathway, that generates various metabolic intermediates glutamate, aspartate, malate, pyruvate, citrate, alanine, and lactate (Dang, 2010a) (Figure 5). In the glutaminolytic pathway, degradation of both amino acids glutamine and glutamate plays a key role in

anabolic process (Dang, 2010a). The donor amino group of glutamine acts as a precursor for the synthesis of certain amino acids like proline, ornithine, and arginine (Wise and Thompson, 2010). Glutaminolysis is also essential for the generation of a series of intermediates from different metabolic cascades: for example (a) synthesis of acetyl CoA serine (for protein and nucleotide synthesis) and for NADH generation (for lipid, nucleotide synthesis and redox balance) (Wise et al., 2008). In addition, the citrate generated through glutaminolysis is found to be essential for fatty acids and cholesterol synthesis (Figure 5) (Dang, 2010b; Wise and Thompson, 2010). Notably, key co-factors such as glutathione, NADH and NADPH generated from glutamine are shown to play key role in protecting the cancer cells from oxidative stress (Dang, 2010b; DeBerardinis et al., 2008). Several recent studies have shown that glutaminolysis is a key metabolic process occurring in many tumor cells. Indeed, cell culture studies indicate that many cancer cells cannot survive without glutamine, often referred to as "glutamine addiction" (Wise et al., 2008; Wise and Thompson, 2010). The enhanced glutamine metabolism in the cancer cells is particularly apparent with the observation of ammonium ion release from the venous effluent of the cancer-bearing patients (Fischer and Chance, 1990; Souba, 1993).

Recent imaging techniques coupled with the improved methods such as nuclear magnetic resonance spectroscopy (NMR) and mass spectrometry (MS) play a key role in quantifying the glutamine metabolism in cancer cells (Wise et al., 2008). These techniques will help in identifying the specific metabolites that can be compared in cancer cells versus normal cells. The significance of glutaminolysis is supported by ^{13}C -

NMR measurements, suggesting cancer cells consume approximately 60% of glutamine for the conversion of lactate or alanine (DeBerardinis et al., 2008).

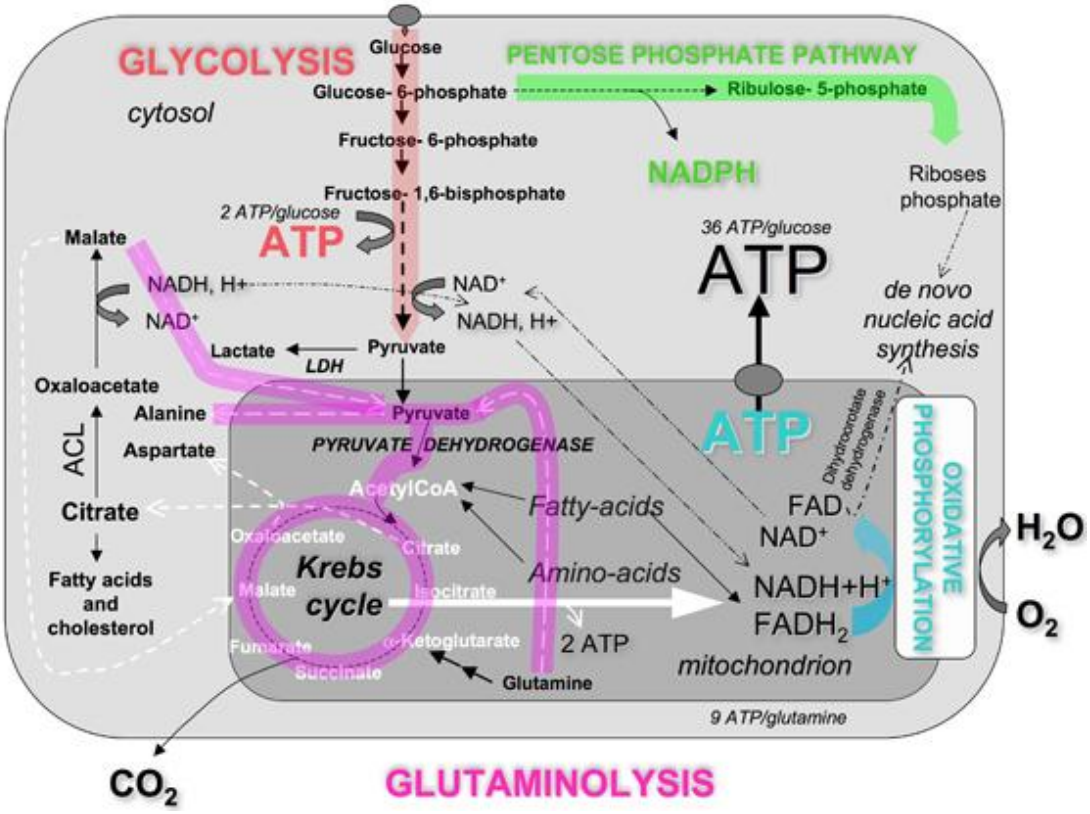

Figure 5: Schematic diagram showing the connection between the glycolysis and glutaminolysis. Cancer cells use both pathways to meet their energy demands. In addition to glucose metabolism, cancer cells undergo glutaminolysis to generate high energy-intermediates. This figure is adapted from (http://www.herbalzym.com/wp-content/uploads/2010/09/glutaminolysis.jpg)**.**

Currently it is believed that targeting the metabolic enzymes which are particularly critical for feeding glutamine to the cancer cells, will have therapeutic impact against many cancers. Glutaminase expression has been shown to be increased in several tumour types such as lymphoma, prostate, brain (glioblastoma) and kidney cancers (Gao et al., 2009; Seltzer et al., 2010). Thus, glutaminase has become an attractive target for the

development of small molecules against cancer therapy. In the next section, I will briefly discuss the role of signaling pathways that regulates the cancer metabolism.

1.3 Signal Transduction

Signaling or signal transduction is a process which involves binding of extracellular signaling molecules (a ligand or growth factors) to its specific receptors and turning on a specific cellular response. Several classes of intracellular signaling pathways exist: MAPK/ERK pathway, Hedgehog pathway, JAK/STAT (Janus kinase-signal transducer and activator of transcription) pathway and cAMP (cyclic Adenosine monophosphate) dependent pathway. Cellular functions are generally mediated by direct modifications of the key molecules or signaling complexes which lead to changes in gene expression. Phosphorylation is one of the common modes of protein modifications found in most signaling pathways. This process involves addition of a phosphate (PO_4) group to a protein, which mainly occurs through serine (Ser), threonine (Thr) and tyrosine (Tyr) residues. Protein kinases are responsible for transferring a terminal phosphate (PO_4) of ATP to a hydroxyl group (OH) of a protein, whereas, phosphatases can reverse the phosphorylation process (Cozzone, 1988) .

1.3.1 Signaling Pathways and Cancer

There are several signaling pathways that play a key role in controlling cell growth and cellular metabolism in response to growth factor stimulation. This is a tightly regulated process and any defect or alterations in the intracellular signaling pathways may lead to cancers (Braun et al., 2011). For example, mammalian target of rapamycin complex 1

(mTORC1) promotes glutamine metabolism in the cancer cells by indirectly regulating the activity of glutamate dehydrogenase (Durán et al., 2012; Sancak et al., 2008). In addition, increasing evidences suggest that different oncogenic transcription factors upregulate metabolic enzymes, which results in altered metabolism and cancer (Kim et al., 2006; Vogelstein and Kinzler, 2004). Three major transcription factors such as HIF (hypoxia-inducible factor 1), Myc, and Srebp-1 are the key regulators of energy metabolism and are often found to be deregulated in most cancers. HIFs are responsible for controlling glucose metabolism (Kim et al., 2006; Kondo et al., 2002) c-Myc, alters both glucose metabolism and glutaminolysis (Gao et al., 2009; Wise et al., 2008), and Srebp-1 increases lipid metabolism in the cancer cells (Figure 6). Taken together, targeting the altered signaling pathways in the cancer cells represents a new approach for cancer treatment.

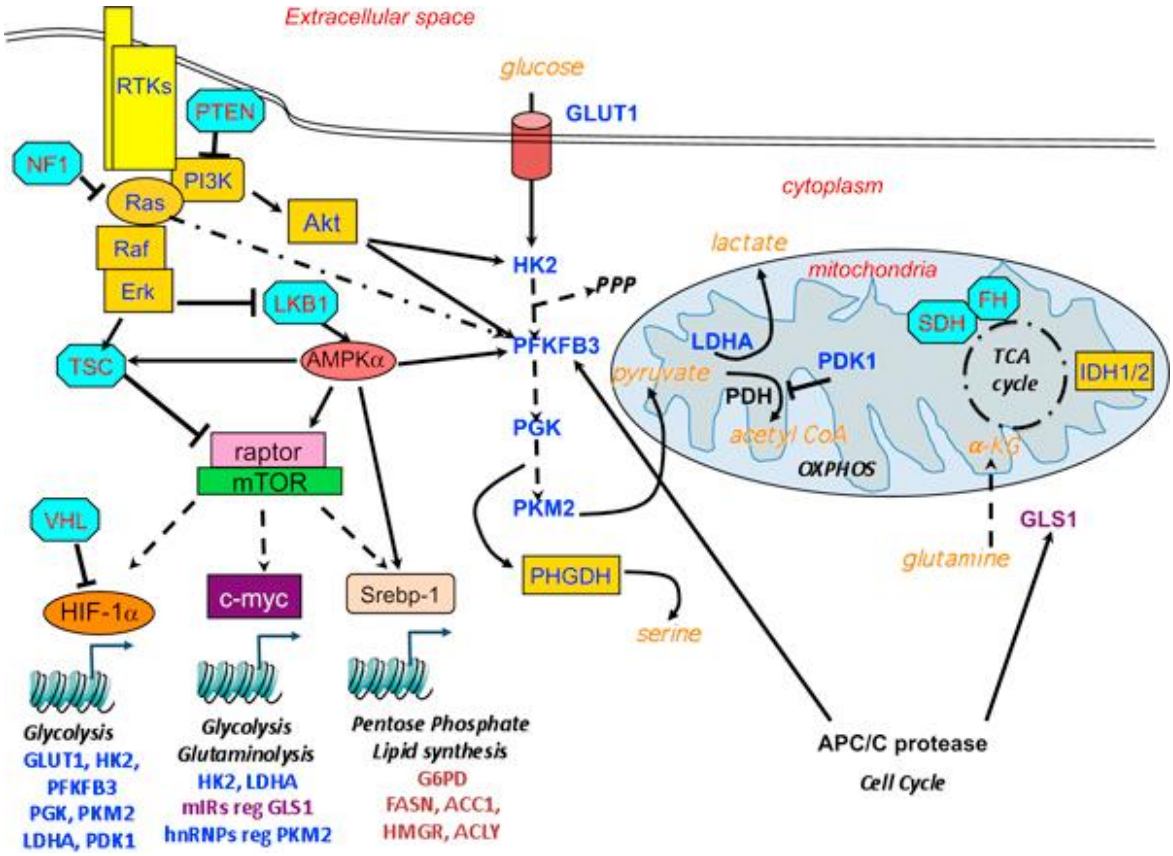

Figure 6: Oncogenic signaling pathways that controls cancer metabolism. Different oncogenes and tumor suppressor genes are illustrated in the figure; which regulates specific enzymes involved in cancer metabolism. This signaling pathway is regulated by the post translational modifications (phosphorylation and proteolysis) are shown. Directly (unbroken lines) and indirectly (unbroken lines) interacting proteins are illustrated. This figure is adapted from (Shaw and Cantley, 2012).

1.3.2 Oncogenic Signaling Pathways and Glutaminolysis

It was recently shown that the activity of glutaminase could be regulated by many oncogenes that are linked with cell metabolism (Figure 7). The oncogenic transcription factor, Myc, plays a crucial role in coordinating glutamine metabolism and proliferation (DeBerardinis et al., 2008). Previously, the unregulated Myc was noticed in many human tumors such as colon, lung, and brain (Nau et al., 1985; Taub et al., 1982). In a search of Myc-regulated mitochondrial proteins, Gao et al., have identified that glutaminase is

unregulated in the cells which express c-Myc (Gao et al., 2009). Interestingly, it has been demonstrated that the c-Myc stimulates the expression of glutaminase through repressing miR-23a and miR-23b in human lymphoma and prostate cancer cells. Indeed, these cells are very sensitive to glutamine withdrawal or glutaminase knockdown, which in turn results in loss of cell growth and survival (Gao et al., 2009). In addition, c-Myc has been shown to be involved in controlling many glycolytic enzymes that promote glucose metabolism and cancers (Kim et al., 2006; Osthus et al., 2000).

One recent study has shown that the elevated activity of glutaminase could promote glutamine metabolism not only in transformed fibroblasts but also in the human breast cancer cells (Wang et al., 2010). It has been found that glutaminase activity was up-regulated by downstream of Rho GTPase signaling in an NF-kB (Nuclear Factor kappa-light-chain-enhancer of activated *B* cells) dependant manner (Figure 7). Rho GTPases are well studied oncogenes and are commonly activated in wide range of tumors such as colon, lung, breast cancers, pancreatic, and urinary tract tumors (Fritz et al., 1999; Schnelzer et al., 2000; Suwa et al., 1998). Further, a study links the glutaminolysis pathway with the cell cycle/cancer progression, through the observation that glutaminase could be targeted by the ubiquitin ligase (APC/C) (Colombo et al., 2010). Taking into all these observations, glutaminase therefore represents a promising anti-cancer drug target.

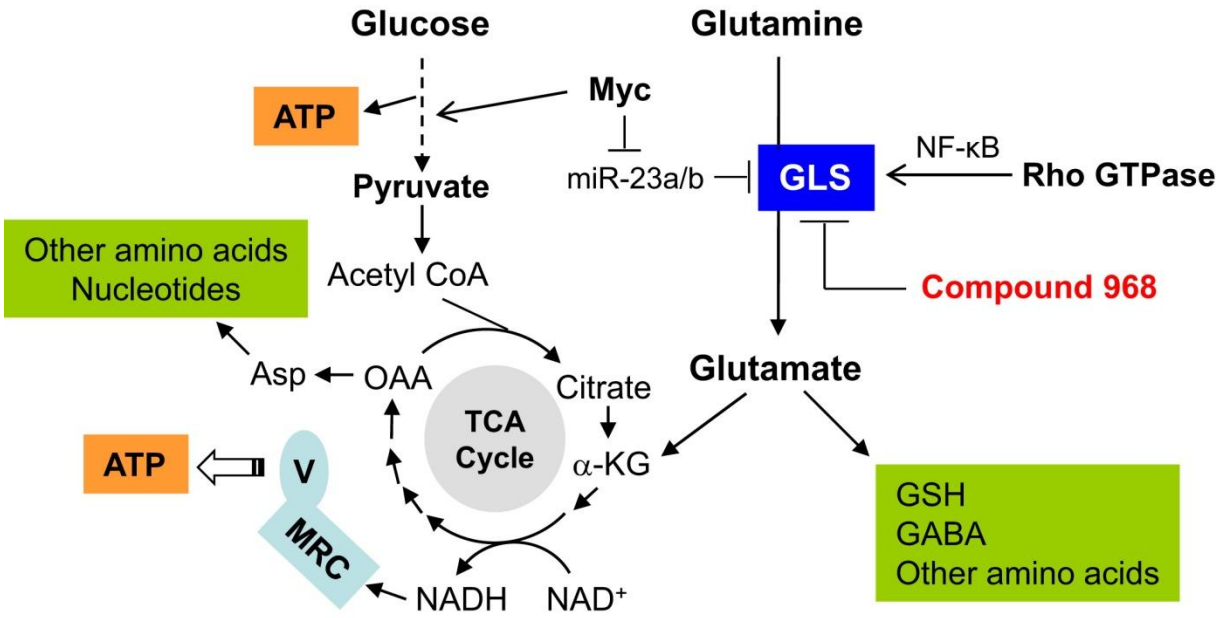

Figure 7: Schematic representation of the oncogenic regulation of glutaminase in the glutaminolysis pathway. Oncogene, Myc regulates glutaminase through miR-23a/b dependent manner; whereas Rho GTPase controls glutaminase in an NF-kB-dependent manner. This figure is adapted from (Lu et al., 2010).

1.3.3 Overview of the Ras/MAPK Signaling Pathways

The Mitogen Activated Protein Kinase (MAPK) pathway has been found in most eukaryotic organisms and is highly conserved. This pathway can be activated by molecules such as mitogens, cytokines, and also by some physical stressors such as UV radiation, osmotic shock and heat. The MAPK module has three protein kinases which act sequentially, it including, MAP kinase kinase kinase (MAPKKK or MEKK), MAP kinase kinase (MAPKK or MEK) and MAP kinase (MAPK). This pathway is known to control diverse cellular functions such as, cell proliferation, differentiation, cell cycle progression, gene expression, embryogenesis, cellular metabolism, and apoptosis (Dhillon et al., 2007; Pearson et al., 2001). The MAPK pathway is further subdivided into four different groups: ERK/MAPK, JNK/SAPK, p38 and ERK5 pathways.

1.3.4 ERK/MAPK Pathway

Receptor tyrosine kinases (RTKs) are the key regulators of cell signaling and are found to play a role in apoptosis, cell growth, proliferation and cancer progression (Zwick et al., 2001). Binding of a growth factor on the extracellular domain of the RTK, induces dimerization and which inturn autophosphorylates tyrosine residues and results in the activation of RTK. The activated RTK further triggers the downstream signaling pathways, for example ERK/MAPK kinase signaling cascade which has been shown in Figure 8. The auto-phosphorylated tyrosine recruits Grb2 (adaptor protein). The guanine nucleotide exchange factor Son of Sevenless (SOS) in turn translocates to the membrane and associates with Grb2 to catalyze the activation of Ras (a small GTPase) by exchanging GDP to GTP. Activated Ras-GTP, further turns on a signaling cascade. Ras-GTP directly binds and activates a protein kinase called Raf, (a serine/threonine kinase). This Raf subsequently phosphorylates either serine or theoronine residues of the MEK (also known as MAP kinase kinase). Consequently, the activated MEK then phosphorylates and activates ERK (also known as MAP kinase).

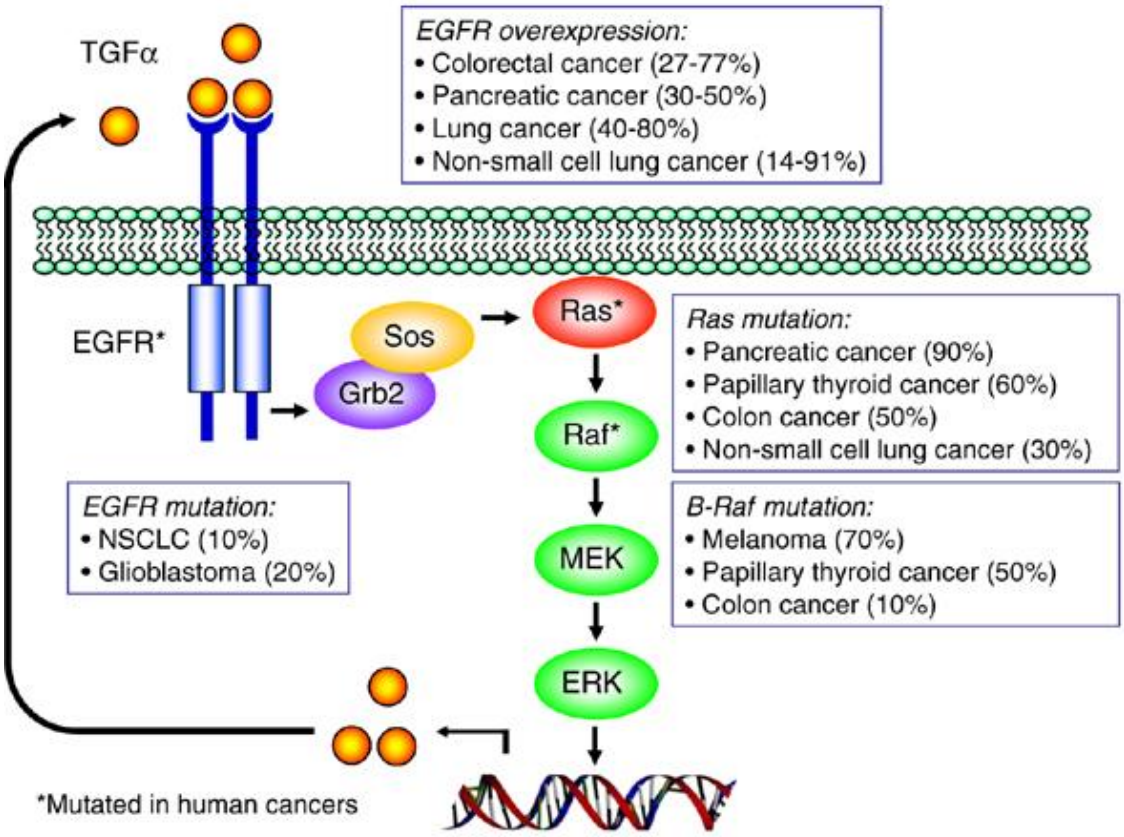

Figure 8: An overview of ERK/MAPK cascade. This pathway is commonly activated by growth factors (eg. TGFα). Activated ERKs regulates various transcription factors inside the nucleus, leading to changes in gene expression. The mutated form of B-Raf, Ras in the ERK/MAPK cascade often found in many human cancers. This figure is adapted from (Roberts and Der, 2007).

Activated Erk then phosphorylates Ser/Thr-Pro motif of many protein substrates to control diverse cellular functions. In the RAS/RAF/MEK/ERK signaling pathway, Mek is a key protein kinase, which plays an important role in regulating cancer cell growth and proliferation. The deregulated activity of MEK is commonly found in wide range of human tumors, particularly, those that express mutant form of RAS and RAF oncogenes (Friday and Adjei, 2008; Roberts and Der, 2007). It is demonstrated from the preclinical studies that MEK inhibitors are found to be synergistic or additive when combined with other pathway inhibitors (Kinkade et al., 2008; Meng et al., 2010).

In this thesis, we have shown that RAS/RAF/MEK/ERK module could act as a regulatory pathway to enhance the activity of glutaminase. These findings are described in detail in Chapter II.

1.4 Current Molecular Targets

From a therapeutic perspective, the effort to develop drugs that could starve the cancer cells by blocking their energy requirements are under development. Currently, there are several potential lead compounds that are undergoing preclinical development and some of them are in clinical trials (Jones and Schulze, 2012) (Table 1). These drugs specifically target the metabolic pathway enzymes (glycolysis, TCA, glutaminolysis, and fatty acid synthesis pathways) which appear to be responsible for feeding the cancer cell energy requirements. Targeting metabolism has the potential to offer an alternative to chemotherapy or radiotherapy and any other treatment regimes where these drugs selectively kill the cancer cell without affecting the normal cells. One striking example in this context is the development of the drug called dicholoro acetate (DCA). DCA is shown to shift the altered glucose metabolism that is found in the cancer cells. By inhibiting a key enzyme pyruvate dehydrogenase **(**PDK1), DCA was shown to prevent the pyruvate conversion to lactate, thus reversing the Warburg effect. More importantly, DCA was shown to effectively shrink the lung, colon cancers (Bonnet et al., 2007). Preliminary clinical trial results suggested that DCA is well tolerated by human patients with fewer side effects (Michelakis et al., 2010).

Drug/compound (Source/reference)	Molecular or pathway target	Biological validation	Current status (if known)
Phloretin	GLUT1/4	Blocks glucose uptake	Early development
2-Deoxyglucose	Hexokinase (glycolysis)	Blocks glycolytic flux	Reported in clinical trials
3-Bromopyruvate	Hexokinase (+ other glycolytic targets?)	Blocks glycolytic flux	Preclinical development
Lonidamine	Hexokinase	Blocks glycolytic flux	Clinical trials ongoing
3PO [+ derivatives] (Advanced Cancer Therapeutics)	Phosphofructose kinase 2 [PFKFB3]	Blocks positive regulation of PFK1 and glycolysis	Preclinical development
Cap-232/TLN-232 (Thallion Pharmaceuticals)	Pyruvate kinase-M2	Blocks pyruvate formation via PK route	Trial suspended owing to licensing dispute
(Agios Pharmaceuticals)	Pyruvate kinase-M2	Blocks pyruvate formation via PK route	Preclinical
(Agios Pharmaceuticals)	Pyruvate kinase-M2 activators	Promotes glycolytic flux reducing synthesis of biosynthetic intermediates	Preclinical
Dichloroacetate	Pyruvate dehydrogenase kinase (+ metabolic targets?)	Activates PDH and promotes oxidative phosphorylation	Basic Phase I trial completed, Phase II studies proposed
FX11 (University of New Mexico/ The John Hopkins University)	Lactate dehydrogenase	Blocks metabolic flux pathways	Early development
Oxamate	Lactate dehydrogenase and aspartate aminotransferase	Blocks metabolic flux pathways	Early development
Amino oxyacetate	Aspartate aminotransferase	Blocks metabolic flux pathways	Early development
AZD-3965 (AstraZeneca)	MCT1	Blocks lactate secretion	Phase I/II trials planned with CRUK
5-Dehydroepiandrosterone [DHEA]	Glucose-6-phosphate dehydrogenase + multiple non-metabolism targets	Blocks oxidative pentose phosphate pathway (PPP)	Early development
Oxythiamine	Transketolase	Blocks non-oxidative PPP	Early development
(Tarvagenix)	Transketolase-like 1 (TKTL1)	Could block non-oxidative PPP in cancer	Early development (no published data)
6-Diazo-5-oxo-L-norleucine	Glutaminase (glutaminolysis)	Blocks glutamine conversion to glutamate	Toxicity issue Early development
968 (Cornell University)	Glutaminase	Blocks glutamine conversion to glutamate	Early development
BPTES	Glutaminase	Blocks glutamine conversion to glutamate	Early development
GSK837149A (GSK)	Fatty acid synthase	Blocks fatty acid synthesis	Preclinical
Orlistat (Roche)	Fatty acid synthase	Blocks fatty acid synthesis	Preclinical
C75	Fatty acid synthase	Blocks fatty acid synthesis	Early development
SB-204990 (GSK)	ATP citrate ligase	Blocks fatty acid synthesis	Preclinical
(Agios Pharmaceuticals)	Mutant IDH1/2	Blocks alternative catalytic function of mIDH	Preclinical
CPI-163 (Cornerstone Pharmaceutical)	Glycolytic target	Blocks glycolytic flux	Phase I/II trials ongoing
Metformin	Energy sensing pathways (AMPK) and other targets	Blocks lipid and protein synthesis and glycolytic regulation	Used in diabetes, clinical trials in cancer ongoing
MPC-9528 (Myrexis)	Nicotinamide phosphoribosyltransferase	Blocks NAD production and reduces glycolysis	Preclinical

Table 1: List of potential compounds that target cancer metabolism. These compounds target metabolic enzymes that are responsible the altered metabolism and cancer formation. Details of compounds, their molecular targets and status are shown. Table adapted from (Jones and Schulze, 2012).

In addition, several metabolic enzymes have been identified in recent studies as a target for small molecules includingIsocitrate dehydrogenase 1 (IDH1), hexokinase, Pyruvate kinase M2 (PKM2) and Glutaminase (GLS). A list of the potential compounds and their molecular targets is summarized in the table (Table 1). The glutaminase inhibitors BPTES and DON have also been proposed as potential anticancer drugs, which are currently in the early stage of clinical development (Table 1). Chapter II and Chapter III of this thesis report the structural basis of the inhibition mechanism of glutaminase by BPTES and DON respectively.

1.5 Glutaminase: A key enzyme in glutaminolysis

Glutaminase (EC number 3.5.1.2.) is an amidohydrolase enzyme which catalyzes the conversion of glutamine to glutamate with the production of an ammonium ion (Figure 9).

Glutamine Glutamate

Figure 4: Reaction catalyzed by glutaminase.

Mitochondrial glutaminase (GA) is the first enzyme in glutaminolysis, and through the subsequent enzymatic reactions, glutamine serves as a major substrate of TCA cycle which ultimately provides enormous bioenergetics to the cancer cells.

1.5.1 Glutaminase Isoforms

In humans, two major glutaminase isoforms have been described, kidney type glutaminase (KGA/GLS/GLS1) and Liver type glutaminase (LGA/GLS2). Both isoforms are encoded by two different but closely related genes. The *Gls* gene that codes for KGA isoform is located in chromosome 2 (Aledo et al., 2000). The *Gls* gene also encodes two different splice variants such as Glutaminase C (GAC) and Glutaminase M (GAM) isoforms, which are collectively referred as KGA (Elgadi et al., 1999). The LGA isoform encoded by *Gls2 gene* is located in chromosome 12 (Aledo et al., 2000). Though, both isoforms of human glutaminase were predicted to have high sequence homology (KGA *vs* LGA is 63% sequence identity), they are found to have difference in their tissue distribution, kinetic and biochemical properties (Curthoys and Watford, 1995; Elgadi et al., 1999).

The KGA isoform is highly expressed in kidney, brain, intestine, fetal liver, lymphocytes, and in many tumors (Curthoys and Watford, 1995). In the kidney, KGA is responsible for the renal ammoniagenesis (Curthoys and Godfrey, 1976; Lupianez et al., 1981); whereas KGA is the major producer of glutamate, an excitatory neurotransmitter of the central nervous system in the brain (CNS) (Yu et al., 1984). Glutaminase C (GAC) is the alternatively spliced isoform of the KGA (GAC *vs* KGA is 83% sequence identity), mainly expressed in heart and pancreas but not in liver (Elgadi et al., 1999; Porter et al., 2002). Similarly, the other alternatively spliced variant of the KGA, namely hGAM, is found only in the heart and skeletal muscle (Elgadi et al., 1999). The expression of Liver type glutaminase (LGA) was originally thought to be only in liver (Elgadi et al., 1999).

Nevertheless, recent studies have demonstrated its expression in extrahepatic tissues such as brain, pancreas and cancers (Gómez-Fabre et al., 2000; Pérez-Gómez et al., 2005; Turner and McGivan, 2003) (Table 2).

Type	Genetic Structure	Cellular Location	Tissue Expresson	References
hLGA	Chromosome 12	Mitochondrial, Nuclear	Liver, Pancreas, Brain	(Aledo et al., 2000; Curthoys and Watford, 1995; Olalla et al., 2002)
hKGA	Chromosome 2, multiple poly-adenylation sites	Mitochondrial	Kidney, Brain, Intestine, Lymphocytes, Fetal Liver	(Elgadi et al., 1999; Porter et al., 2002; Shapiro et al., 1985)
hGAC	KGA isoform: Unique 3' tail derived from exon 15	Mitochondrial	Cardiac muscle, Pancreas, Placenta, Kidney, Lung, Brain	(Elgadi et al., 1999; Porter et al., 2002)

Table 2: Glutaminase isoforms. Different isoforms of human glutaminase, their location, and tissue expression are given. This table is adapted from (Erdmann et al., 2006).

The important difference between KGA and LGA isoform is their mode of inhibition and activation mechanism. KGA is activated by phosphate and inhibited by glutamate (the product), whereas LGA is less dependent on phosphate for its activation and not inhibited by glutamate (Curthoys and Godfrey, 1976). The activation of recombinant KGA requires inorganic phosphate that converts the inactive dimeric form to active tetrameric or oligomeric form (Godfrey et al., 1977; Morehouse and Curthoys, 1981). Besides phosphate, acetyl-coA, and ADP were shown to stimulate the activity of KGA (Kvamme and Torgner, 1974; Masola and Ngubane, 2010).

1.5.2 Sequence Analysis of Glutaminase

The isoforms of human glutaminase contains distinct combination of signature motifs and functional domains, and is often referred to as "multifaceted protein" (Márquez et al., 2006) (Figure 10 and Figure 11). The glutaminase isoforms KGA and GAC have high sequence homology in the N-terminal region of the protein, and only 12% sequence identity was found in the C-terminals. Starting from N-terminal, the first 16 amino acids of all three isoforms (KGA, GAC and LGA) have conserved sequence, known as transit peptides. This is shown to be responsible for the localization of enzyme into mitochondria (Gómez-Fabre et al., 2000). In addition, the nuclear receptor targeting box (NR box) has been found in all three glutaminase isoforms, which specifically interacts with nuclear receptors (Heery et al., 1997).

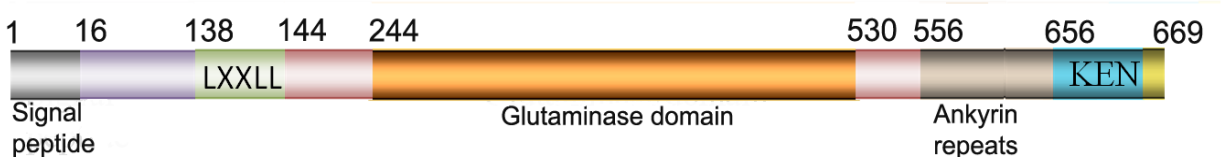

Figure 10: Domain architecture of human KGA. The signature domains and functional motifs of KGA are illustrated in the figure. KGA contains Signal peptide (amino acids 1-16), nuclear targeting box (amino acids 138-144), glutaminase domain (244-530), ankyrin repeats (amino acids 556-656), and KEN box (amino acids 656-669) (Thangavelu et al., 2012).

Human KGA has NR box with the sequence of LDDLL on the N-terminal residues from 138-144 whereas LGA has the similar motif from 72-76. Pfam data base suggests the presence of glutaminase domain (aa 244-530) in KGA and residues 177–463 form glutaminase domain in LGA (Finn et al., 2010). The C-terminal of glutaminase has a protein-protein interaction module, known as ankyrin repeats.

```
KGA             MMRLRGSGMLRDLLLRSPAGVSATLRRAQPLVTLCRRPRGGGRPAAGPAAAARLHPWWGG 60
GAC             MMRLRGSGMLRDLLLRSPAGVSATLRRAQPLVTLCRRPRGGGRPAAGPAAAARLHPWWGG 60
LGA             --------------MRSMKALQKALSRAG---SHCGR----------------------- 20
                             :**  .:. :* **    : * *

KGA             GGWPAEPLARGLSSSPSEILQELGKGSTHPQPGVSPPAAPAAPGPKDGPGETDAFGNSEG 120
GAC             GGWPAEPLARGLSSSPSEILQELGKGSTHPQPGVSPPAAPAAPGPKDGPGETDAFGNSEG 120
LGA             GGWGHP------SRSP-----LLGGGVRHH---LSEAAAQGRETPHSHQPQHQDHDSSE- 65
                ***         * **      ** *  *    :* .** .   *:.   : : ...**

KGA             KELVASGENKIKQGLLPSLEDLLFYTIAEGQEKIPVHKFITALKSTGLRTSDPRLKECMD 180
GAC             KELVASGENKIKQGLLPSLEDLLFYTIAEGQEKIPVHKFITALKSTGLRTSDPRLKECMD 180
LGA             ------------SGMLSRLGDLLFYTIAEGQERIPIHKFTTALKATGLQTSDPRLRDCMS 113
                            .*:*. * ************:**:*** ****:***:******::**.

KGA             MLRLTLQTTSDGVMLDKDLFKKCVQSNIVLLTQAFRRKFVIPDFMSFTSHIDELYESAKK 240
GAC             MLRLTLQTTSDGVMLDKDLFKKCVQSNIVLLTQAFRRKFVIPDFMSFTSHIDELYESAKK 240
LGA             EMHRVVQESSSGGLLDRDLFRKCVSSNIVLLTQAFRKKFVIPDFEEFTGHVDRIFEDVKE 173
                 :: .:* :*.* :**:***:***.***********:******* .**.*:*.::*..*:

KGA             QSGGKVADYIPQLAKFSPDLWGVSVCTVDGQRHSTGDTKVPFCLQSCVKPLKYAIAVNDL 300
GAC             QSGGKVADYIPQLAKFSPDLWGVSVCTVDGQRHSTGDTKVPFCLQSCVKPLKYAIAVNDL 300
LGA             LTGGKVAAYIPQLAKSNPDLWGVSLCTVDGQRHSVGHTKIPFCLQSCVKPLTYAISISTL 233
                 :***** ******* .*******:*********.*.**:**********.***::. *

KGA             GTEYVHRYVGKEPSGLRFNKLFLNEDDKPHNPMVNAGAIVVTSLIKQGVNNAEKFDYVMQ 360
GAC             GTEYVHRYVGKEPSGLRFNKLFLNEDDKPHNPMVNAGAIVVTSLIKQGVNNAEKFDYVMQ 360
LGA             GTDYVHKFVGKEPSGLRYNKLSLNEEGIPHNPMVNAGAIVVSSLIKMDCNKAEKFDFVLQ 293
                **:***::*********:*** ***:. *************:**** . *:*****:*:*

KGA             FLNKMAGNEYVGFSNATFQSERESGDRNFAIGYYLKEKKCFPEGTDMVGILDFYFQLCSI 420
GAC             FLNKMAGNEYVGFSNATFQSERESGDRNFAIGYYLKEKKCFPEGTDMVGILDFYFQLCSI 420
LGA             YLNKMAGNEYMGFSNATFQSEKETGDRNYAIGYYLKEKKCFPKGVDMMAALDLYFQLCSV 353
                :*********:**********:*:****:*************:*.**:. **:******:

KGA             EVTCESASVMAATLANGGFCPITGERVLSPEAVRNTLSLMHSCGMYDFSGQFAFHVGLPA 480
GAC             EVTCESASVMAATLANGGFCPITGERVLSPEAVRNTLSLMHSCGMYDFSGQFAFHVGLPA 480
LGA             EVTCESGSVMAATLANGGICPITGESVLSAEAVRNTLSLMHSCGMYDFSGQFAFHVGLPA 413
                ******.***********:****** ***.*****************************

KGA             KSGVAGGILLVVPNVMGMMCWSPPLDKMGNSVKGIHFCHDLVSLCNFHNYDNLRHFAKKL 540
GAC             KSGVAGGILLVVPNVMGMMCWSPPLDKMGNSVKGIHFCHDLVSLCNFHNYDNLRHFAKKL 540
LGA             KSAVSGAILLVVPNVMGMMCLSPPLDKLGNSHRGTSFCQKLVSLFNFHNYDNLRHCARKL 473
                **.*:*.************* ******:*** :*  **:.**** ********** *:**

KGA             DPRREGGDQRVKSVINLLFAAYTGDVSALRRFALSAMDMEQRDYDSRTALHVAAAEGHVE 600
GAC             DPRREGGDQ---------------------RHSFGPLDYES--LQQELALKETVWK---- 573
LGA             DPRREGAEIRNKTVVNLLFAAYSGDVSALRRFALSAMDMEQKDYDSRTALHVAAAEGHIE 533
                ******.:                      *.::..:* *.   :.. **: :. :

KGA             VVKFLLEACKVNPFPKDRWNNTPMDEALHFGHHDVFKILQEYQVQYTPQGDSDNGKENQT 660
GAC             ---------KVSPESNEDISTTVVYRMESLGEKS-------------------------- 598
LGA             VVKFLIEACKVNPFAKDRWGNIPLDDAVQFNHLEVVKLLQDYQDSYTLSETQAEAAAEAL 593
                         **.* .::  ..  :     :.. .

KGA             VHKNLDGLL 669
GAC             --------- 
LGA             SKENLESMV 602
```

Figure 11: Sequence-based analysis of human glutaminase isoforms. The sequence alignments of three isoforms KGA, GAC and LGA was performed by ClustalW (Thompson et al., 1994).

The ankyrin repeats has approximately 30 amino acids and found in several signaling proteins whose functions include transcriptional initiation, cell cycle regulation, cytoskeleton, and signal transducers (Li et al., 2006). According to the Pfam database, KGA contains three ankyrin repeats, whereas LGA contains two ankyrin repeats. The exact function of ankyrin repeats in human glutaminase is still not known. Interestingly, KGA has a KEN box in the C-terminal end that is specifically targeted by ubiqutin ligase APC/C during cell-cycle progression (Colombo et al., 2011). On the other hand, LGA contains a unique motif EMSV in the C-terminal end which specifically interacts with PDZ domain containing proteins (Olalla et al., 2002).

1.5.3 Structure of Glutaminase

Glutaminase have been reported to present in many organisms including, bacteria, yeast, fungi and mammals but not found in thermophiles, archaea and plants (Yoshimune et al., 2009). A PSI-BLAST search with the KGA sequence suggested the presence of over 50 homologs from various species and all of them belong to the glutaminase superfamily. Besides, a BLAST search with the KGA sequence against protein data bank (PDB) showed several homologs in the PDB. The closest homolog includes microbial glutaminase from *Micrococcus luteus* (PDB: 1U60) and probable glutaminase from *Geobacillus Kaustophilus* (PDB: 2PBY), both shares 38% sequence identity with KGA. The monomeric structure of probable glutaminase YbgJ (*Geobacillus Kaustophilus)* consists of two domains; α/β/α sandwich and associated α-helical domain. The crystal structure of YbgJ revealed the presence of five anti parallel β strands (β1, β2, β8, β9, and β10) that are surrounded by several α helices and loops (Figure 12). Furthermore, YbgJ

structure revealed the presence of β lactamase motif 1 (Ser- X-X-Lys), where Ser74 was identified to act as a catalytic nucleophile (Brown et al., 2006). The sequence alignment of KGA with the selected homologs from *E. coli* and *Micrococcus luteus* suggested the presence of β-lactamase-like motif in KGA.

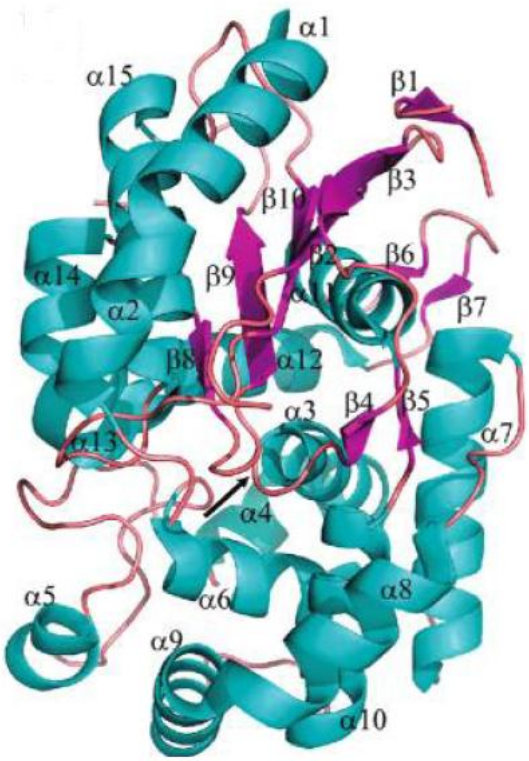

Figure 12. Crystal structure of *E.Coli* glutaminase. The secondary structure elements such as α-helices (cyan), β-strands (magenta), loops (magenta) are shown. The location of the active site is indicated by black arrow. This figure adapted from (Yoshimune et al 2009).

1.5.4 Binding Partners of Glutaminase

A recent study by Buschdorf et al., has identified Caytaxin or BNIP-H (brain-specific BNIP-2-homology protein) as an interacting partner of KGA (Buschdorf et al., 2006). Interestingly, the C-terminal part of the BNIP-H contains a novel protein-protein interaction domain, called the BCH domain (BNIP-2 and Cdc42GAP Homology) that

directly interacts with KGA. The BCH domain approximately contains 145 residues and was initially identified in two proteins; BNIP-2 and Cdc42GAP (Low et al., 2000). It has been established that the BCH domain in several proteins regulates a wide range of cellular functions including cell apoptosis, cell elongation, migration, rounding and Ras-MAPK signaling (Low et al., 2000; Lua and Low, 2004, 2005).

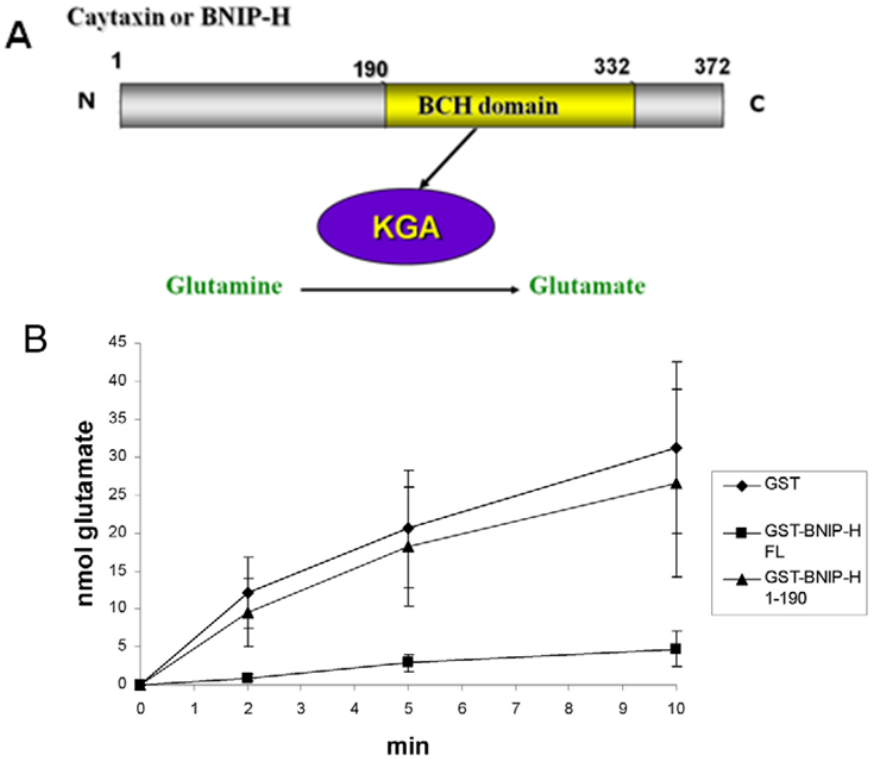

Figure 13: Schematic representation showing the direct interaction of Caytaxin and glutaminase (KGA). (A) The C-terminal caytaxin contains a novel domain called BCH that directly binds and inhibits the activity of KGA, (B) thereby it reduces the steady-state level of glutamate (Buschdorf et al., 2006).

Caytaxin or BNIP-H is encoded by gene ATCAY and mutation in this gene has been implicated in human Cayman cerebellar ataxia (Bomar et al., 2003). The BCH domain of

Caytaxin, has been found to directly inhibit the activity of KGA; thereby reducing the level of glutamate (Figure 13). Furthermore, it was also found that KGA interaction is mediated via atleast two different region of the BCH domain; (aa 191-235) and (aa 288-331) (Buschdorf et al., 2006). The other isoform LGA is known to directly interact with PDZ domain containing proteins such as SNT and GIP (Banerjee et al., 2008; Olalla et al., 2008).

1.5.5 Glutaminase in Neurodegenerative Diseases

In the brain, the role of KGA is briefly described in glutamine-glutamate cycle (Masson et al., 2006). Once glutamine is released from the glial cell, mitochondria glutaminase (KGA) converts glutamine into glutamate. Upon nerve stimuli, glutamate is released from presynaptic terminals and activates glutamate receptors to exert its physiological functions. Subsequently, glutamate is converted back into glutamine by glutamine synthetase. The glutamine-glutamate cycle is an essential event to maintain low level of glutamate in the synapse, avoiding glutamate accumulation and its associated glutamate excitotoxicity (Choi and Rothman, 1990). Glutamate excitotoxicity is a principal mediator for several neurological disorders including seizures, stroke, trauma, multiple sclerosis, and schizophrenia. The excess activity of mitochondrial glutaminase (KGA isoform) was found to be associated with stroke and schizophrenia, due to the KGA-mediated glutamate excitotoxicity (Masson et al., 2006; Newcomb et al., 1997). In multiple sclerosis (MS) animal model studies, the activated microglia has been shown to play a key role in the generation of excessive glutamate through the release of KGA (Shijie et al., 2009). Release of KGA from the HIV-1 infected mononuclear phagocytes

was noticed to induce glutamate toxicity that leads to Human immunodeficiency virus Associated Dementia (HAD) (Figure 14). Consequently, inhibition of KGA activity by small molecule inhibitors resulted in decreased level of glutamate in the cell (Erdmann et al., 2009; Erdmann et al., 2006). Taken together, these findings indicate that KGA has been considered as a potential target for the development drugs towards several neurological conditions.

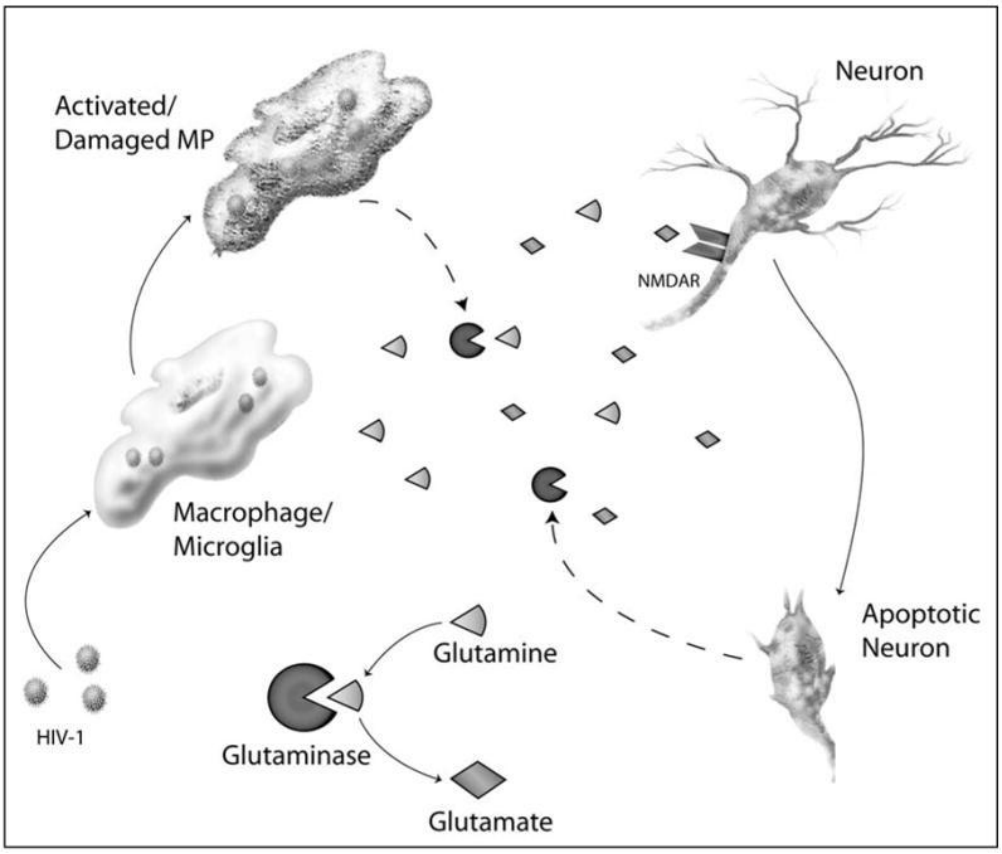

Figure 14: A schematic model for glutaminase activity in HAD. Glutaminase (KGA isoform) releases from the infected microglia converts glutamine to glutamate. Over stimulation of glutamate receptor NMDAR by glutamate, leads to neuron death. This figure is adapted from (Erdmann et al., 2006).

1.6 Glutaminase inhibitors

Numerous studies suggest that KGA is a potential therapeutic target for many cancers includes lymphoma, prostate, brain and kidney cancers (Erickson and Cerione, 2010; Gao et al., 2009; Seltzer et al., 2010; Wang et al., 2010). In this regard, small-molecules targeting this enzyme could potentially be used to arrest glutamine-dependent cell growth and tumor formation. To date, few small molecule inhibitor of glutaminase have been reported. The active site inhibitor that includes 6-Diazo-5-Oxo-l-Norleucine (DON) and L-2-amino-4-oxo-5-chloropentanoic acid (CK) are glutamine and glutamate analogs respectively (Shapiro et al., 1978, 1979) (Figure 15).

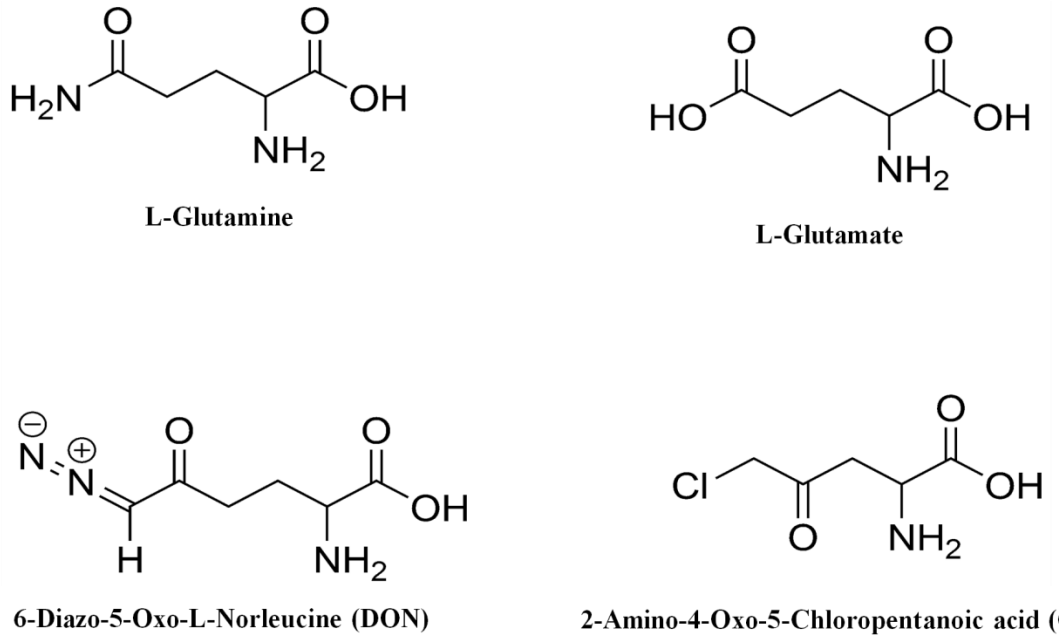

Figure 5: Chemical structures of glutamine and glutamate analogs. 6-Diazo-5-Oxo-l Norleucine (DON) and L-2-amino-4-oxo-5-chloropentanoic acid (CK) are active site inhibitors of KGA.

The inhibitor DON is non-specific to human glutaminase, because it not only inhibits glutaminase but also is shown to inhibit other glutamine or glutamate utilizing enzymes such as glutamine amidotransferase and glutamine synthetase (Barclay and Phillipps, 1966; Ortlund et al., 2000; Pinkus, 1977). The potential anticancer activity of DON has been studied in different animal models, however, it has not progressed to clinical trials due to the toxicity concerns (Ahluwalia et al., 1990; Ovejera et al., 1979).

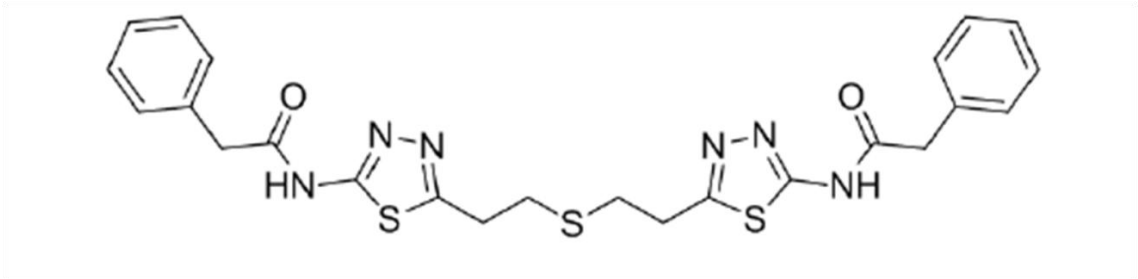

BPTES

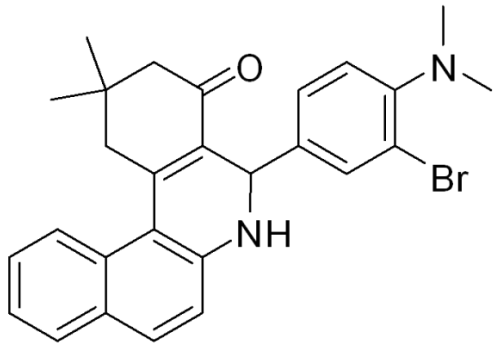

Compound 968

Figure 6: Chemical structure of glutaminase–allosteric inhibitors: BPTES [bis-2-(5-phenylacetamido-1,2,4-thiadiazol-2-yl) ethyl sulfide] and compound 968, [-(3-bromo-4 (dimethylamino) phenyl)-2,2-dimethyl-2,3,5,6-tetrahydrobenzo [a] phenanthridin-4(1H)-one].

In recent years, much effort has been taken to develop potent and selective inhibitors of glutaminase with better therapeutic efficacy towards human cancers. Recently, BPTES [bis-2-(5-phenylacetamido-1,2,4-thiadiazol-2-yl) ethyl sulfide] (Figure 16) was identified as a potent and selective inhibitor for KGA (Robinson et al., 2007). This compound was originally thought to have therapeutic potential towards the neurological disorders where it reduces the glutamate level through the inhibition of glutaminase in cultured neurons. However, recent studies highlighted BPTES as a cancer metabolism inhibitor, as it inhibits glutaminase that feeds the cancer cells with glutamine. Strikingly, BPTES was recently shown to be effective against glioblastoma tumors (low-grade gliomas and secondary glioblastomas), by indirectly reducing the activity of R132H mutant form of isocitrate dehydrogenase-1 (IDH1) (Figure 17). The enzyme IDH1 usually converts α-ketoglutarate (α-KG) into isocitrate. However, R132H mutant form of IDH1 is commonly found in the brain cancers (glioblastoma cells) that unusually converts α-ketoglutarate (α-KG) into 2-hydroxyglutaric acid (2-HG), an "onco-metabolite" which supports tumorigenesis (Dang et al., 2010). By inhibiting glutaminase, BPTES reduces the glutamate derived α-ketoglutarate levels and delays the growth of cells harboring IDH mutations (Seltzer et al., 2010).

Furthermore in animal model studies, BPTES has proven to be effective in delaying tumor xenograft growth (Keibler et al., 2012). In addition, BPTES is known to be the most potent among all the inhibitors studied so far (DeLaBarre et al., 2011; Hartwick and Curthoys, 2011; Thangavelu et al., 2012). The selectivity and high potency of BPTES against KGA makes this inhibitor an ideal candidate for the therapeutics and notably, this

compound has entered in preclinical trials (Garber, 2010; Jones and Schulze, 2012). Similarly, Wang et al., identified a compound 5-(3-bromo-4 (dimethylamino) phenyl)-2,2-dimethyl-2,3,5,6-tetrahydrobenzo[a] phenanthridin-4(1H)-one, named 968 as an allosteric inhibitor of glutaminase. This compound has been shown to inhibits recombinant GAC *invitro*, and as well blocks the growth of tumors in mouse xenograft models *invivo* (Wang et al., 2010).

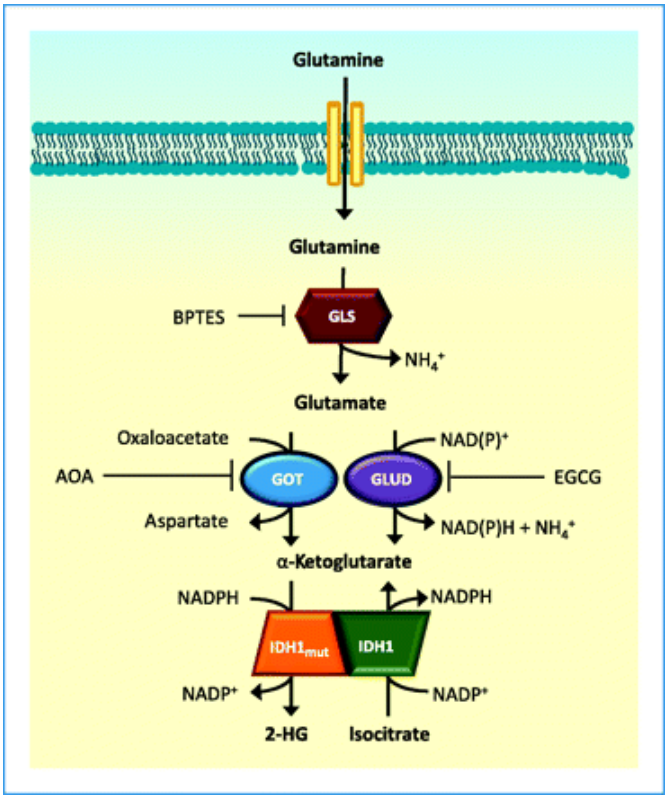

Figure 7: BPTES inhibits IDH1 mutant isoform indirectly. The pathway shows the production of 2-HG (an oncometabolite) by IDH1 mutant isoform. BPTES specifically inhibits of GLS/KGA in glioblastoma cells and it reduces the glutamate derived α-ketoglutarate level, a substrate of tumor specific IDH1 mutant isoform. This figure is adapted from (Seltzer et al., 2010).

1.7 Objectives

The major objective of this thesis is to understand the structural and functional basis of human kidney type glutaminase (KGA) and its implications in arresting cancer cell metabolism. This will be accomplished through the combination of structural, biochemical, molecular, and cell-based studies. Our objectives will be achieved through the following studies:

(a) To study the structure based inhibition mechanism of KGA by small molecule inhibitors BPTES and DON.

(b) To study the regulatory role of KGA in the Raf-Mek-Erk signaling pathway in cancer metabolism.

(c) To identify the growth factors which are connected to Raf-Mek-Erk signaling pathway in regulating KGA activity.

(d) To validate the effect of BPTES in inhibiting cancer cell growth and proliferation using different cancer cell lines which express full length KGA.

(e) To study the functional importance of inhibitors-interacting residues and also to explore the specificity of BPTES towards KGA.

(h) To establish a synergistic inhibitory mechanism between both KGA and Raf-Mek-Erk signaling pathway and their implications in cancer cell metabolism.

Chapter II

Structural basis for the allosteric inhibitory mechanism of human kidney type glutaminase (KGA) and its regulation by Raf-Mek-Erk signaling in cancer cell metabolism

2.1 Introduction

The Warburg effect in cancer biology describes the tendency of cancer cells to take up more glucose than most normal cells despite the availability of oxygen (DeBerardinis et al., 2008; WARBURG, 1956a). In addition to altered glucose metabolism, glutaminolysis (catabolism of glutamine to ATP and lactate) is another hallmark of cancer cells (DeBerardinis et al., 2008; Reitzer et al., 1979). In glutaminolysis, mitochondrial glutaminase (GA) catalyzes the conversion of glutamine to glutamate (Curthoys and Watford, 1995), which is further catabolized in the Krebs cycle for the production of ATP, nucleotides, certain amino acids, lipids and glutathione (DeBerardinis et al., 2008; Wise et al., 2008) .

Humans express two glutaminase isoforms, KGA (Kidney-type) and LGA (Liver-type) from two closely related genes (Aledo et al., 2000). Although KGA is important for promoting growth, nothing is known about the precise mechanism of its activation or inhibition and how its functions are regulated under physiological or patho-physiological conditions. Inhibition of rat KGA activity by antisense mRNA results in decreased growth and tumourigenicity of Ehrlich ascites tumor cells (Lobo et al., 2000), reduced level of glutathione, and induced apoptosis (Lora et al., 2004), whereas Myc, an oncogenic transcription factor, stimulates KGA expression and glutamine metabolism (Wise et al., 2008). Interestingly, direct suppression of miR23a and miR23b (Gao et al., 2009) or activation of TGF (Andratsch et al., 2007) enhances KGA expression. Similarly, Rho GTPase that controls cytoskeleton and cell division also up-regulates KGA expression in an NF-kB dependent manner (Wang et al., 2010). In addition, KGA is a

substrate for the ubiquitin ligase anaphase-promoting complex/cyclosome (APC/C)-Cdh1, linking glutaminolysis to cell cycle progression (Colombo et al., 2010). In comparison, function and regulation of LGA is not well studied although it was recently shown to be linked to p53 pathway (Hu et al., 2010; Suzuki et al., 2010). Although intense efforts are being made to develop a specific KGA inhibitor such as BPTES [bis-2-(5-phenylacetamido-1, 2, 4-thiadiazol-2-yl) ethyl sulfide] (Robinson et al., 2007), its mechanism of inhibition and selectivity is not yet understood. Equally important is to understand how KGA function is regulated in normal and cancer cells so that a better treatment strategy can be considered.

The previous crystal structures of microbial (Mglu) and *Escherichia coli* glutaminases show a conserved catalytic domain of KGA (Brown et al., 2008; Yoshimune et al., 2010). However, detailed structural information and regulation are not available for human glutaminases especially the KGA, and this has hindered our strategies to develop inhibitors. In this chapter, we report the crystal structure of the catalytic domain of human *apo* KGA and its complexes with substrate (L-glutamine), product (L-glutamate), BPTES, and its derived inhibitors. Further, Raf-Mek-Erk module is identified as the regulator of KGA activity. Although BPTES is not recognized in the active site, its binding confers a drastic conformational change of a key loop (Glu312-Pro329), which is essential in stabilizing the catalytic pocket. Significantly, EGF (epidermal growth factor) activates KGA activity, which can be abolished by the kinase-dead, dominant negative mutants of Mek2 (Mek2-K101A) or its upstream activator Raf-1 (Raf-1-K375M), which are the kinase components of the growth-promoting Ras-Mek2-Erk signaling node.

Furthermore, co-expression of phosphatase PP2A and treatment with Mek-specific inhibitor or alkaline phosphatase all abolished enhanced KGA activity inside the cells and *in vitro*, indicating that stimulation of KGA is phosphorylation-dependent. Our results therefore provide novel mechanistic insights into KGA inhibition by BPTES and its novel regulation by EGF-mediated Raf/Mek/Erk module in cell growth and possibly cancer manifestation. This paves the way for developing more specific therapeutic inhibitors for KGA in glutamine-addicted cancers.

2.2 Materials and Methods

2.2.1 Cloning, Protein Expression, and Purification

The human KGA consists of 669 amino acids. We refer to Ile221-Leu533 as the catalytic domain of KGA (cKGA) (Figure 11). The cKGA was cloned into a pET-28(b) vector fusion with N-terminal His tag (pNICBsa4 cleavable with tobacco etch virus (TEV) protease, and the protein was expressed in *Escherichia coli* BL21 (DE3)-RIL-Codon plus cells grown in 6 L LB broth medium. Cells were sonicated in lysis buffer [50 mM Hepes (pH 7.5), 500 mM NaCl, 5 mM imidazole, 10% glycerol, 1 mM DTT, 0.1% (vol/vol) Triton X-100, and one tablet of complete protease inhibitor mixture] (Roche Diagnostics) and further lysed by French press. The soluble fraction was passed on to a Ni-NTA affinity column (Qiagen), and the bound protein was eluted with 500 mM imidazole. The His_6 tag was cleaved with TEV protease at 4 °C for 20 h. The protein was further purified by gel filtration column (Superdex-200; GE Healthcare) and then concentrated to 20 mg/mL in a buffer containing 20 mM Hepes (pH 7.5), 200 mM NaCl, 10% glycerol, and 3 mM DTT. The recombinant cKGA mutants were generated by site-directed

mutagenesis on the pET-28(b)-cKGA plasmid using the KAPA polymerase site-directed mutagenesis kit (Kapa Bio-systems) (Table 4). All cKGA mutants were expressed and purified using similar protocol as described above.

2.2.2 Inhibitor Synthesis

All inhibitors (**1–5**) were synthesized by following the reported procedure (Newcomb, 2002). The diamino compounds (**2–4**) were prepared by refluxing thiosemicarbazide (5 mmol) and appropriate dicarboxylic acid (15 mmol) in the presence of $POCl_3$ for 2 h. Upon cooling the reaction mixture was poured over 200 g of ice. The turbid suspension was filtered, and the filtrate was basified with potassium carbonate to precipitate the product. The precipitate was filtered and washed with plenty of water and dried at vacuum to afford the target amines in moderate yield of ≈50%. The amide derivatives (**1** and **5**) were synthesized by condensing the diamino compound (**1**) (1 mmol) and corresponding acid chloride (3 mmol) in dry pyridine for 12 h. After cooling, the reaction mixture was poured into 50 mL of methanol. The precipitated product was filtered and washed with plenty of methanol to afford the target compounds.

General procedure for the synthesis of diamino bis-thiazole derivatives (**1–3**): thiosemicarbazide (0.45 g, 5 mmol) and appropriate dicarboxylic acid (15 mmol) were refluxed in 10 mL of $POCl_3$ for 2 h. Upon cooling the reaction mixture was poured over 200 g of ice. The turbid suspension was filtered, and the filtrate was basified with potassium carbonate to precipitate the product. The precipitate was filtered and washed with plenty of water and dried at vacuum.

Bis-2′-[5-amino-1,3,4-thiazol-2-yl]ethylsulfide (**1**):

3,3′-thiodipropionic acid (5.67 g). 0.75 g of product (yield = 53%)

1,5-(5-amino-1,3,4-thiadiazol-2yl)pentane (**2**):

Pentane-1,5-dicarboxylic acid (2.4 g). 0.6 g of product (yield = 45%)

1,5-(5-amino-1,3,4-thiadiazol-2yl]butane (**3**):

1,6-hexanedioic acid (2.2 g). 0.5 g of product (yield = 40%)

General procedure for amide synthesis (**4** and **5**): diamino compound **1** (1 mmol) and corresponding acid chloride (3 mmol) were refluxed in 10 mL of dry pyridine for 12 h. Upon cooling, the reaction mixture was poured into 50 mL of methanol. The precipitated product was filtered and washed with plenty of methanol to afford the target compound.

Bis-2′-[5- (phenylacetamido)-1,3,4-thiazol-2-yl]ethylsulfide (**4**):

Phenyl acetyl chloride (0.45 g). 0.3 g of product (yield = 57%)

Bis-2′-[5-(3,4,5-trimethoxybenzamido)-1,3,4-thiazol-2-yl]ethyl sulfide (**5**):

3,4,5-trimethoxybenzoyl chloride (0.69 g). 0.28 g of product (yield = 41%)

Inhibitors were synthesized in collaboration with A/P Valiyaveettil Suresh, Department of Chemistry, NUS.

2.2.3 Glutaminase Assay

Glutaminase assay was performed using a two step assay described previously (Kenny et al., 2003). Briefly, 10 µL of wild-type cKGA or cKGA mutant was incubated separately with 10 µL of first assay mix [20 mM glutamine, 50 mM Tris·acetate (pH 8.6), 80–150 mM phosphate, and 0.2 mM EDTA] at 37 °C for 10 min, and the reaction was quenched with adding 2 µL of 3 M HCl. Subsequently 200 µL of the second assay mix [2.2 U glutamate dehydrogenase, 80 mM Tris·acetate (pH 9.4), 200 mM hydrazine, 0.25 mM ADP, and 2 mM nicotinamide adenine dinucleotide] was added and incubated for 30 min at room temperature. The absorbance at 340 nm was recorded using a microplate reader (SpectraMax 340; Molecular Devices). Compounds were prepared as a 10-mM stock in 100% (vol/vol) DMSO, and necessary controls were established. The IC_{50} values were calculated from the fitted regression equation using the-log plot (Graphpad prism). Each value represents the means ± SD of three independent experiments, each with at least three replicates. Statistical significance was analyzed using ANOVA and the Student-Newman-Kuels multiple range test (StatsDirect). Data are means ± SD ($P < 0.05$) and expressed as fold increase over the control cells.

2.2.4 Crystallization and Data collection

Crystallization screening was carried out by hanging drop vapor diffusion methods at 20 °C using crystallization screens from Hampton Research (Aliso Viejo, CA, USA) and Jena Bioscience screens (Jena, Germany). *apo* cKGA crystals were grown in 0.1 M Bis-Tris propane (pH 7.0), 1.7 M $LiSO_4$, and 5% DMSO. cKGA-L-glutamine complex crystals were obtained by adding 10 mM L-glutamine with cKGA in 0.1 M Hepes Na

(pH 7.5), 2% PEG 400, and 2.1 M $(NH4)_2SO_4$. cKGA-L-glutamate complex crystals were obtained by adding 10 mM L-glutamate with cKGA in 0.1 M Bis-Tris propane (pH 7.0), and 1.4 M $LiSO_4$. The cKGA: BPTES complex was prepared by mixing cKGA (1 mg/mL) with BPTES (inhibitor **1**) to the final molar ratio of 1:7 and incubated at room temperature (23 °C) for 1 h. The complex was then concentrated to 22 mg/mL by centrifugation. Crystals of the cKGA: BPTES complex were grown in 0.1 M Bis-Tris propane (pH 7.0) and 1.8 M $LiSO_4$. Similarly cKGA-inhibitors **2**, **3**, and **4** complexes were prepared and crystals obtained using a similar condition as BPTES complex. Crystals were cryoprotected in the reservoir solution with 20% glycerol and flash cooled in a N_2 cold stream (100 K). Diffraction data were collected at the synchrotron beam lines [X12C, Brookhaven National Laboratory, New York, NY; BL13B1, National Synchrotron Radiation Research Center (NSRRC), Taiwan; and I911-3, MAX-lab, Lund, Sweden]. Data were processed and scaled using HKL2000 (Otwinowski Z and W., 1993) and XDS (Kabsch, 2010). The crystallographic data collection statistics are provided in Table 5.

2.2.5 Structure Solution and Refinement

We solved the crystal structure of glutaminase (cKGA)- L-glutamate complex [Protein Data Bank (PDB) code 3CZD] by molecular replacement with MolRep (Vagin and Teplyakov, 2010) using the coordinates of a homolog from *Micrococcus luteus* K-3 (PDB 2DFW; 36% sequence identity with cKGA) as search model (Yoshimune et al., 2010). This structure was refined using Refmac5 (Murshudov et al., 1997) and the models were examined and built in COOT (Emsley and Cowtan, 2004). Similarly the *apo*

cKGA and other complex structures are determined by molecular replacement with MolRep using the cKGA coordinates from cKGA–L-glutamate complex. All crystals were in space group $I4_122$, and in all cases one *apo*/complex molecule of cKGA was observed in the asymmetric unit. The initial model with the electron density map was examined, and the model was fitted with COOT and subsequent refinement carried out with CNS (Brünger et al., 1998). Manual fitting of the inhibitor and refinements were carried out in O (Jones et al., 1991) and CNS programs respectively, with appropriate entries made in their respective libraries. Overall geometry of final models was analyzed by PROCHECK (Laskowski RA et al., 1993). The refinement statistics are provided in Table 5.

2.2.6 Cell Culture, Growth Factor Stimulation, and Inhibitors Treatment.

Human embryonic kidney epithelial 293T cells were maintained in RPMI-1640 (HyClone) with 10% (vol/vol) FBS (from PPA, Cell Culture Company, Austria), 2 mM L-glutamine, 100 U/mL penicillin, and 100 μg/mL streptomycin (HyClone), whereas human breast epithelial cancer MCF7 cells were grown in high-glucose DMEM (HyClone). All cells were grown at 37 °C, 5% CO_2. Confluent cells grown on six-well plates were transfected using Mirus (TransIT) with 2 μg of either vector plasmid or plasmids encoding wild-type KGA (full length), Raf-1, Mek2, or the various mutants as indicated. Twenty-four hours later, cells were treated with indicated doses of BPTES or DMSO for 48 h. For growth factor stimulation [using 100 ng/mL of EGF (Sigma), 20 μM of LPA (Sigma), 50 ng/mL of PDGF (Sigma), 1 ng/mL of TGF-β (R&D Systems), and 10 ng/mL of basic FGF (bFGF; Promega)], the transfected cells were starved for 18 h and

stimulated with various growth factors and for the time indicated. Quiescent cells were treated with 20 μM of U0126 (Promega) and incubated at 37 °C for 30 min before growth factor stimulation. Cells were lysed with Hepes buffer [20 mM Hepes (pH 7.4), 150 mM NaCl, 1% Nonidet P-40, 20 mM glycerol-2-phosphate, 1 mM sodium orthovanadate, and 20 mM sodium fluoride and protease inhibitors (Roche Applied Science)], and 260 μL of aliquots were used for the glutaminase assays as described.

2.2.7 Phosphatase Treatment

Beads with immunoprecipitated complex were resuspended with 50 μL of Tris buffer (100 mM NaCl, 50 mM Tris·HCl, 10 mM $MgCl_2$, and 1 mM DTT; pH 7.9) and incubated with 20 U of calf intestine alkaline phosphatase (NEB) for 3 h at 37 °C. The beads were washed thrice with chilled Hepes buffer before glutaminase assay.

2.2.8 Plasmids Construction and Site-Directed Mutagenesis

The full length KGA cDNA is a generous gift from Norman P. Curthoys (Colorado State University, Fort Collins, CO; GenBank accession no. AF327434) and was cloned into pXJ40 vector with the addition of HA-tag (previously obtained from Dr. Ed Manser, Institute of Molecular and Cell Biology, Singapore). The full-length cDNA was generated through PCR with appropriate primers containing either a BamHI or XhoI restriction site for cloning into the pXJ40 expression vectors. The residues Phe318, Leu321, Phe322, Leu323, and Tyr394 of full-length human KGA were mutated to Ala, respectively, as a single-point mutant. Similarly, triple (Leu321- Phe322-Leu323) and

tetra (Leu321-Phe322-Leu323-Tyr394) mutant constructs were mutated to multiple alanines (Table 3). We used a polymerase site-directed mutagenesis kit (Kapa Biosystems) to create all mutants. The wild-type, constitutive active, or dominant negative mutants of the human Raf-1, mouse Mek2 cDNAs were gifts from Dr. Graeme Guy, Institute of Molecular and Cell Biology (IMCB), Singapore and their inserts were subcloned into Flag or HA-tagged pXJ40 vectors and propagated in *E. coli* strains DH5α. The plasmids were purified, transfected, and Mek2 was validated to activate downstream Erk/MAPK as previously described (Pan et al., 2010). Plasmids for protein phosphatase PP2A were a gift from Sheng-cai Lin (Xiamen University, Xiamen, China).

Table 3: Deoxyoligonucleotides used to generate mutants of full length KGA

F318A	5'-GCCGAGTGGACTAAGAGCCAACAAACTATTTTTGAAT-3’
	5'-ATTCAAAAATAGTTTGTTGGCTCTTAGTCCACTCGGC-3’
L321A	5'-GTGGACTAAGATTCAACAAAGCATTTTTGAATGAAGATGA-3’
	5'-TCATCTTCATTCAAAAATGCTTTGTTGAATCTTAGTCCAC-3’
F322A	5'-GTGGACTAAGATTCAACAAACTAGCTTTGAATGAAGATGATAAACC-3’
	5'-GGTTTATCATCTTCATTCAAAGCTAGTTTGTTGAATCTTAGTCCAC-3’
L323A	5'-GACTAAGATTCAACAAACTATTTGCGAATGAAGATGATAAACCACA-3’
	5'-TGTGGTTTATCATCTTCATTCGCAAATAGTTTGTTGAATCTTAGTC-3’
Y394A	5'- GAAATTTTGCAATAGGATATGCCTTAAAAGAAAAGAAGTGTTTTC-3’
	5'- GAAAACACTTCTTTTCTTTTAAGGCATATCCTATTGCAAAATTTC-3’
L321A-L323A	5'-GTGGACTAAGATTCAACAAAGCAGCTGCGAATGAAGATGATAAACC-3’
	5'-GGTTTATCATCTTCATTCGCAGCTGCTTTGTTGAATCTTAGTCCAC-3’

Table 4: Deoxyoligonucleotides used to generate mutants of recombinant cKGA

F318Y	5'- CCGTCGGGGCTGCGCTATAATAAACTGTTTCTGAAC -3'
	5'- GTTCAGAAACAGTTTATTATAGCGCAGCCCCGACGG -3'
F322S	5'- CGCTTTAATAAACTGTCTCTGAACGAAGATGACAAACCG -3'
	5'- CGGTTTGTCATCTTCGTTCAGAGACAGTTTATTAAAGCG -3'
F318Y/F322S	5'- TCGGGGCTGCGCTATAATAAACTGTCTCTGAACGAAGAT -3'
	5'- ATCTTCGTTCAGAGACAGTTTATTATAGCGCAGCCCCGA -3'
F394I	5'- CGCAACTTCGCAATTGGGTATATTCTGAAAGAAAAAAAATGCT-3'
	5'- AGCATTTTTTTTCTTTCAGAATATACCCAATTGCGAAGTTGCG -3'

2.2.9 Cell Proliferation Assays

293T cells transfected with vector, KGA, or the KGA mutant plasmids were trypsinized and replated into 96-well plates, followed by treatment with BPTES for 48 h, and amounts of cell proliferations were determined using an MTT proliferation assay kit (Promega) as described by the manufacturer. The assay was repeated with at least three independent experiments, each with multiple replicates. Statistical significance was analyzed using ANOVA and the Student-Newman-Kuels multiple range test (StatsDirect). Data are means ± SD ($P < 0.05$) and expressed as fold increase over control cells.

2.2.10 Coimmunoprecipitation and Western Blot Analyses

Transfected 293T cells were lysed with Hepes buffer and immunoprecipitated with anti-Flag M2 affinity gel (Sigma) as previously described (Low et al., 2000). Samples were separated in SDS/PAGE gels, followed by Western blot analyses. Blots were probed with

polyclonal anti-Flag (Sigma), polyclonal anti-HA (Zymed), anti-KGA (Santa Cruz), anti-myc (Santa Cruz), anti-Raf (Santa Cruz), anti-Pan-Erk (Cell Signaling Technology), and anti-phospho-ERK (Sigma). The luminescence signals were generated by incubation with Pierce Pico ECL (Thermo Scientific) as described by the manufacturer.

Cell biology related studies are performed in collaborations with Prof Low Boon Chuan, Mechnobiology Institute of Singapore (MBI), NUS.

2.2.11 PDB Accession Codes

The coordinates of the *apo* cKGA and its complexes with L-glutamine, L-glutamate, BPTES, L-glutamate- BPTES, and inhibitors **2**, **3**, and **4** have been deposited under accession codes 3VOY, 3VP0, 3CZD, 3VOZ, 3VP1, 3VP2, 3VP3, and 3VP4, respectively.

2.3 Results

2.3.1 Purification of Recombinant cKGA

The human KGA consists of 669 amino acids. We refer to Ile221-Leu533 as the catalytic domain of KGA (cKGA) (Figure 11). The plasmid was expressed in *Escherichia coli* BL2 (DE3) RIL-Codon plus cells and the cell pellets were lysed by sonication and followed by French press. The protein purification was carried out by two steps: affinity purification and followed by gel filtration chromatography. The His_6-tagged-cKGA was

first purified through affinity purification with the Ni-NTA agarose column. The bound protein was eluted in buffer containing 200 mM and 500 mM imidazole, respectively (Figure 18).

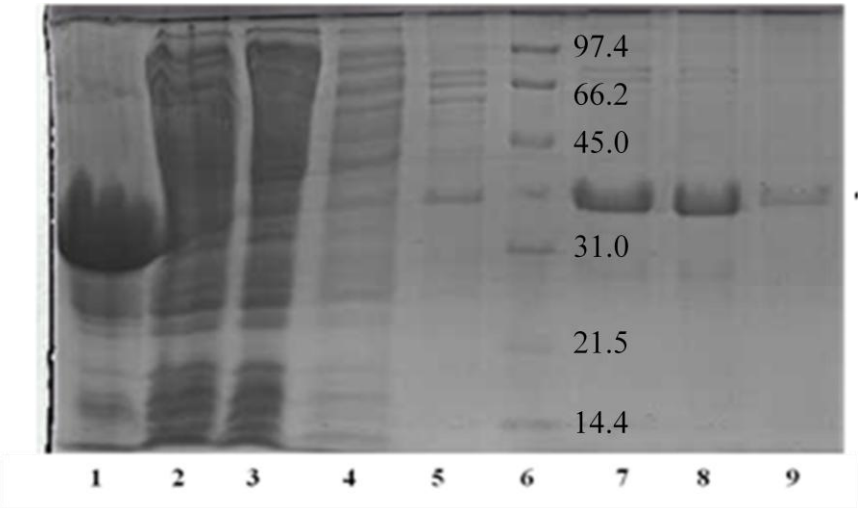

Figure 8: SDS-PAGE showing the expression and affinity purification profile of His-tagged cKGA. Samples from different stages of Ni affinity purification were collected, verified by coomassie blue stained SDS-PAGE (12.5% gel). Lane 1 – soluble fraction, Lane 2 – insoluble fraction, Lane 3 – Flow through, Lane4– wash 1, Lane5– wash 2, Lane6–low molecular weight ladder, Lane7–elution1, Lane8– elution2, Lane9 –protein bound to Ni-NTA beads after elution.

The eluted protein was further purified through gel filtration chromatography using FPLC Hiload 16/200 Superdex200 gel filtration column. A single peak corresponding to the molecular weight of cKGA (approximately 36 kDa) was obtained (Figure 19). The eluted protein was finally concentrated to 20 mg/ml by ultracentrifugation.

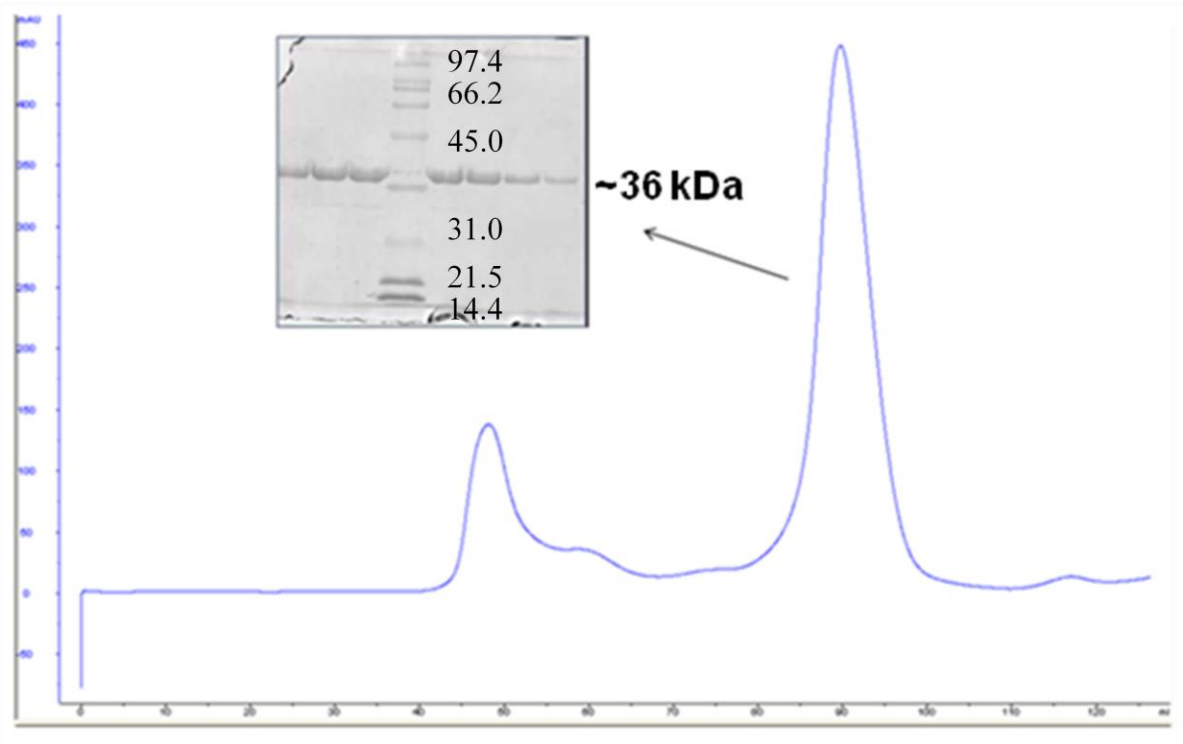

Figure 9: Gel filtration profile of cKGA in a 120 ml column volume 16/60 Superdex-200 column. The cKGA protein was purified to homogeneity, as cKGA was eluted as a single peak in the gel filtration. Gel filtration fractions from the peak were analyzed through 12.5% SDS-PAGE analysis. The X-axis indicates the elution volume in mL; Y-axis indicates the UV absorbance (at 280 nm) measured in mAU (arbitrary units).

Dynamic Light Scattering (DLS) experiment was performed during concentrating the protein and prior to the crystallization screenings, to analyze the homogeneity of the protein. DLS experiment indicated a dispersity index of 0.11 at 20 mg/ml of protein, and this indicates that the cKGA was mono-dispersed (Figure. 20).

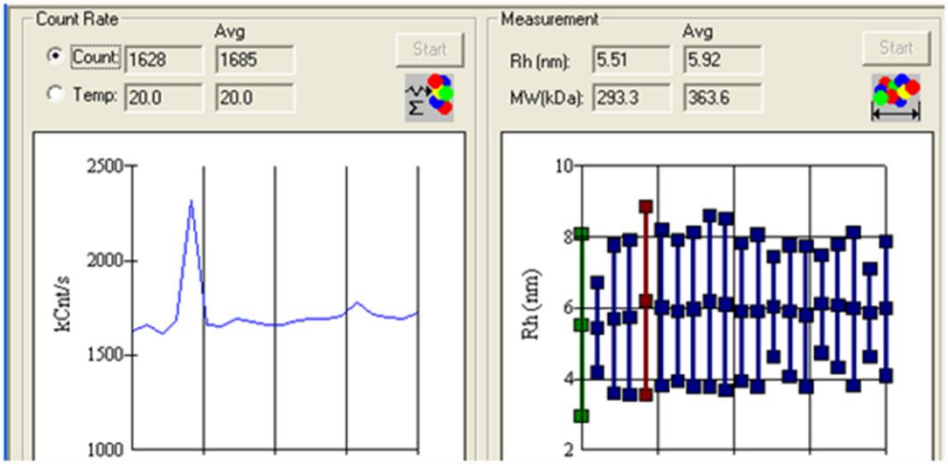

Msr#	Time(s)	Temp(C)	Count Rate	Ampl	Diff Coeff	Radius(nm)	Polyd(nm)	PolydIndx	MW(KDa)	%Mass	Baseline	Sos Error
1*	10.0	20.0	1628766	0.466	388.	5.51	2.56	0.22	293.	100.0	1.086	41.2
2	20.0	20.0	1660062	0.582	394.	5.44	1.26	0.05	281.	100.0	1.000	4.49
3	30.0	20.0	1614406	0.637	377.	5.68	2.09	0.14	320.	100.0	1.000	6.07
4	40.0	20.0	1685246	0.598	374.	5.73	2.18	0.14	329.	100.0	1.002	6.64
5*	50.0	20.0	2321021	0.503	345.	6.21	2.66	0.18	419.	100.0	1.031	7.73
6	60.0	20.0	1657751	0.563	356.	6.00	2.21	0.14	379.	100.0	1.005	5.87
7	70.0	20.0	1650025	0.609	362.	5.92	1.98	0.11	363.	100.0	1.000	4.92
8	80.0	20.0	1691459	0.589	359.	5.96	2.18	0.13	371.	100.0	0.999	5.12
9	90.0	20.0	1678680	0.600	346.	6.18	2.41	0.15	413.	100.0	1.000	8.68
10	100.0	20.0	1657664	0.594	351.	6.10	2.41	0.16	397.	100.0	1.001	7.97
11	110.0	20.0	1659637	0.600	363.	5.89	1.95	0.11	358.	100.0	1.000	3.58
12	120.0	20.0	1682731	0.590	362.	5.92	2.14	0.13	362.	100.0	1.001	4.98
13	130.0	20.0	1691874	0.590	354.	6.04	1.40	0.05	385.	100.0	1.000	5.49
14	140.0	20.0	1694578	0.593	361.	5.92	1.84	0.10	363.	100.0	1.000	3.23
15	150.0	20.0	1710261	0.588	371.	5.77	1.99	0.12	337.	100.0	1.000	4.07
16	160.0	20.0	1779974	0.576	350.	6.11	1.38	0.05	399.	100.0	1.001	11.3
17	170.0	20.0	1711697	0.557	353.	6.07	1.73	0.08	391.	100.0	1.000	4.80
18	180.0	20.0	1696591	0.600	358.	5.97	2.17	0.13	372.	100.0	1.000	4.73
19	190.0	20.0	1694975	0.597	365.	5.86	1.23	0.04	353.	100.0	1.000	3.52
20	200.0	20.0	1725762	0.608	358.	5.97	1.89	0.10	373.	100.0	1.000	3.21
Aves:												
Mono		20.0	1685742	0.593	362.	5.92	1.91	0.11	364.	100.0	1.000	5.48
Bi-1		0.0	0	0.000	0.000	0.000	****	****	0.000	0.0	0.000	0.000

Figure 10: Dynamic Light Scattering (DLS) results for purified cKGA. The Polydispersity index, and SOS error are indicated in red and blue boxes respectively.

2.3.2 Crystallization

The initial crystals obtained from the screen were too small to diffract. However, better diffraction-quality crystals were obtained through the grid screen optimization process

using the crystallization condition of 0.1 M Bis-Tris Propane pH 7.0 and 1.8-2.1 M $LiSO_4$ (Figure 21).

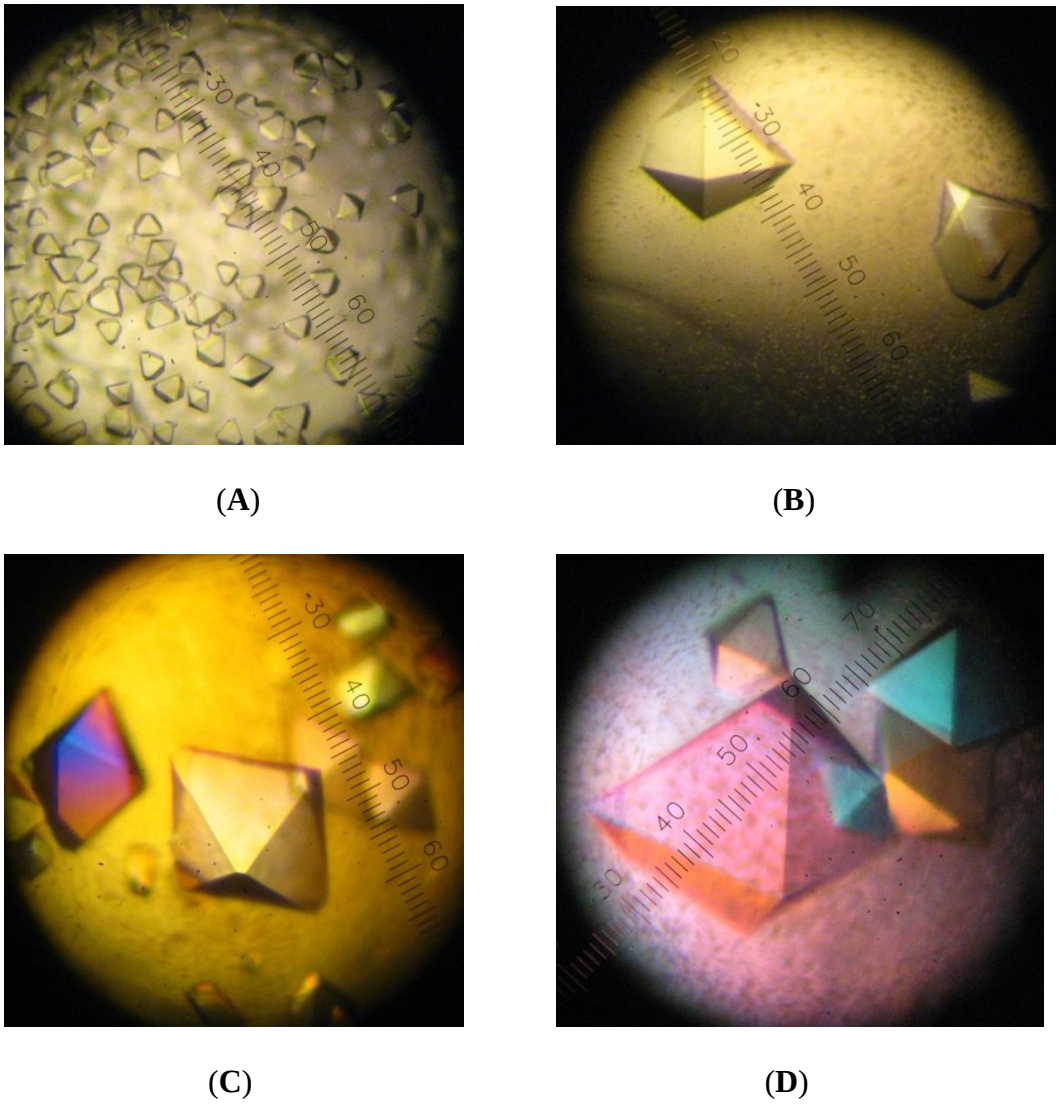

(**A**) (**B**)

(**C**) (**D**)

Figure 11: A representative crystals of cKGA. Crystals were obtained from the hanging drop vapour diffusion method: (A) *apo* cKGA crystal (Small), (B) *apo* cKGA crystal (Large), (C) cKGA -L-glutamine complx, (D) cKGA -BPTES complex.

2.3.3 Data collection, Structure Determination and Refinement

The crystals were cryo-protected with 15% glycerol and the diffraction data were collected at synchrotron beamlines (Figure 22). The *apo* cKGA and all other complexes

crystallized in *I4$_1$22* space group. The structures of the *apo*-cKGA, and other complex structures were determined by molecular replacement method using the program Molrep (Vagin and Teplyakov, 2010) (Table 5).

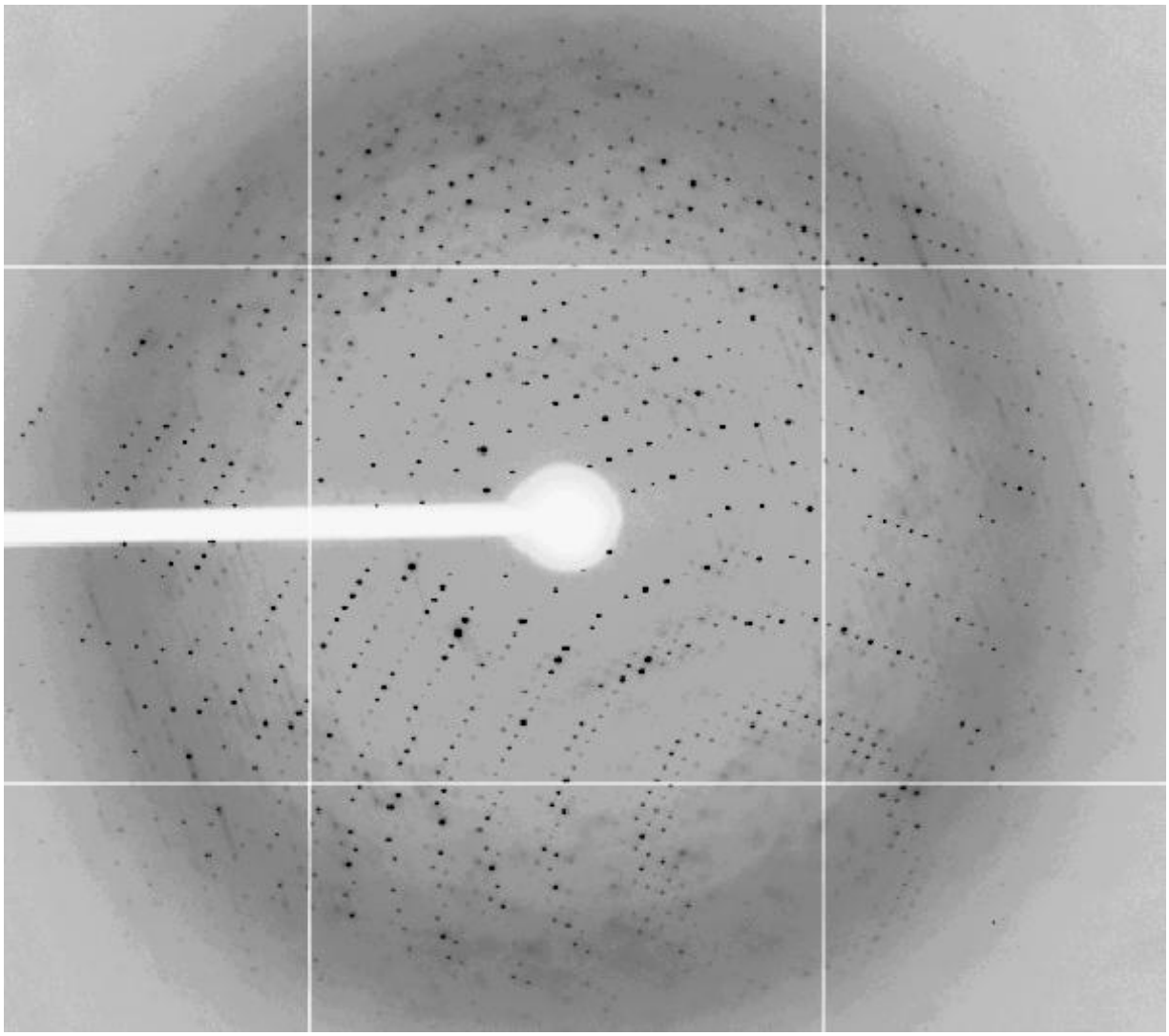

Figure 12: A representative diffraction pattern of *apo* cKGA crystal. The data collected from ADSC Q315 (Area Detector System Corporation) diffractometer system at 13-b1beamline (NSRRC, Taiwan).

Data collection	*apo*-cKGA	cKGA-L-glutamine (substrate)	cKGA-L-glutamate (product)	cKGA–BPTES (inhibitor 1)	cKGA–BPTES-L-glutamate	cKGA–inhibitor 2	cKGA–inhibitor 3	cKGA–inhibitor 4
Space group	$I4_122$	$I4_122$	$I4_122$	$I4_122$	$I4_122$	$I4_122$	$I4_122$	$I4_122$
Cell parameters (Å, °)	a = 139.60	a = 139.74	a = 139.52	a = 139.54	a = 139.64	a = 139.88	a = 139.83	a = 139.56
	b = 139.60	b = 139.74	b = 139.52	b = 139.54	b = 139.64	b = 139.88	b = 139.83	b = 139.56
	c = 156.62	c = 156.64	c = 153.95	c = 156.79	c = 156.47	c = 158.00	c = 158.04	c = 156.87
	α = β = γ = 90	α = β = γ = 90	α = β = γ = 90	α = β = γ = 90	α = β = γ = 90	α = β = γ = 90	α = β = γ = 90	α = β = γ = 90
Resolution range (Å)	50–2.2 (2.28–2.20)	50–2.4 (2.44–2.40)	30–2.4 (2.46–2.40)	50–2.4 (2.49–2.40)	50–2.3 (2.38–2.30)	50–2.7 (2.75–2.70)	50–2.70 (2.75–2.7)	50–2.45 (2.49–2.45)
Wavelength (Å)	1.000	1.000	0.9789	1.000	1.000	1.000	1.000	1.000
Observed *hkl*	326,149	193,140	279,860	394,838	420,212	367,644	338,983	246,002
Unique *hkl*	38,287	30,131	29,652	30,507	34,726	21,862	21,755	28,767
Completeness (%)	97.2 (89.8)	99.0 (98.3)	99.0 (96.7)	99.9 (99.9)	99.9 (100)	100 (99.9)	99.6 (95.9)	99.7 (100)
Overall $I/\sigma I$	17.9	23.1	26.9	19.9	14.6	12.9	9.3	10.6
R_{sym}*	0.054 (0.396)	0.056 (0.278)	0.051 (0.292)	0.058 (0.289)	0.090 (0.432)	0.063 (0.293)	0.072 (0.331)	0.067 (0.365)
Refinement and quality of the model								
Resolution range (Å)†	20.0–2.20	30.0–2.40	29.0–2.40	30.0–2.40	20.0–2.30	20.0–2.70	30.0–2.70	30.0–2.45
R_{work} (%, no. reflections)‡	20.03 (32,444)	20.76 (26,408)	18.85 (27,871)	20.87 (24,159)	20.51 (29,273)	20.74 (18,747)	19.53 (18,670)	19.75 (22,751)
R_{free} (%, no. reflections)§	22.17 (2,092)	22.62 (1,674)	21.00 (1,780)	23.85 (1,799)	23.20 (1,862)	23.31 (2,067)	21.51 (2,075)	21.62 (1,979)
Bond length (Å)¶	0.008	0.008	0.014	0.008	0.014	0.010	0.008	0.006
Bond angle (°)¶	1.29	1.29	1.41	1.33	1.57	1.44	1.42	1.26
Ramachandran plot (%)								
Favored region	86.3	82.5	90.8	87.3	88.1	84.5	84.2	86.0
Allowed region	12.2	16.7	8.4	11.6	10.8	14.7	15.1	12.5
Generously allowed Region	1.5	0.8	0.8	0.7	1.1	0.8	0.8	1.5
Disallowed region	0	0	0	0.4	0	0	0	0
Average B-factors (Å^2)‖								
Main chain atoms	48.09	60.49	46.07	33.66	39.56	53.70	49.44	49.47
Side chain atoms	50.97	63.40	47.80	36.08	42.56	55.74	51.36	51.53
Overall protein atoms (no. atoms)	49.48 (2,428)	61.89 (2,382)	46.90 (2,358)	34.83 (2,412)	41.01 (2,412)	54.67 (2,386)	50.36 (2,386)	50.46 (2,395)
Waters	50.61 (107)	63.18 (85)	51.38 (83)	40.88 (147)	43.07 (103)	49.29 (59)	45.40 (64)	50.52 (87)
Ligand(s) (no. atoms)	—	64.54 (10)	47.29 (10)	39.39 (18)	44.14 (18) 53.94 (10)	66.04 (9)	67.01 (9)	72.21 (8)

*$R_{sym} = |I_i - \langle I \rangle| / |I_i|$ where I_i is the intensity of the i^{th} measurement, and $\langle I \rangle$ is the mean intensity for that reflection.
†Reflections greater than $I > \sigma I$ where used in the refinement.
‡$R_{work} = |F_{obs} - F_{calc}| / |F_{obs}|$ where F_{calc} and F_{obs} are the calculated and observed structure factor amplitudes, respectively.
§R_{free} = as for R_{work}, but for 6–10% of the total reflections chosen at random and omitted from refinement.
¶rmsd from ideal.
‖Individual B-factor refinement were carried out.

Table 5: Crystallographic data and refinement statistics

2.3.4 Structures of cKGA and Its Complexes with L-Glutamine and L-Glutamate

The human KGA consists of 669 amino acids. We refer to Ile221-Leu533 as the catalytic domain of KGA (cKGA) (Figure 23A). The crystal structures of the *apo* cKGA and in complex with L glutamine or L-glutamate were determined (Figure 23B and Figure 24).

A

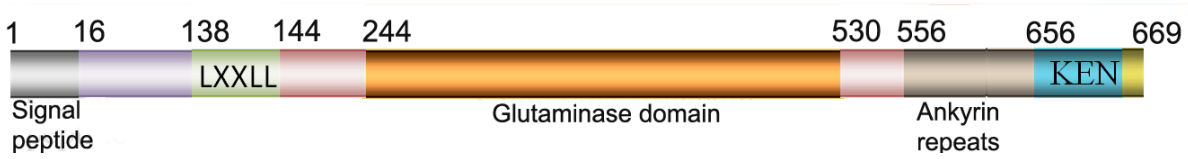

B

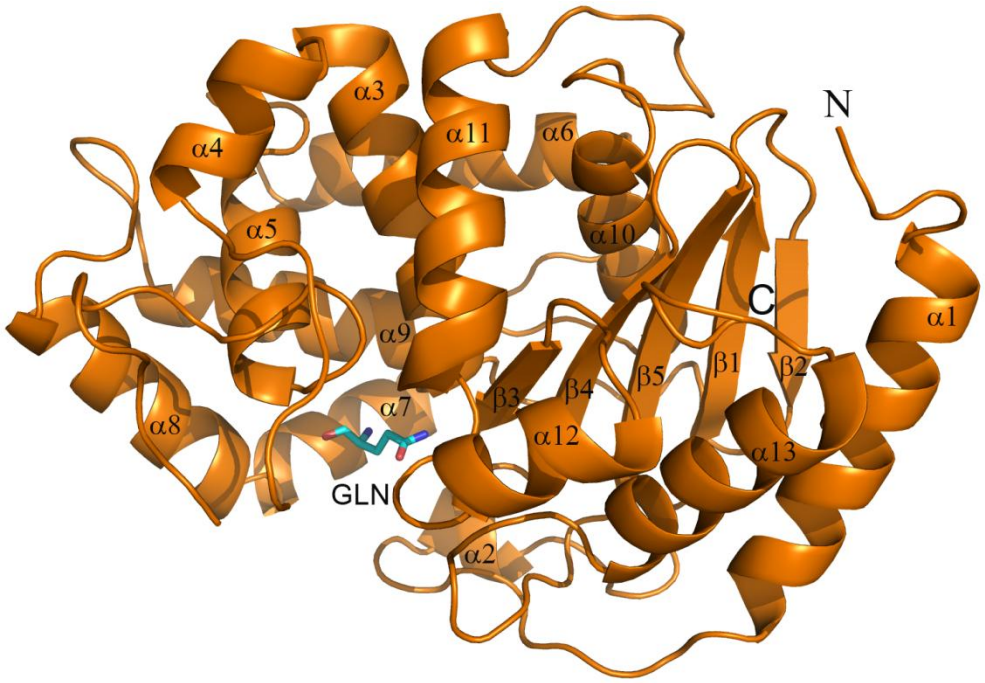

Figure 13: Schematic view and structure of the cKGA-L-glutamine complex. (**A**) Human KGA domains and signature motifs (refer to introduction 1.5.2 for details). (**B**) Structure of the of cKGA and bound substrate (L-glutamine) is shown as a cyan stick. The N- and C- termini and the secondary structures such as α-helices and β-sheets are labeled. This figure and the following figures of this chapter are prepared by PyMol (DeLano, 2002).

The structure of cKGA has two domains with the active site located at the interface. Domain I comprises (Ile221-Pro281 and Cys424 -Leu533) of a five-stranded anti-parallel β-sheet (β2↓β1↑β5↓β4↑β3↓) surrounded by six α-helices and several loops. The domain II (Phe282-Thr423) mainly consists of seven α-helices (Figure 25A).

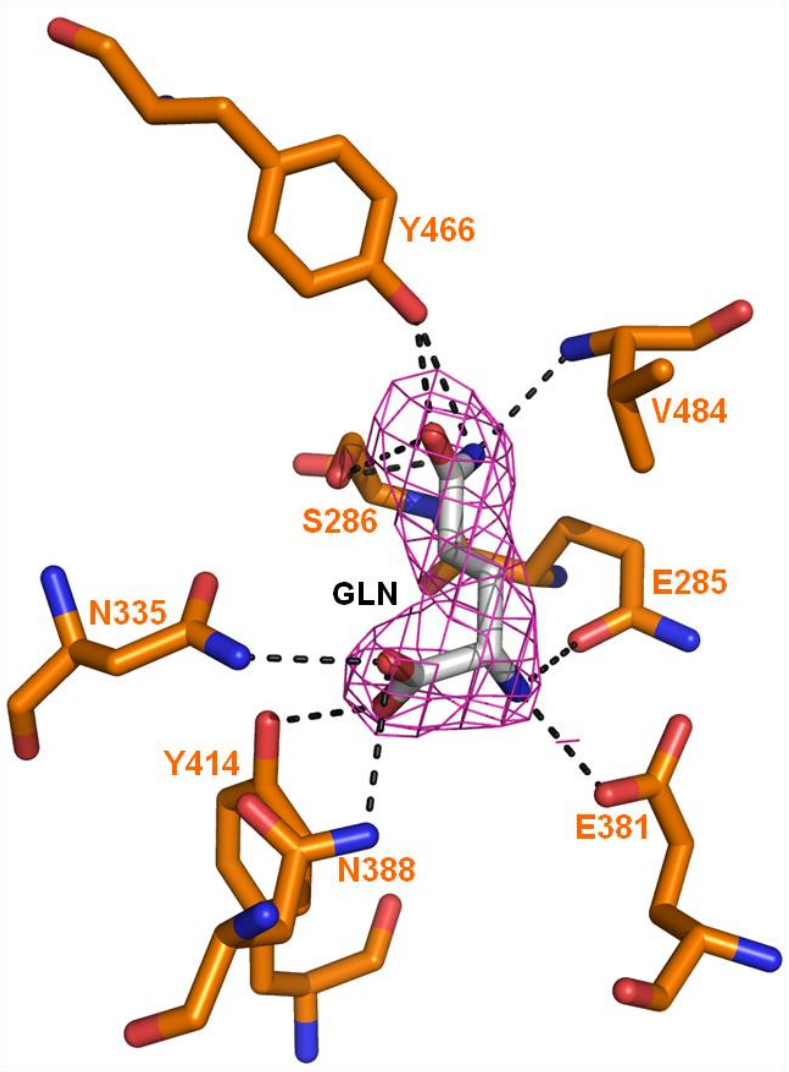

Figure 14: Interactions of cKGA with L-Glutamine. Final *2Fo- Fc* electron density map in the active-site region of cKGA, map contoured at a level of 1 σ. L-Glutamine is shown as a cyan stick that makes hydrogen bond interactions with active site residues (orange).

L-Glutamine/L-glutamate is bound in the active site cleft (Figure 25B). Overall the active site is highly basic, and the bound ligand makes several hydrogen-bonding contacts to Gln285, Ser286, Asn335, Glu381, Asn388, Tyr414, Tyr466, and Val484, and these residues are highly conserved among KGA homologs (Figure 26).

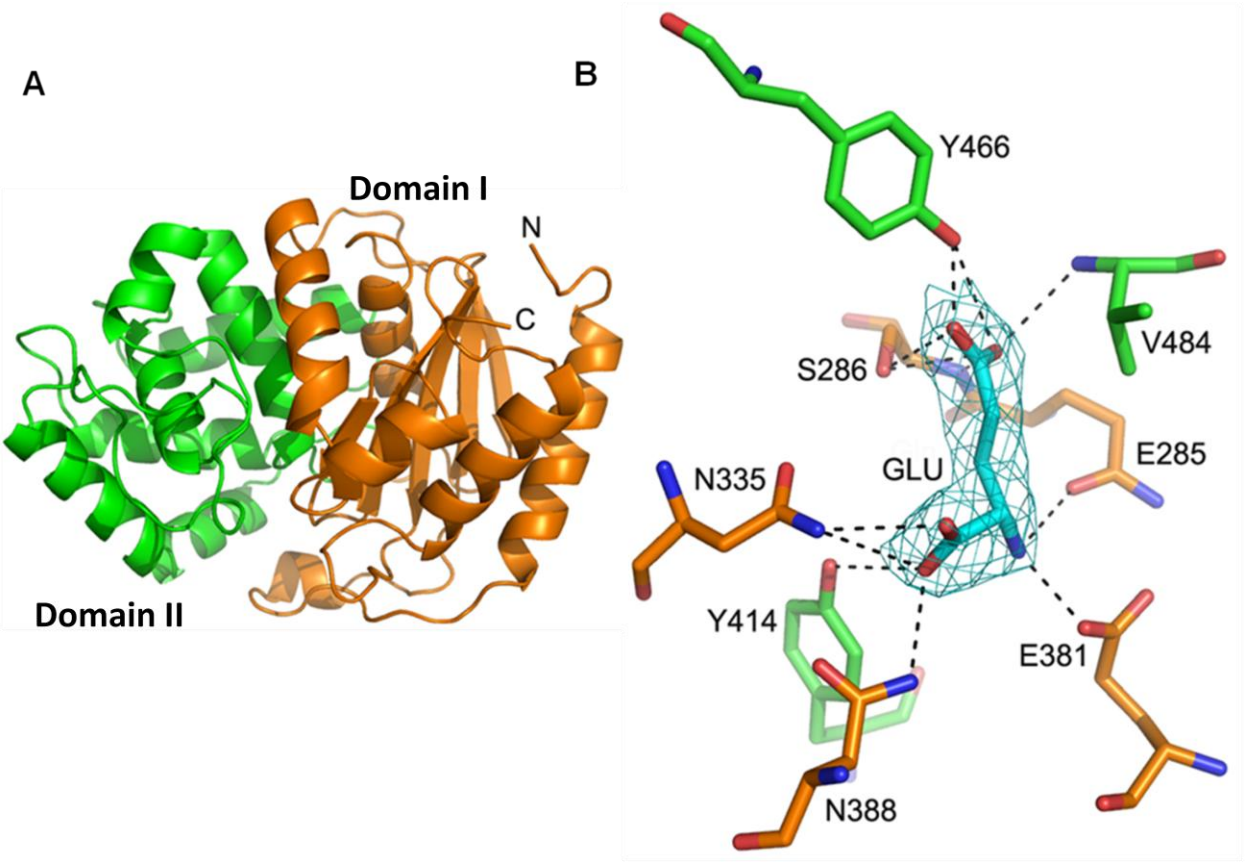

Figure 15: Structure of cKGA and its complex with L-Glutamate. **(A**) Cartoon representation of the apo cKGA structure. Domain I (amino acids 221–281 and 424–533) is shown in orange; domain II (amino acids 282–423) in green. The active site cleft is located between the interfaces of the domains. (**B**) Final *2Fo- Fc* electron density map in the active-site region of cKGA, map contoured at a level of 1 σ. L-Glutamate is shown as a cyan stick that makes hydrogen bond interactions with active site residues.

Notably, the putative serine-lysine catalytic dyad (286-SCVK-289), corresponding to the SXXK motif of class D β-lactamase (Brown et al., 2008), is located in close proximity to the bound ligand. In the *apo* structure, two water molecules were located in the active site, one of them being displaced by glutamine in the substrate complex. The substrate side chain is within hydrogen-bonding distance (2.9 Å) to the active site Ser286. Other key residues involved in catalysis, such as Lys289, Tyr414, and Tyr466, are in the vicinity of the active site. Lys289 is within hydrogen-bonding distance to Ser286 (3.1 Å) and acts as a general base for the nucleophilic attack by accepting the proton from Ser286. Tyr466, which is close to Ser286 and in hydrogen bonding contact (3.2 Å) with glutamine, is involved in proton transfer during catalysis. Moreover, the carbonyl oxygen of the glutamine is hydrogen-bonded with the main chain amino groups of Ser286 and Val484, forming the oxyanion hole. Thus, we propose that in addition to the putative catalytic dyad (Ser286 XX Lys289), Tyr466 could play an important role in the catalysis (Figure 26 and Figure 27).

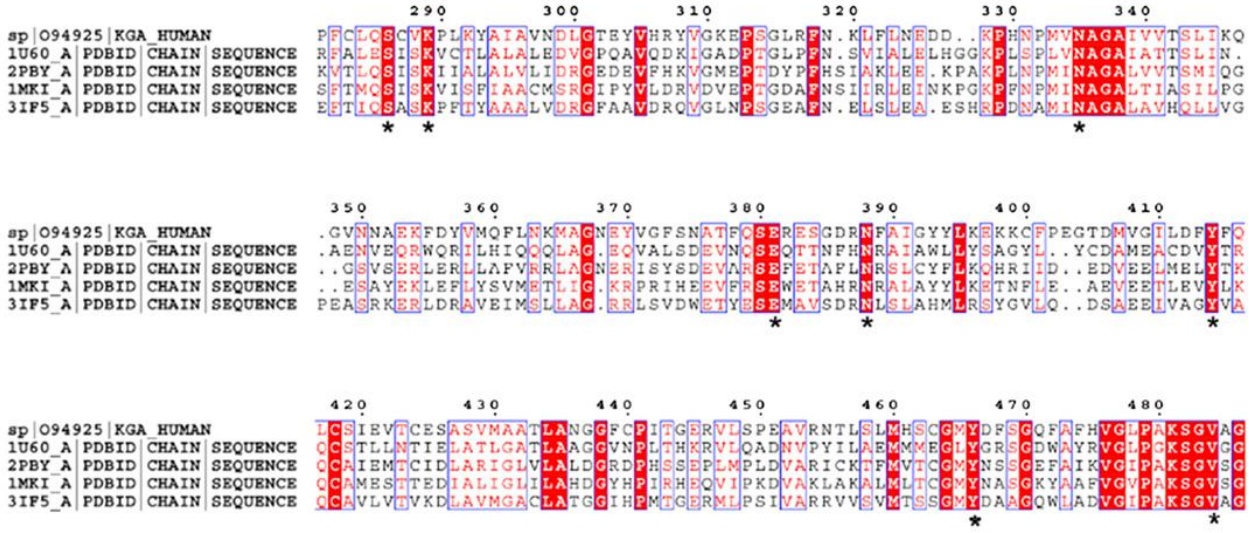

Figure 16: Sequence alignment of cKGA homologs. The amino acids are in one-letter codes, and the conserved residues are in red. Strictly conserved residues are highlighted in red (identity <36%). Numbering is shown for the KGA sequence. The key conserved catalytic residues of cKGA are shown with asterisks. This figure was prepared using the program Espript2.2 (Gouet et al., 1999). The compared cKAG homologs are E. coli YbaS (PDB code IU60), Geobacillus kaustophilus (PDB code 2PBY), Bacillus subtilis (PDB code 1MKI), and M. luteus (PDB code 3IF5).

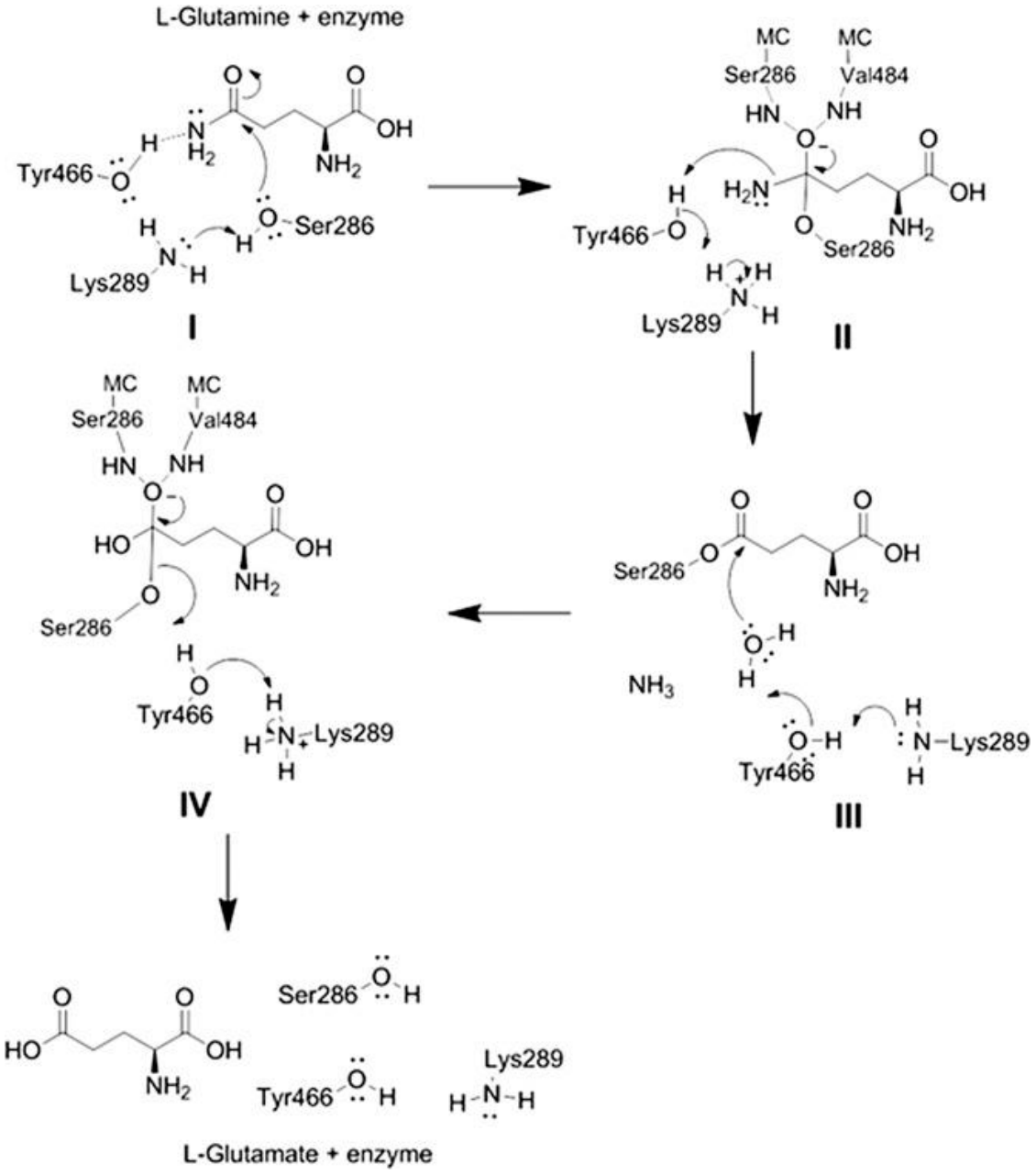

Figure 17: Proposed catalytic mechanism of KGA. The reaction mechanism proceeds with the following steps. (i) Formation of tetrahedral intermediate by nucleophilic attack of Ser286 on glutamine, which is assisted by Lys289. (ii) Breakdown of tetrahedral intermediate to form ammonia and the enzyme intermediate. (iii) Nucleophilic attack of water on the enzyme intermediate aided by Lys289 and Try466. (iv) Formation of glutamate and free enzyme.

2.3.5 Allosteric Binding Pocket for BPTES

The crystal structure of cKGA: BPTES complex shows that BPTES occupies a previously unsuspected allosteric pocket, in the solvent-exposed region at the dimer interface of cKGA, located ≈18 Å away from the active site serine (Ser286). The chemical structure of BPTES has an internal symmetry, with two exactly equivalent parts including a thiadiazole, amide, and a phenyl group and it equally interacts with each monomer (Figure 28 and 29).

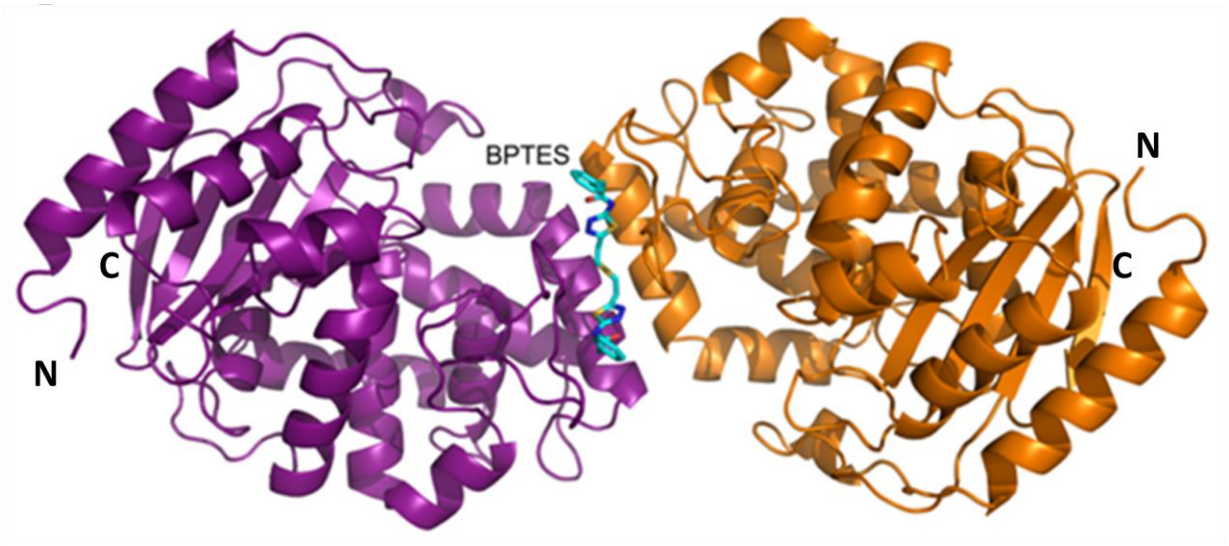

Figure 18: Structure of cKGA: BPTES complex. The cKGA homodimer figure is shown in ribbon representation. The monomer A and monomer B are shown in purple and orange color, respectively, and BPTES is shown as a cyan stick representation.

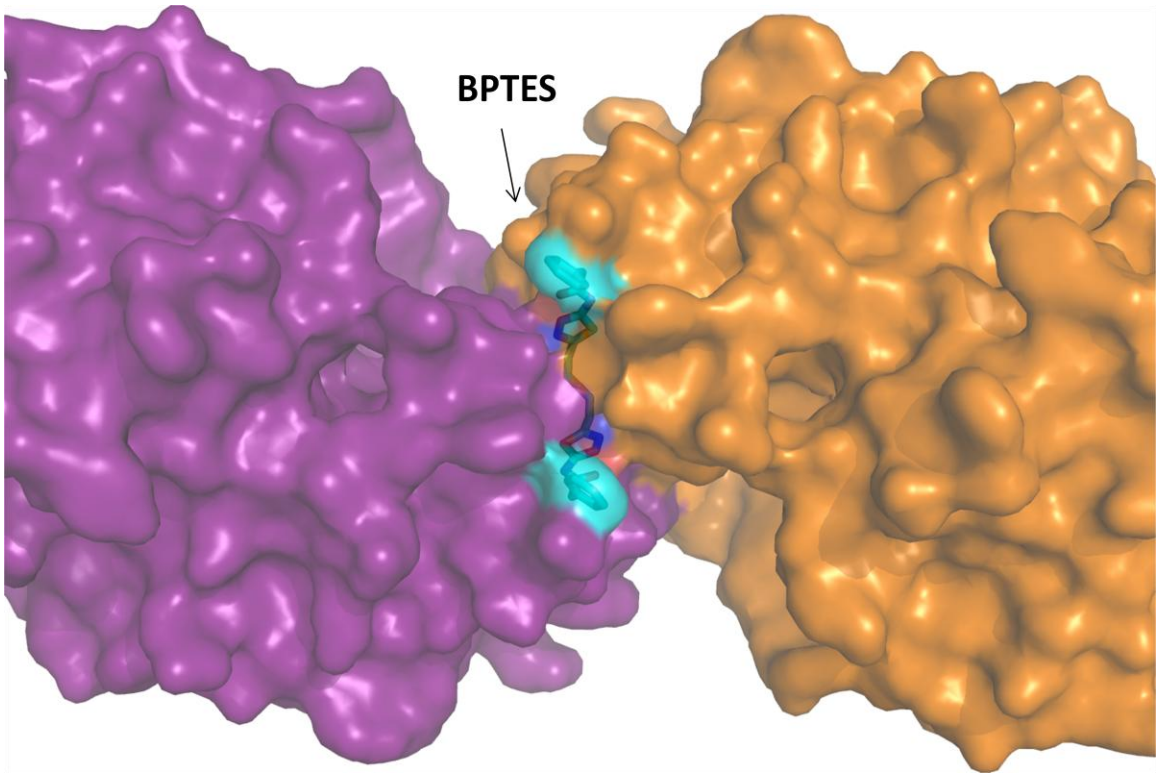

Figure 19: Binding pocket for BPTES. A surface representation of the inhibitor binding pocket of BPTES; one molecule of BPTES wedged at the interface of two cKGA monomers. BPTES is shown as a stick in the transparent view of the surface of cKGA.

The thiadiazole group and the aliphatic linker are well buried in a hydrophobic cluster that consists of Leu321, Phe322, Leu323, and Tyr394 from both monomers, which forms the allosteric pocket (Figure 30A and 30B). The side chain of Phe322 is found at the bottom of the allosteric pocket. The phenylacetamido moiety of BPTES is partially exposed on the loop (Asn324-Glu325), where it interacts with Phe318, Asn324, and the aliphatic part of the Glu325 side chain. The side chain of Tyr394, backbone amide of the Phe322 and Leu323, makes hydrogen-bonding contacts to inhibitors. Moreover, the residues Leu321 and Phe322 flipped out ≈180° to enhance the hydrophobic interactions

with the inhibitors (Figure 31). Thus, the conformational changes are required to form the allosteric pocket.

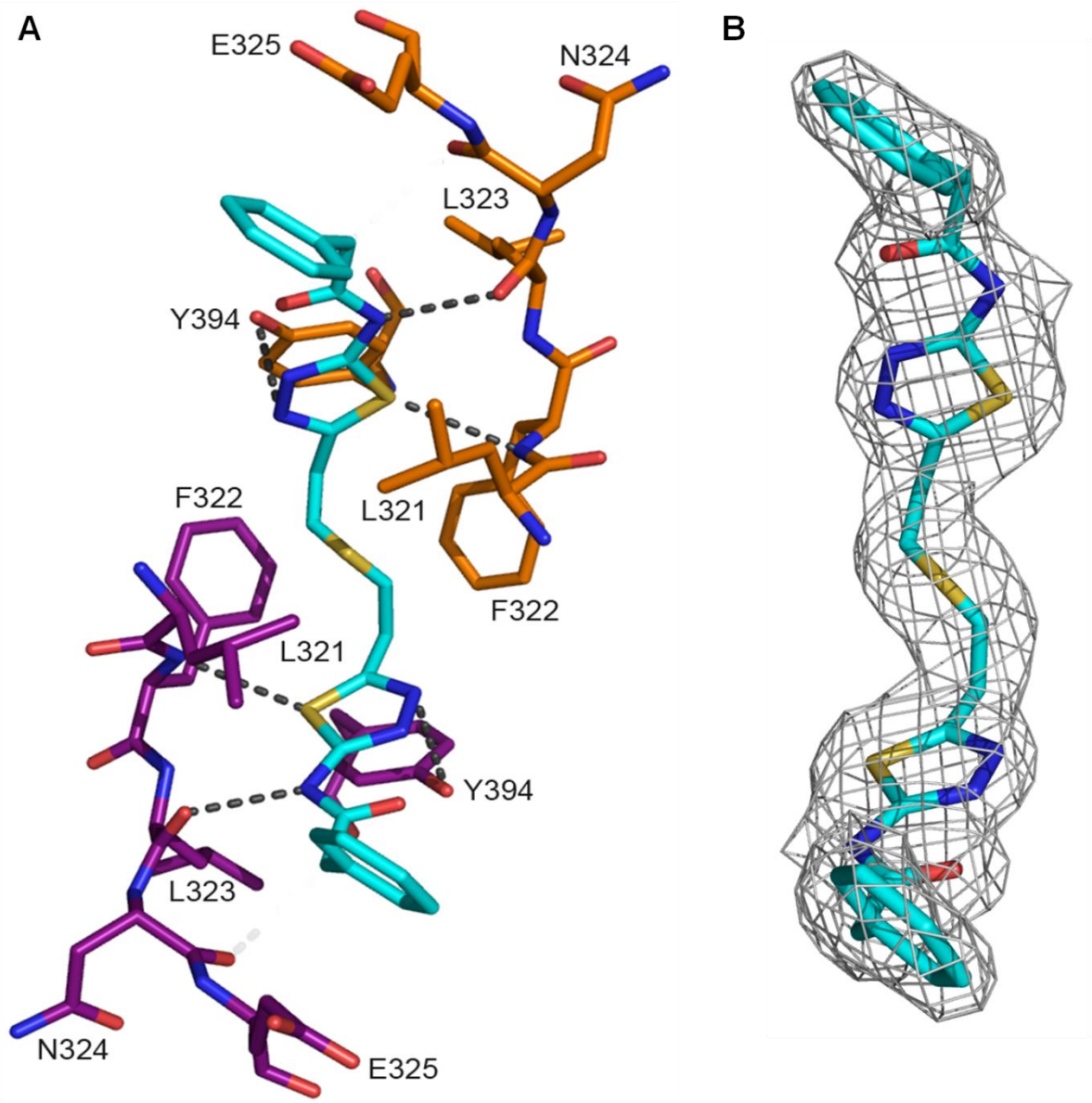

Figure 20: A close-up view of the interactions of BPTES in the cKGA allosteric inhibitor binding pocket. (**A**) The residues that interact with BPTES from each monomer are labeled and shown in different colors consistent with Figure 28. (**B**) Electron density map (*2Fo – Fc* map contoured at 1.0 σ) for BPTES (cyan sticks) is shown in grey mesh.

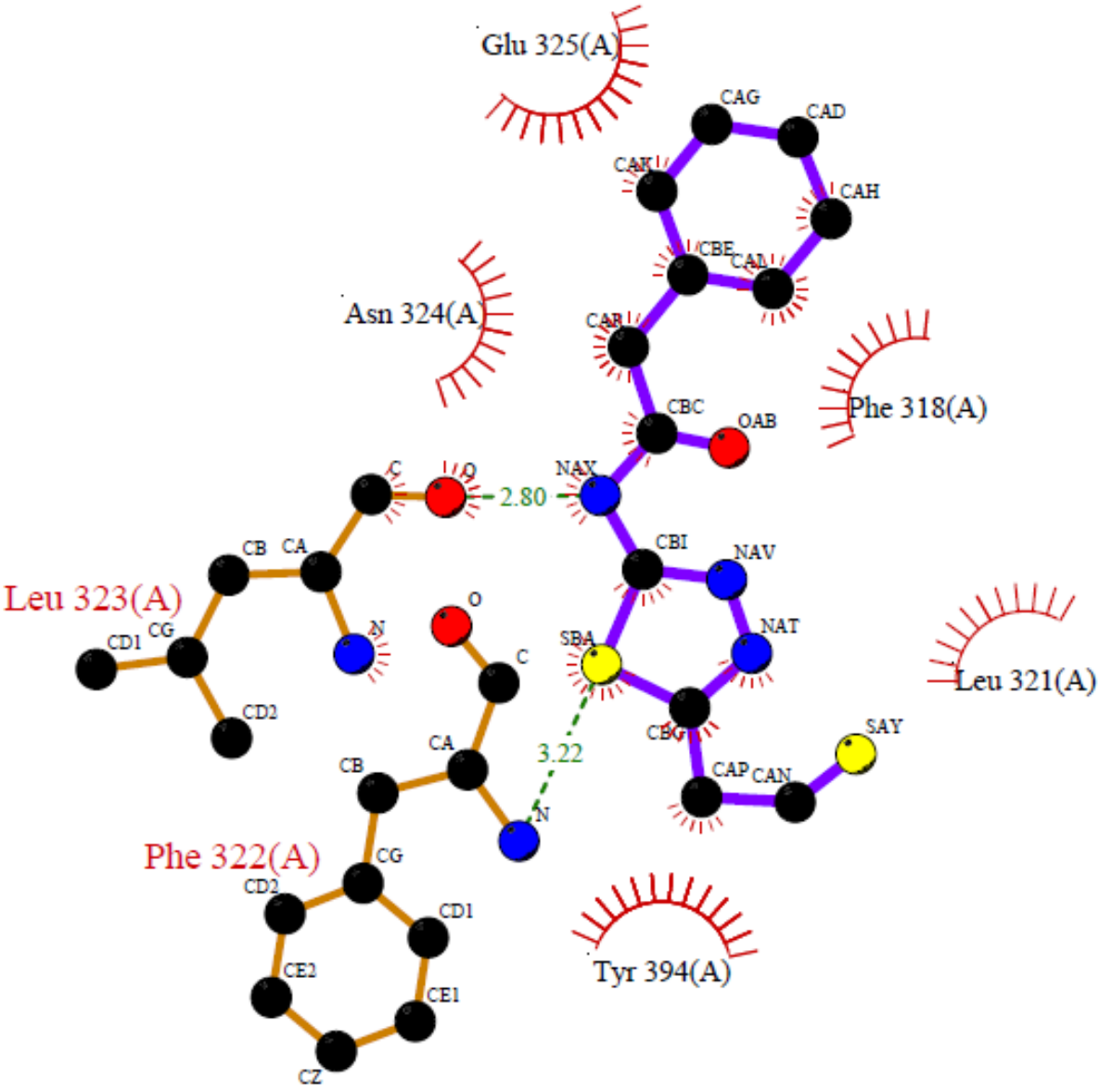

Figure 21: A schematic view of cKGA monomer interactions with BPTES. For clarity, only half of the BPTES inhibitor that interacts with a monomeric cKGA and the interaction residues are shown. The Figure was prepared using LIGPLOT (Wallace et al., 1995).

2.3.6 Inhibitor Optimization of KGA

The crystal structure of catalytic domain of KGA (cKGA) in complex with BPTES (Figure 28) shows that one molecule of BPTES is wedged between two cKGA monomers, forming equivalent interactions with each of them. Each of the terminal phenylacetamino groups forms fewer interactions with cKGA than the rest of the inhibitor. These observations led us to further optimize its inhibitory properties, and initially three inhibitors were synthesized (inhibitors **2**, **3**, and **4**) (Figure 32A). Inhibitors **2**, **3**, and **4** inhibited cKGA with IC_{50} values of 8 μM, 11 μM, and 19 μM, respectively (Figure 32B). However, BPTES (inhibitor **1**) inhibits cKGA with an IC_{50} of 0.16 μM. This clearly indicated the important role of the phenylacetamido group, the length and the hydrophobic groups of the linker in cKGA inhibition. To further understand the binding mode of these inhibitors, the complex structures of inhibitors **2**, **3**, and **4** bound to cKGA were determined (Table 5 and Figure 33 and 34). Similar to BPTES, compounds **2**–**4** all resides within the hydrophobic cluster of the allosteric pocket and also the side chain of Tyr394, backbone amide of the Phe322 and Leu323, makes hydrogen-bonding contacts to inhibitors. With these complex crystal structures along with BPTES complex, we observed that the inhibitor binding pocket might accommodate larger hydrophobic groups and result in synthesizing inhibitor **5** with three methoxy substitutions on both side phenyl rings (Figure 32A and Figure 32B). Inhibitor **5** shows an IC_{50} of 5 μM. This demonstrated that adding more hydrophobic groups did not enhance the efficiency of BPTES.

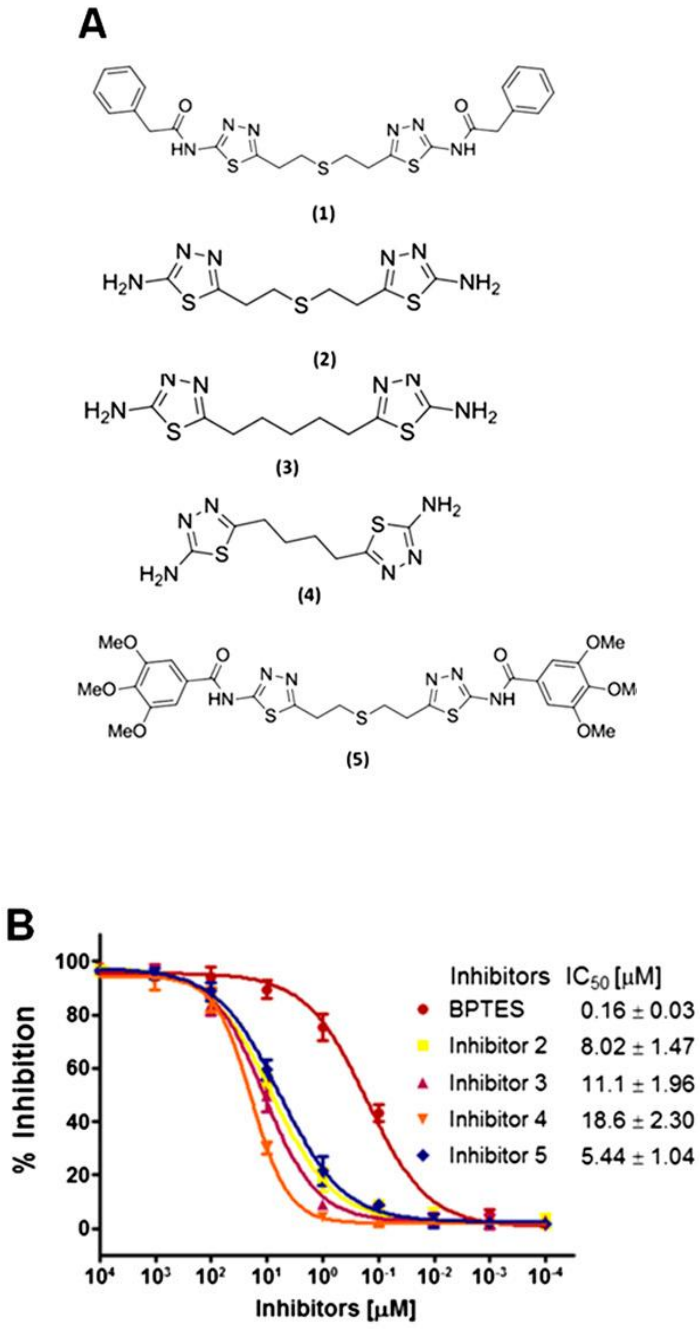

Figure 22: Enzymatic and structural details of BPTES and its derived inhibitors. (**A**) Chemical structure of BPTES (inhibitor 1) and its derivatives. (**B**) IC_{50} determination for synthesized inhibitors with cKGA. The IC_{50} values were determined from a plot of percentage inhibition against various inhibitors concentration. Each value represents the means ± SD of three independent experiments, each with at least three replicates. This figure was prepared using Graphpad prism.

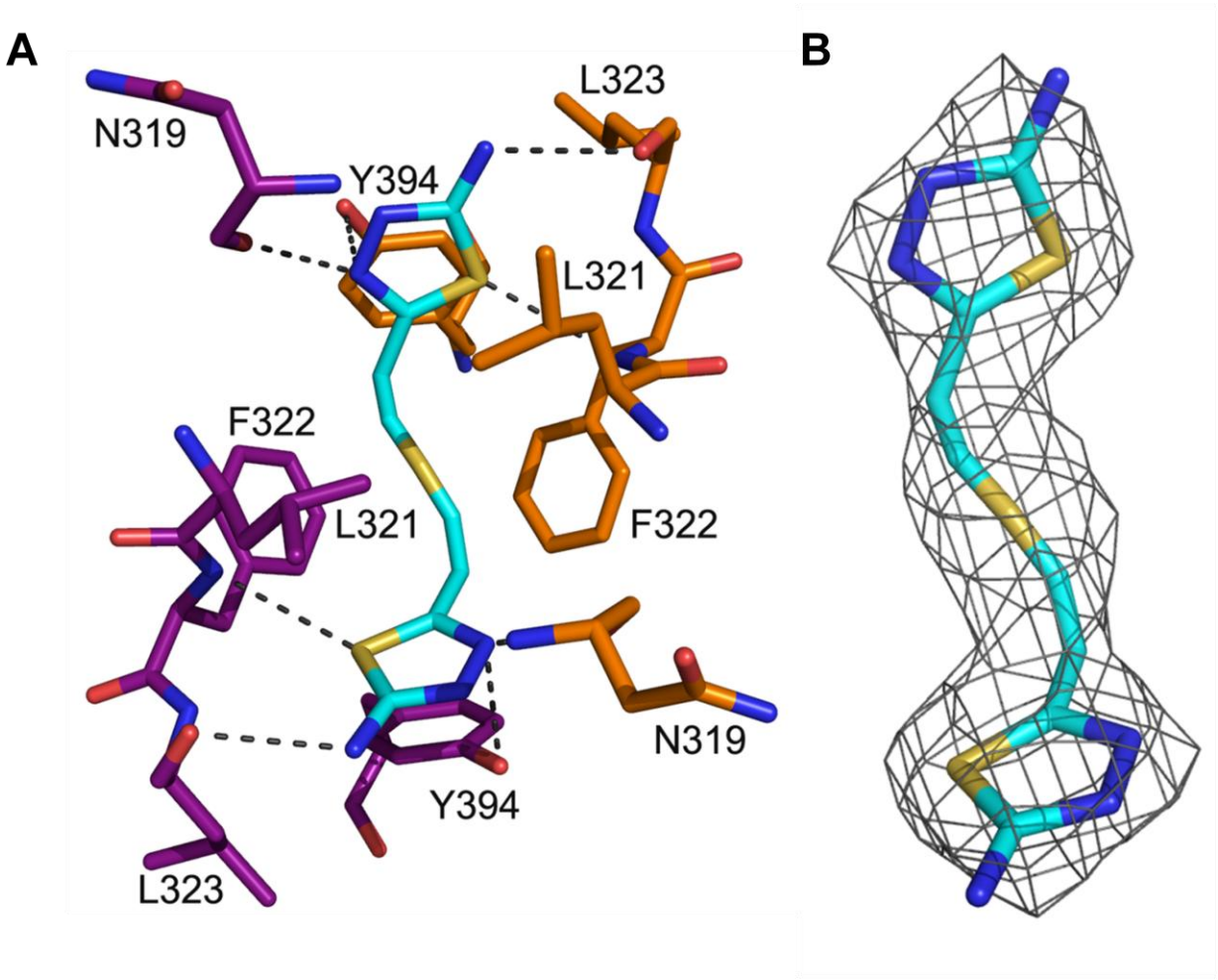

Figure 23: Details of the interactions of inhibitor 2 in the cKGA inhibitor binding pocket. (**A**) The residues that interact with inhibitor 2 from each monomer are labeled. (**B**) Electron density map (*2Fo – Fc* map contoured at 1.0σ) for inhibitor 2 (cyan stick) is shown in grey mesh.

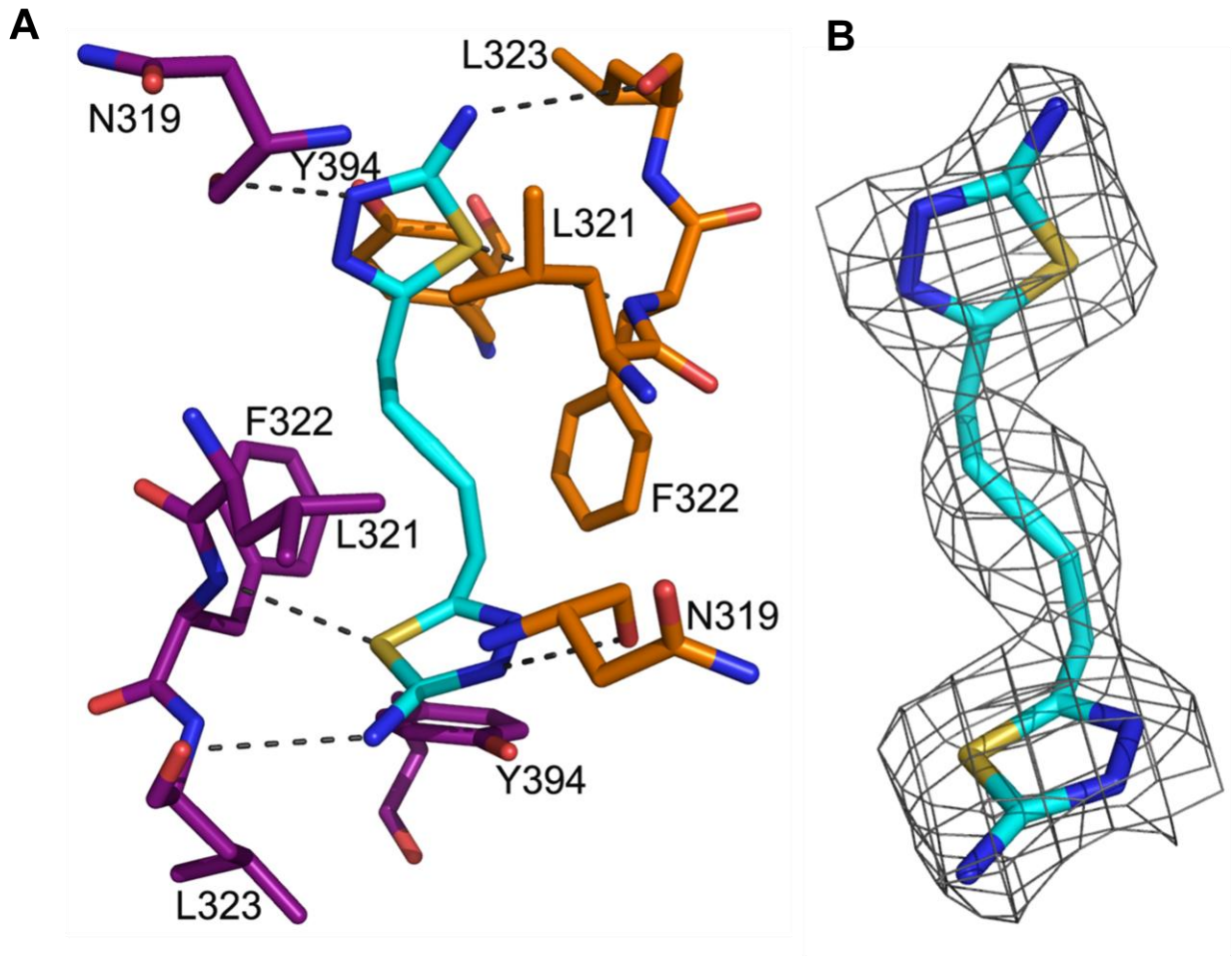

Figure 24: Details of the interactions of inhibitor 3 in the cKGA inhibitor binding pocket. (A) The residues that interact with inhibitor 3 from each monomer are labeled. (B) Electron density map (*2Fo – Fc* map contoured at 1.0 σ) for inhibitor 3 (cyan stick) is shown in grey mesh.

Although inhibitors **2-5** showed moderate inhibition compared with BPTES, their structural details reveal the key determinants for the high potency and selectivity of the inhibitors, and guide the design of next-generation inhibitors. Taken together, we propose that the binding specificity of BPTES is dictated by the thiadiazole, amide, and the

hydrophobic linker regions, whereas the potency is primarily determined by the presence of phenyl rings at both ends. Thus, BPTES was subsequently used to further delineate the structural, functional, and regulation aspects of KGA.

2.3.7 Allosteric Binding of BPTES Triggers Major Conformational Change in the Key Loop Near the Active Site

The overall structure of these inhibitor complexes superimposes well with *apo* cKGA. However, a major conformational change at the Glu312 to Pro329 loop was observed in the BPTES complex (Figure 35). The most conformational changes of the backbone atoms that moved away from the active site region are found at the center of the loop (Leu316- Lys320). The backbone of the residues Phe318 and Asn319 is moved ≈9 Å and ≈7 Å, respectively, compared with the apo structure, whereas the side chain of these residues moved ≈14 Å and ≈12 Å, respectively. This loop rearrangement in turn brings Phe318 closer to the phenyl group of the inhibitor and forms the inhibitor binding pocket, whereas in the *apo* structure the same loop region (Leu316-Lys320) was found to be adjacent to the active site and forms a closed conformation of the active site. Specifically, in *apo* structure Phe318 makes hydrophobic interactions with Tyr466, and side chain of the Asn319 makes hydrogen- bonding contact with backbone of the Asn335 (≈2.8 Å). Notably, the residues Tyr466 and Asn335 are involved in binding to L-glutamine and catalysis. These observations suggest that binding of BPTES induces conformational changes of the key residues of the loop (Glu312-Pro329) to stabilize an open and inactive conformation of the catalytic site. Figure 36A and B show the electrostatic surface potential of the open and closed conformation of active site.

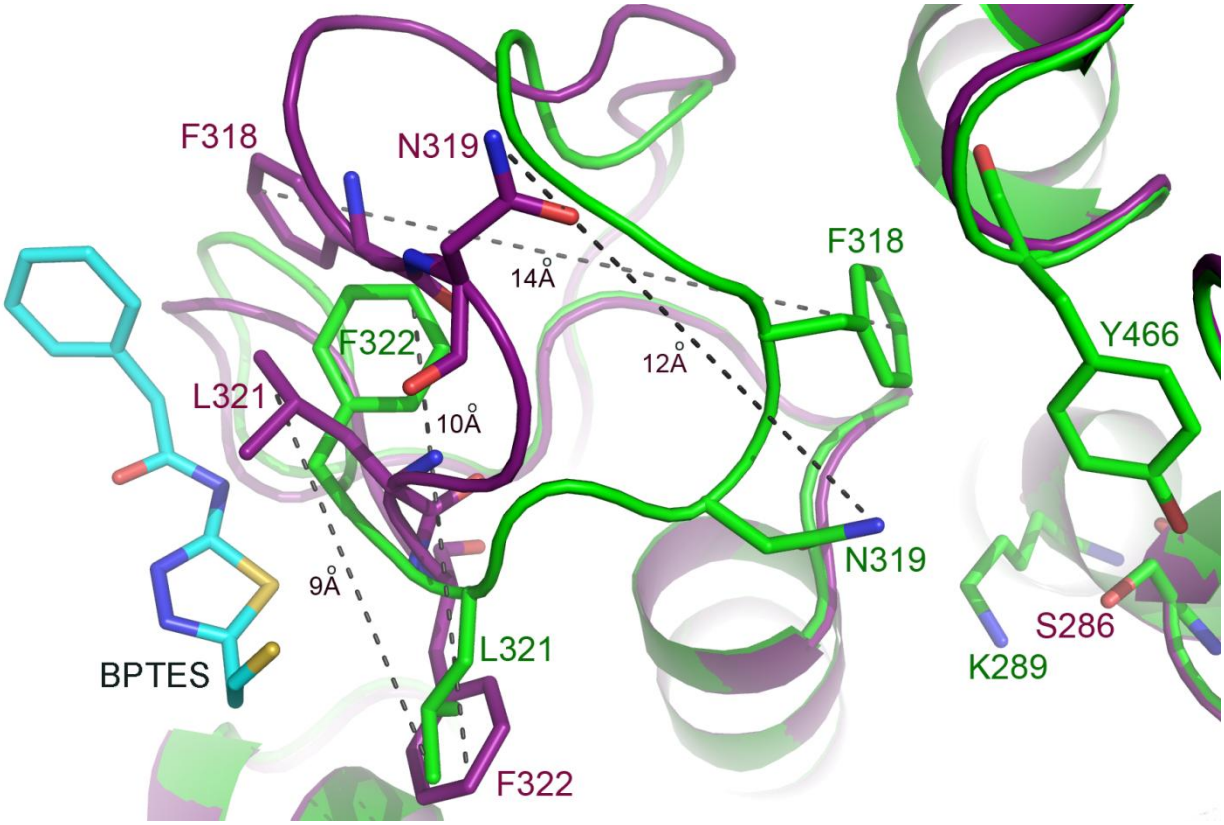

Figure 25: Conformational changes on cKGA induced by binding of the BPTES. Structure superposition of monomeric BPTES complex (magenta) and *apo* cKGA (green), showing conformational changes of key residues on the loop Glu312-Pro329. BPTES binding site and active site residues are labeled. The BPTES binding site is located ~18 Å away from the active site (Ser286) region. For clarity, only half of the BPTES inhibitor that interacts with a monomeric cKGA and the relevant conformational changes are shown.

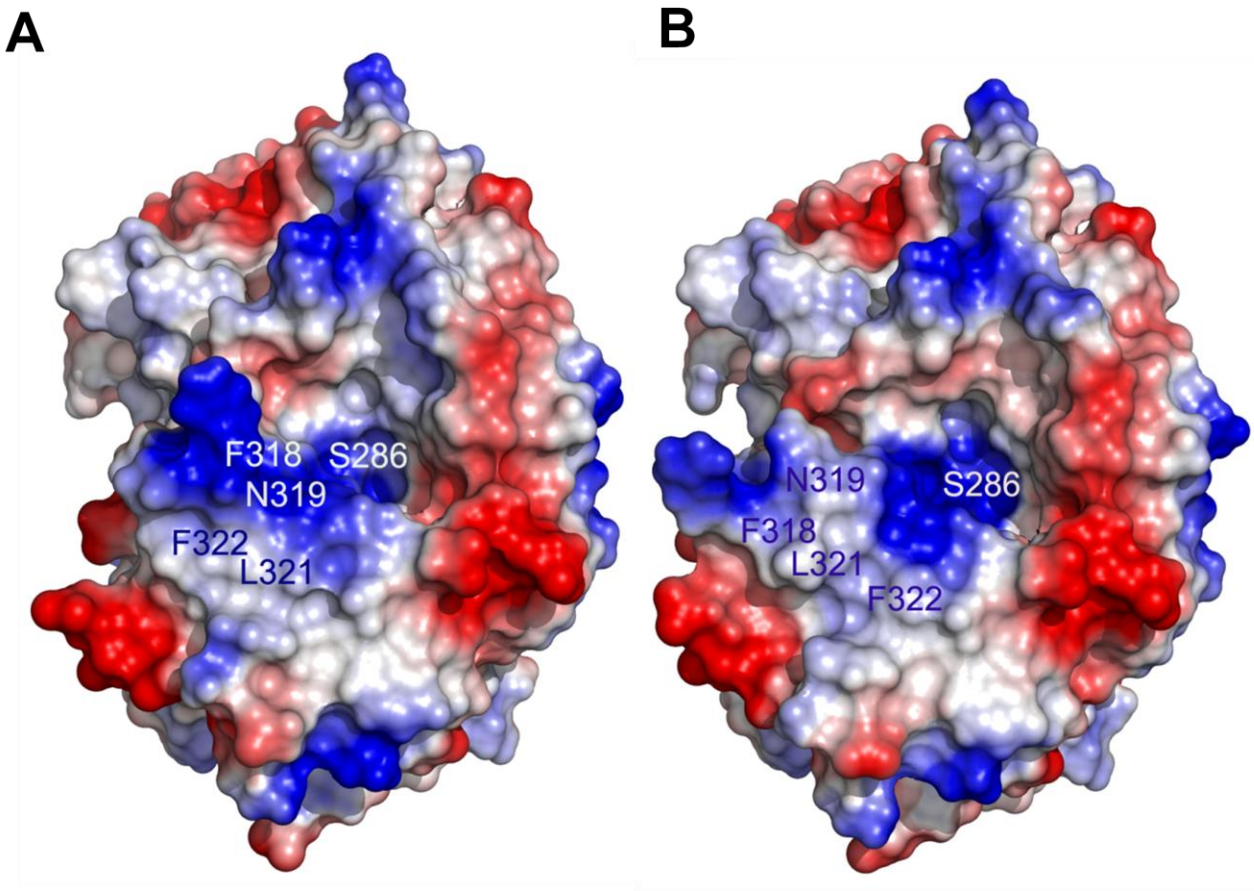

Figure 26: Electrostatic surface representation for *apo* cKGA and cKGA: BPTES complex. (**A**) Electrostatic surface potential of the *apo* cKGA monomer. Active site (Ser286) and BPTES binding site residues were labeled. The active site region is in the closed conformation. Blue indicates the positive charge, and red indicates negative charge. The position of key residues of the loop Glu312-Pro329 is labeled. (**B**) Electrostatic surface potential of the BPTES: cKGA monomer. Same residues as described in A are shown here. The active site is in the open conformation with the residues Phe318 and Asn319 are moved away. The position of the key residues is labeled. A and B show the difference in the electrostatic surface potential and molecular surface between the *apo* cKGA and BPTES complex.

Besides, we have determined the cKGA-glutamate-BPTES structure and revealed similar conformational changes, suggesting that BPTES can stabilize an inactive glutamate-bound form of the enzyme (Figure 37). This result is consistent with previous kinetics studies showing that BPTES, which is an uncompetitive inhibitor, can inhibit both the enzyme–substrate or enzyme–product complex (Robinson et al., 2007).

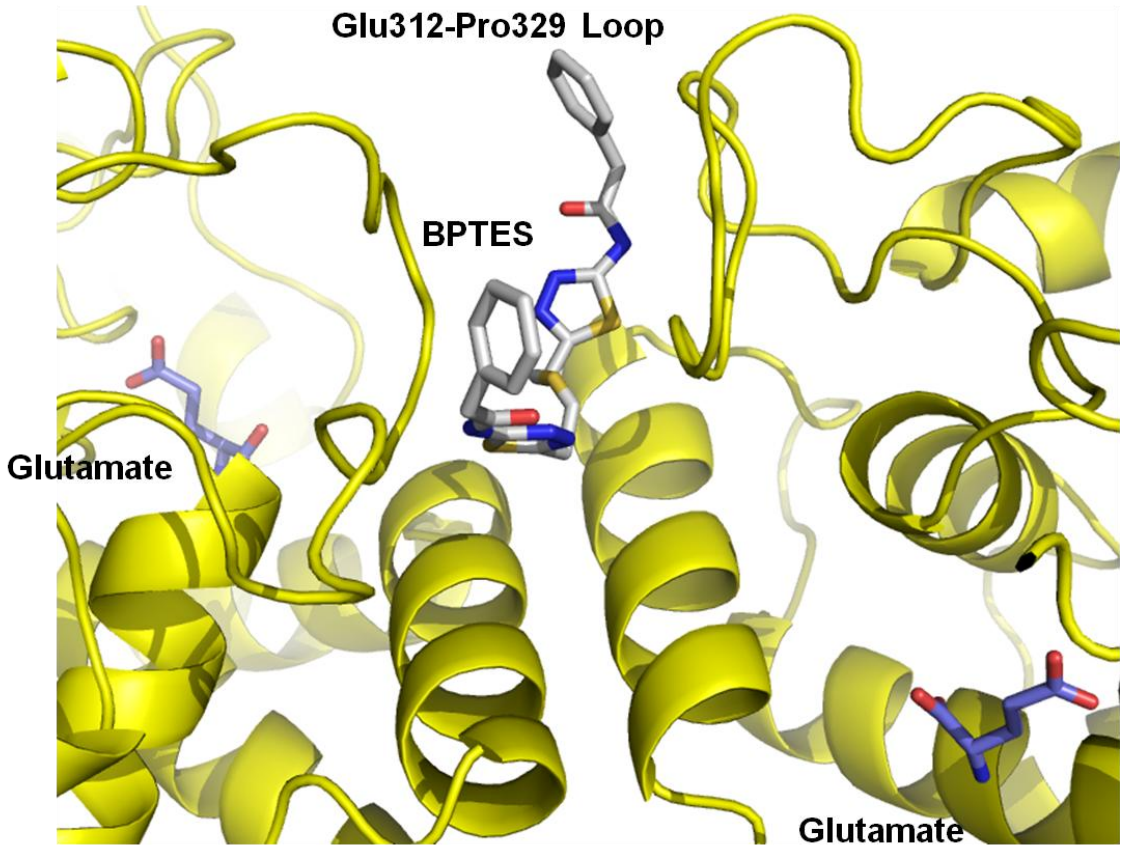

Figure 27: Structure of cKGA-glutamate-BPTES complex. The BPTES molecule, shown as a cyan stick, is located at the dimer interface and its interacting loops (Glu312-Pro329) from each monomer. The glutamate molecules are shown as magenta stick in the active site of each monomer.

2.3.8 Binding of BPTES Stabilizes the Inactive Tetramers of cKGA

To understand the role of oligomerization in KGA function, dimers and tetramers of cKGA were generated using the symmetry-related monomers (Figure 38).

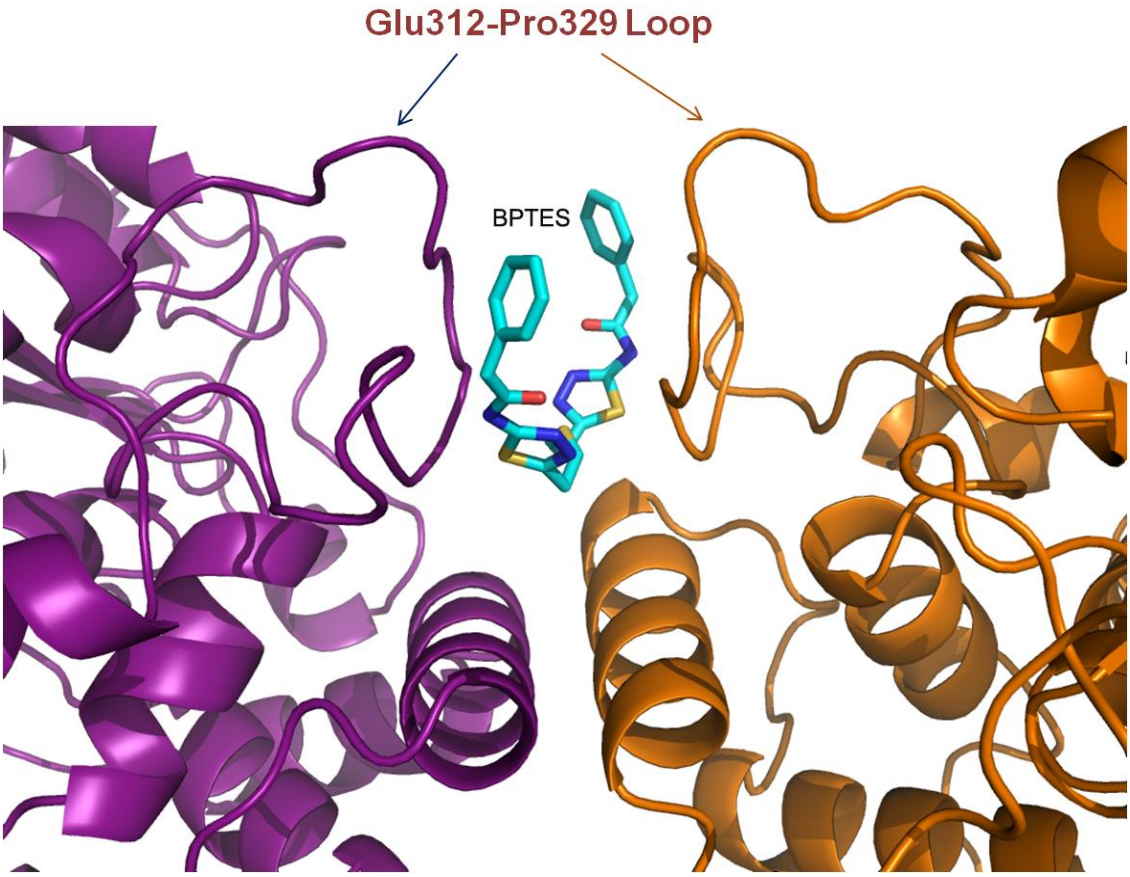

Figure 28: A close-up view of the BPTES binding pocket. BPTES binding pocket is located on the surface exposed region of the loop Glu312-Pro329 at the dimer interface.

The dimer interface in the cKGA: BPTES complex is formed by residues from the helix Asp386-Lys398 of both monomers and involves hydrogen bonding, salt bridges, and

hydrophobic interactions (Phe389, Ala390, Tyr393, and Tyr394), besides two sulfate ions located in the interface (Figure 38 and Figure 39).

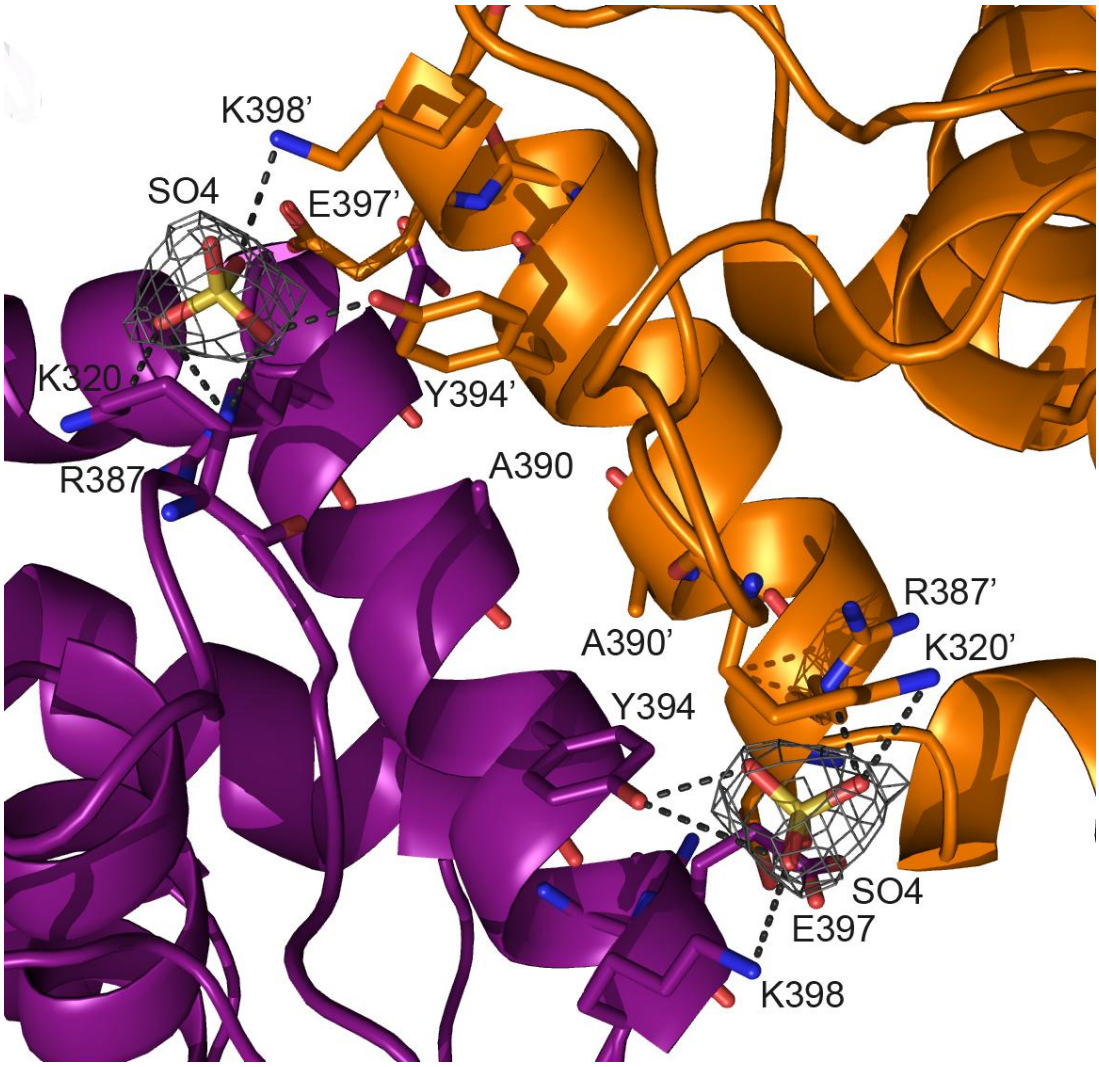

Figure 29: Perpendicular view of dimer interface of the cKGA-BPTES homodimer and showing the residues involved in the interaction as sticks. The dimerization interface is formed by the sulphate ion, hydrogen bonding, salt bridge, and hydrophobic interactions between residues from each monomer. The sulphate ion and the hydrogen bonding contacts are shown.

The dimers are further stabilized by binding of BPTES, where it binds to loop residues (Glu312-Pro329) and Tyr394 from both monomers. Similarly, residues from Lys311-Asn319 loop and Arg454, His461, Gln471, and Asn529-Leu533 are involved in the interface with neighboring monomers to form the tetramer in the BPTES complex. Furthermore, the tetrameric structure of the *apo* and BPTES: cKGA complex reveals a significant difference in the interface area of each monomer. These interactions are relatively weak in the *apo* tetramer compared with the BPTES complex. The *apo* tetramer has a total of 16 intermolecular hydrogen bond contacts (<3.2 Å) with a buried area of ≈1,700 $Å^2$ of each monomer, whereas in the cKGA: BPTES complex there are 25 intermolecular hydrogen bond contacts with a buried area of ≈1900 $Å^2$. The interactions among the monomers are relatively weaker in the *apo* tetramer than in the BPTES complex Figure 40A and B). We infer that the binding of BPTES promotes the formation of a stable but inactive tetramer.

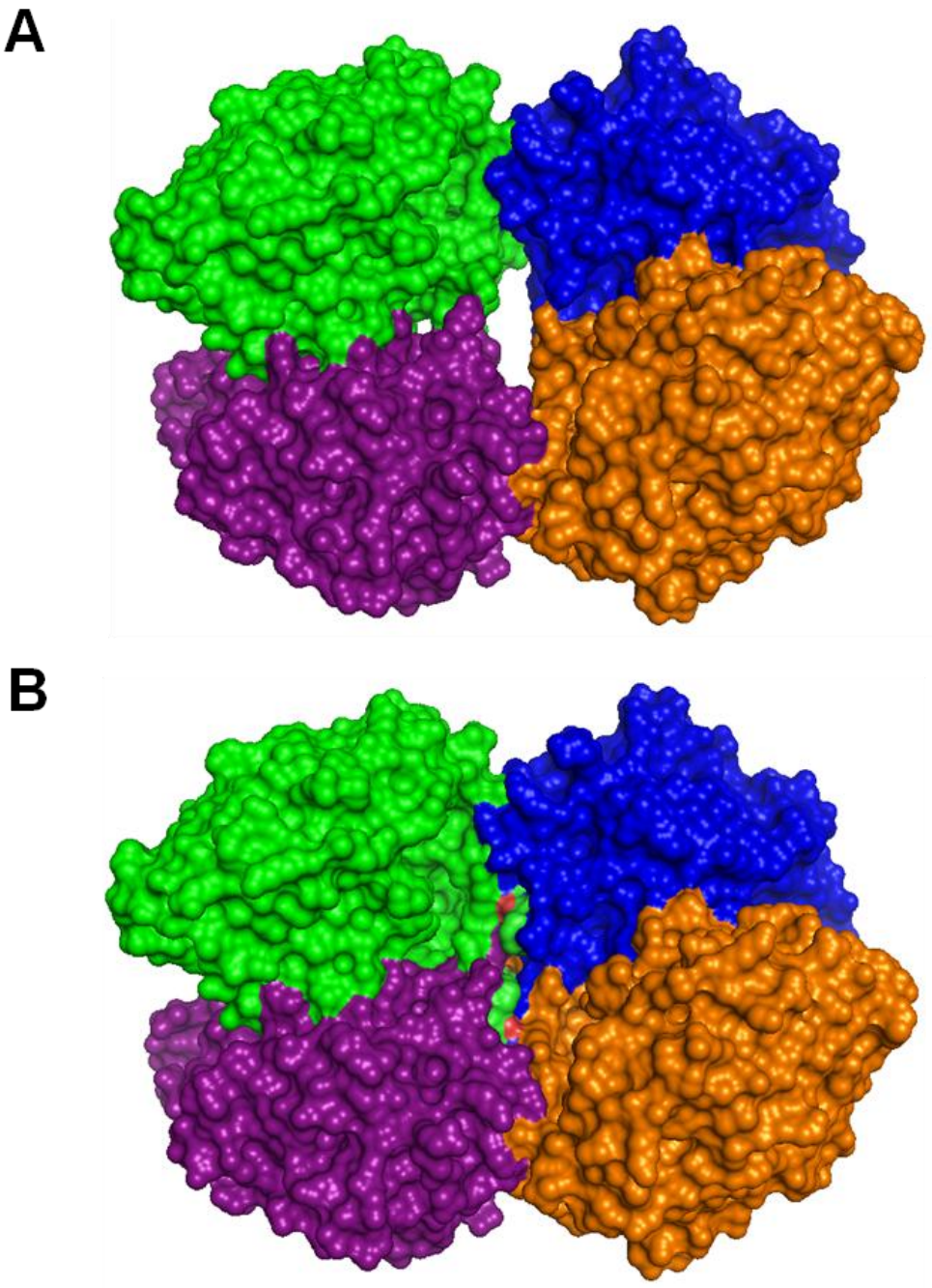

Figure 30: Surface representation showing the *apo* cKGA and cKGA: BPTES tetramer (**A**) Surface representation showing the symmetry-related *apo* cKGA molecules forms a tetramer. Each monomer is colored differently (A, orange; B, purple; C, blue; D, green). (**B**) Surface representation showing the symmetry-related BPTES: cKGA forms tetramer. Each monomer is shown in same color as described in **A**. The BPTES: cKGA forms tight tetramer compared with *apo* cKGA.

2.3.9 BPTES Induces Allosteric Conformational Changes That Destabilize Catalytic Function of KGA

Subsequently we examined how BPTES binding could inhibit KGA activity by comparing the structures of the cKGA: BPTES inhibitor complex with the *apo* cKGA structure. Because the loop Glu312-Pro329 is located near the active site, we hypothesize that BPTES binding induces conformational changes of the key residues of the loop (Glu312-Pro329) to stabilize an open and inactive conformation of the catalytic site. To test this hypothesis, wild-type KGA and structure-guided KGA mutants Phe318Ala, Leu321Ala, Phe322Ala, and Leu323Ala, as well as a Tyr394Ala variant from the dimerization helix, were each expressed in human embryonic kidney epithelial cells 293T at equal levels, and homeostasis levels of glutamate inside the cells were determined. Figure 41 shows that HEK 293T cells overexpressing KGA produced a higher level of glutamate compared with the vector control cells. Most significantly, all of these mutants, except Phe322Ala, greatly diminished the KGA activity.

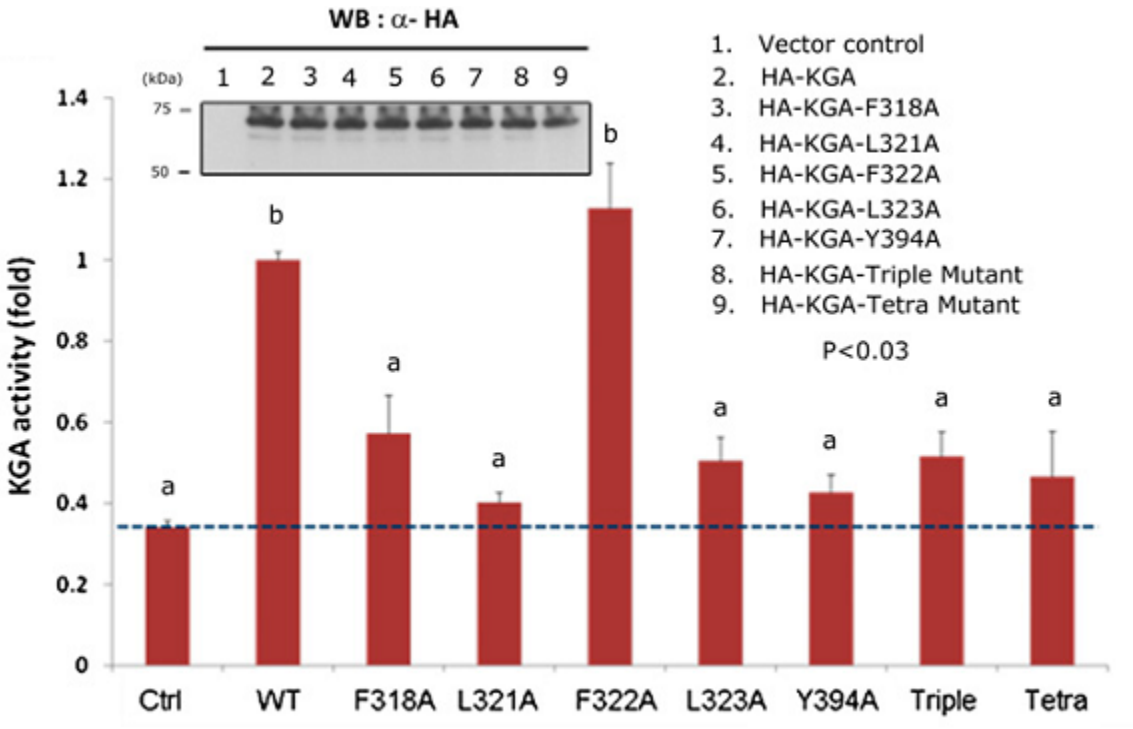

Figure 31: Mutations at allosteric loop and BPTES binding pocket abrogate KGA activity. HEK 293T cells were transfected with vector control or plasmids expressing wild-type, single, or multiple point mutants of HA-tagged KGA for 24 h before cell lysates were prepared for glutaminase assays. For clarity, the dotted line was included to indicate the basal level. Equal expression levels of the wild-type and mutants KGA were verified with Western blots. Each value represents the mean ± SD of three independent experiments.

Next, we examined whether these residues are specifically involved in stabilizing the BPTES–KGA interactions. Unlike all of the previous mutants that have Ala substitutions to knock out their direct contribution to the actual enzymatic activities, a set of recombinant cKGA mutants (Phe318Tyr, Phe322Ser, Phe318Tyr/Phe322Ser, and Tyr394Ile) were instead generated to test their BPTES sensitivity. In particular, Phe318Tyr/Phe322Ser double mutant was used to mimic the corresponding residues in the liver form of glutaminase, LGA. Results show that all these mutants still retain the

same KGA activity as the wild-type control (Figure 42). However, the three mutants Phe322Ser or Phe318Tyr/ Phe322Ser and Tyr394Ile showed significantly reduced sensitivity to BPTES (1,140-, 970-, and 910-fold, respectively) (Figure 43). In contrast, Phe318Tyr, which retains the aromatic ring and is still active, remains highly sensitive to BPTES. In summary, consistent with our structural analysis, all of the key residues in the loop Glu312 to Pro329 and Tyr394 are essential for conferring KGA activity, and at least Phe322 and Tyr394 are involved in stabilizing the BPTES–KGA interaction. Any conformational change upon BPTES binding would severely affect the stability of the catalytic core of KGA, hence affecting its activity.

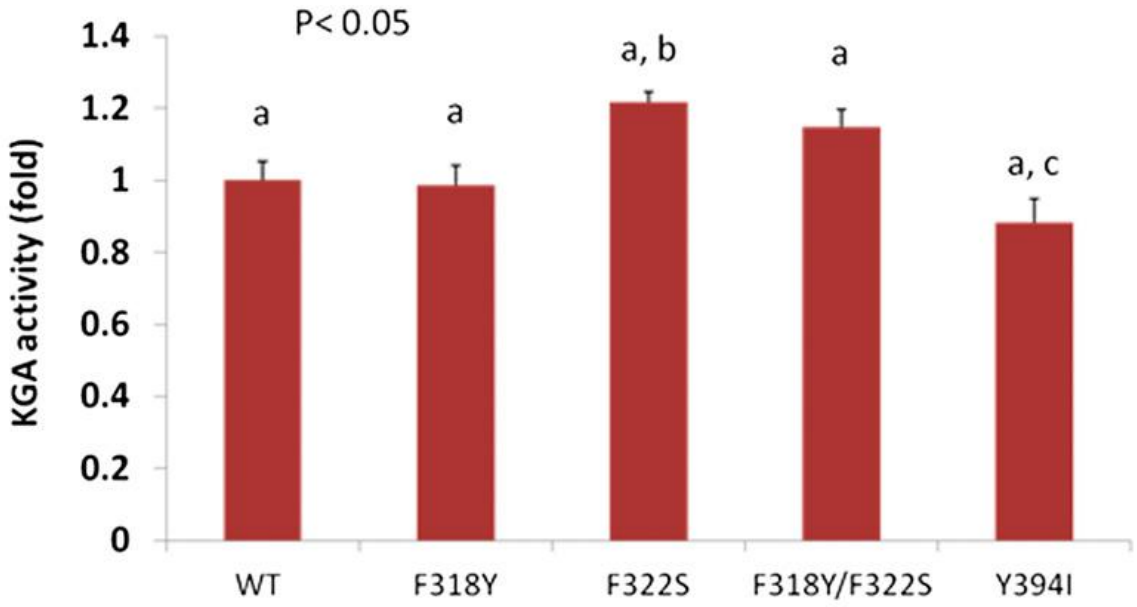

Figure 32: Glutaminase assay of cKGA mutants. Wild-type, F318Y, F322S, F318Y/F322S (a double mutant), and Y394I mutant of the cKGA were expressed, purified, and used for in vitro glutaminase assays.

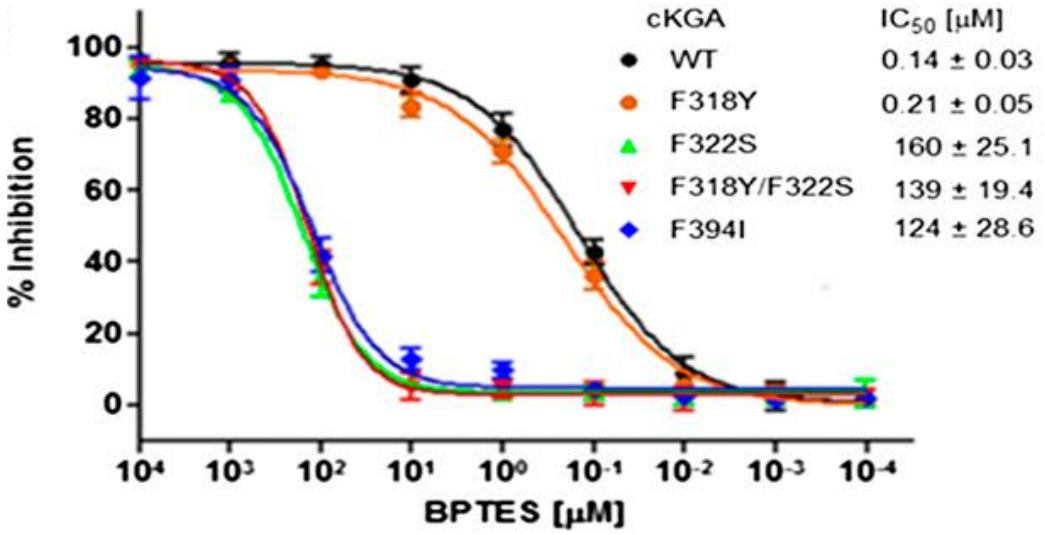

Figure 33: Mutational analyses of cKGA residues in the BPTES binding pocket. BPTES sensitivity for the wild-type and cKGA mutants indicated were measured and their IC_{50} values calculated. Each value represents the mean ± SD of three independent experiments performed in duplicate.

2.3.10 Raf-Mek-Erk Signaling Module Regulates KGA Activity

To demonstrate that treatment of cells with BPTES indeed inhibits KGA activity and cell proliferation, both 293T and MCF7 cells were treated with various concentrations of BPTES. Figure 44A and B show that BPTES abolished any increase in the glutamate levels in 293T and MCF7 cells overexpressing KGA, down to the basal level in a dose dependent manner, with more than 75% of the activity inhibited with 10 μM and completely inhibited with 50 μM of BPTES (Figure 44C). Consequently, treatment with BPTES in these cells also reduced cell proliferation in a dose-dependent manner (Figure 44D). BPTES therefore specifically inhibits KGA activity and cell proliferation.

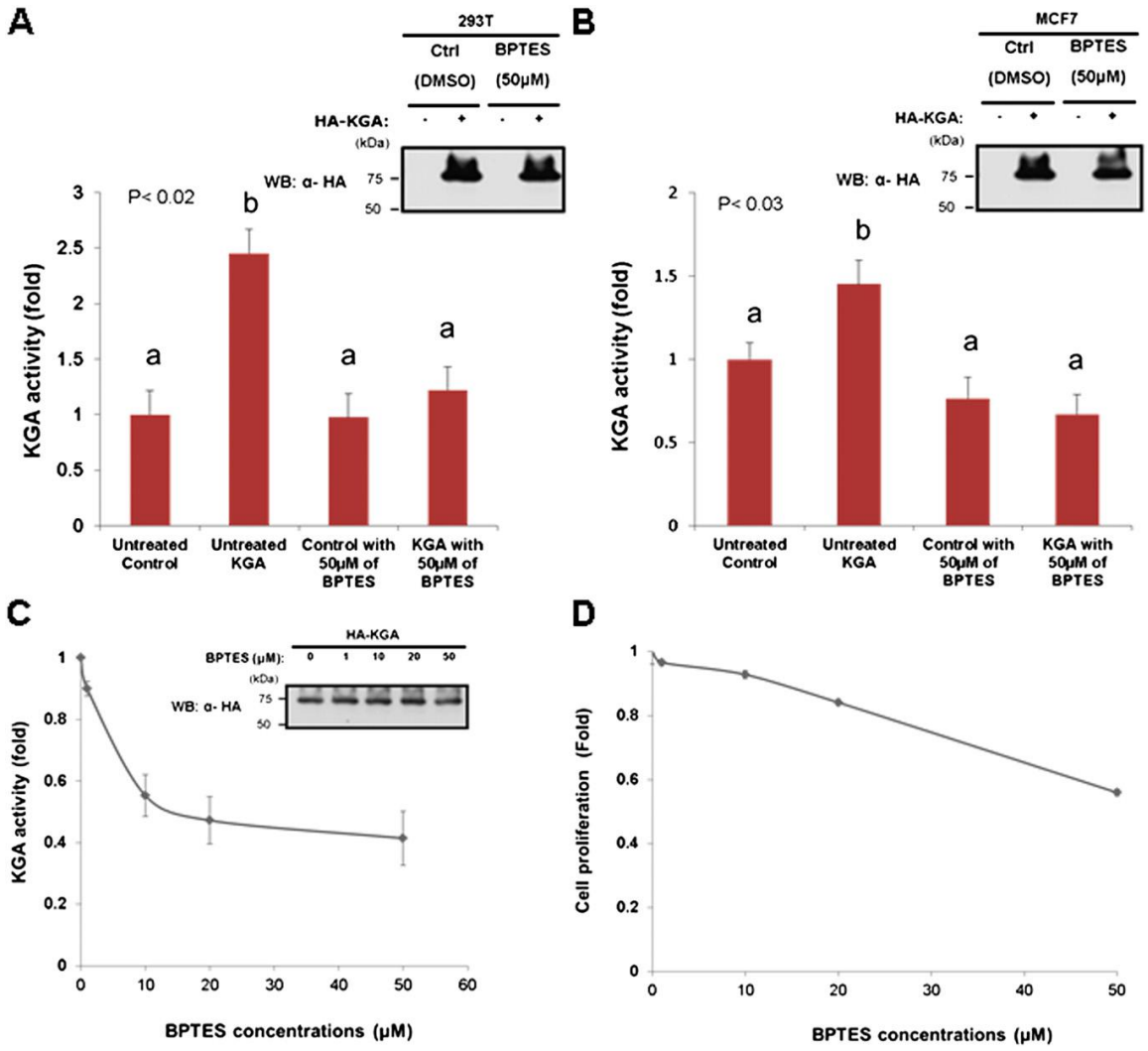

Figure 34: BPTES inhibits both KGA activity and cell proliferation in a dose-dependent manner. HEK 293T (**A**) and MCF7 (**B**) cells expressing a vector control or HA-tagged KGA were treated with DMSO or 50 μM of BPTES for 48 h. Cells were lysed and assayed for glutaminase activity. Equal expression levels of KGA were verified by Western blots. All values are means ± SD of three independent experiments, each with at least three replicates. Data sharing different letters are statistically significant at P values as indicated, as tested by ANOVA. (**C**) BPTES inhibits KGA activity in HEK 293T cells in a dose-dependent manner. HEK 293T cells expressing KGA were treated with the range of BPTES concentration as indicated. Cells were lysed and assayed for glutaminase activity. Equal expression levels of KGA were verified with Western blot analyses. (**D**) BPTES inhibits cell proliferation in HEK 293T cells in a dose-dependent manner. HEK 293T cells were seeded into 96-wells and treated with various indicated concentrations of BPTES for 48 h, and cell proliferation assays were measured. All values are means ± SD of three independent experiments, each with at least three replicates. Data sharing different letters are statistically significant at P values as indicated, as tested by ANOVA.

Next, as cells respond to various physiological stimuli to regulate their metabolism, with many of the metabolic enzymes being the primary targets of modulation (Tennant et al., 2010), we examined whether KGA activity can be regulated by physiological stimuli, in particular EGF (epidermal growth factor), which is important for cell growth and proliferation. Cells overexpressing KGA were made quiescent and then stimulated with EGF for various time points. Figure 45 shows that the basal KGA activity remained unchanged 30 min after EGF stimulation, but the activity was substantially enhanced after 1 h and then gradually returned to the basal level after 4 h. Because EGF activates the Raf-Mek-Erk signaling module (Roberts and Der, 2007), treatment of cells with Mek-specific inhibitor U0126 could block the enhanced KGA activity with parallel inhibition of Erk phosphorylation (Figure 45). Interestingly, such Mek-induced KGA activity is specific to EGF and lysophosphatidic acid (LPA) but not with other growth factors, such as PDGF, TGF-β, and basic FGF (bFGF), despite activation of Mek-Erk by bFGF (Figure 46).

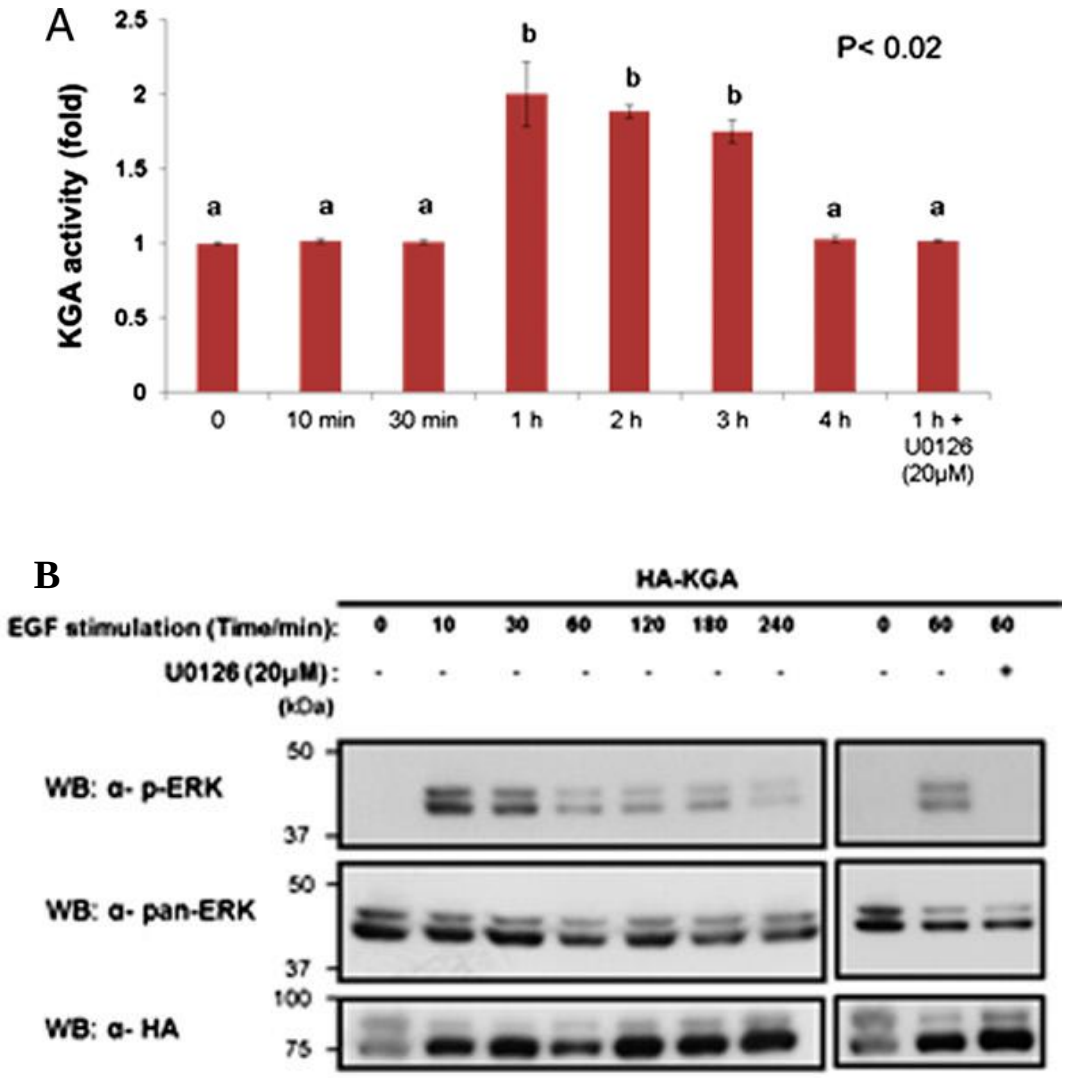

Figure 35: EGFR-Raf-Mek-Erk signaling stimulates KGA activity (*i*). (**A**) 293T cells expressing HA-tagged KGA were starved for 24h and then stimulated with EGF (100 ng/mL) for the times indicated. Cells were lysed and assayed for their glutaminase activities. (**B**) The expression levels of KGA and the Erk activation profile (as indicated by levels of phosphorylated Erk) were verified by Western blot analyses. All values are mean ± SD of three independent experiments, each with multiple replicates. Data sharing different letters are statistically significant at P values as indicated, tested by ANOVA or t test.

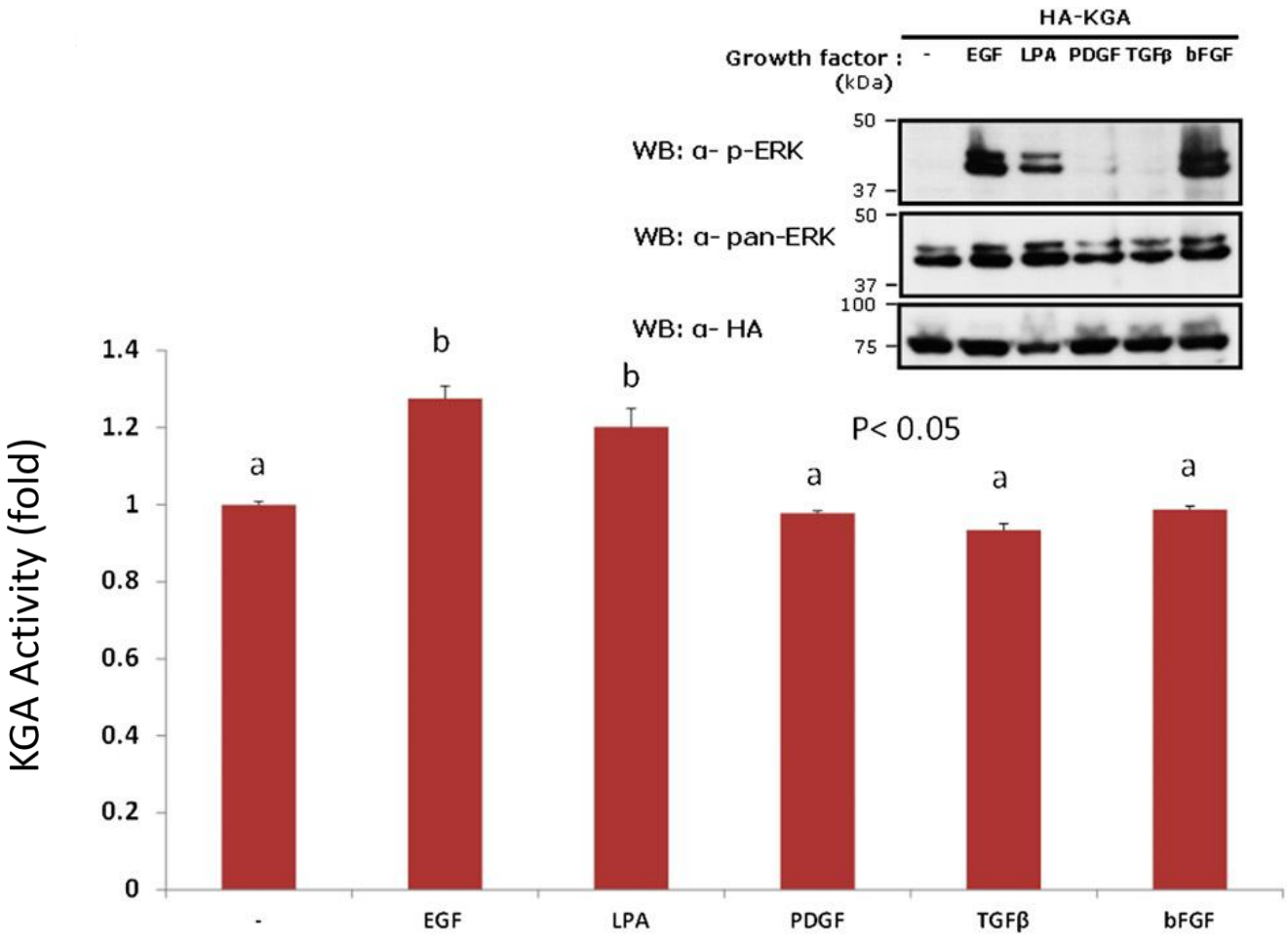

Figure 36: Regulation of KGA by different growth factors and stimuli. 293T cells expressing HA-tagged KGA were starved and stimulated with various mitogens including EGF (100 ng/mL), LPA (20 μM), PDGF (50 ng/mL), TGF-β (1 ng/mL), and bFGF (10 ng/mL) as indicated for 3 h. The cells were lysed and assayed for glutaminase activity. Equal expression of KGA and signaling activation (as indicated by levels of phosphorylated Erk) were verified with Western blot. Values are means ± SD of three independent experiments, each with multiple replicates. Data sharing different letters are statistically significant at P values as indicated, as tested by ANOVA.

We next investigated whether Raf-Mek-Erk activated by EGF could indeed directly regulate the KGA activity. Cells were transfected with KGA with wild-type, the "dominant negative and kinase-dead," or the constitutive active mutants of Raf-1 and

Mek2 and the levels of glutamate determined. Strikingly, KGA activity was completely inhibited by both the dominant negative mutants of Raf-1 (K375M) and Mek2 (K101A), whereas both wild-type and constitutive active mutants of Raf-1 (Raf-1-Y340D) and Mek2 (Mek2-S222, 226D) did not lead to any further increase in the glutamate production (Figure 47A). Moreover, expression of these mutants did not affect the expression levels of either ectopically expressed or the endogenous level of KGA (Figure 47B and 47C), indicating that any changes in the KGA activity was not due to their protein stability but was due to some posttranslational modifications of KGA. To examine whether such regulation is directly associated with the Raf-Mek-Erk complex, overexpressd KGA was immunoprecipitated from the cells, and the presence of Raf-1, Mek2, or Erk1/2 (endogenous or overexpressed) was examined. The results show that KGA could interact equally well with the wild-type or mutant forms of Raf-1 and Mek2 (Figure 47C). Importantly, endogenous Raf-1 or Erk1/2, including the phosphorylated Erk1/2 (Figure 47C and 47D), could be detected in the KGA complex. Taken together, these results indicate that the activity of KGA is directly regulated by Raf-Mek-Erk downstream of EGF receptor.

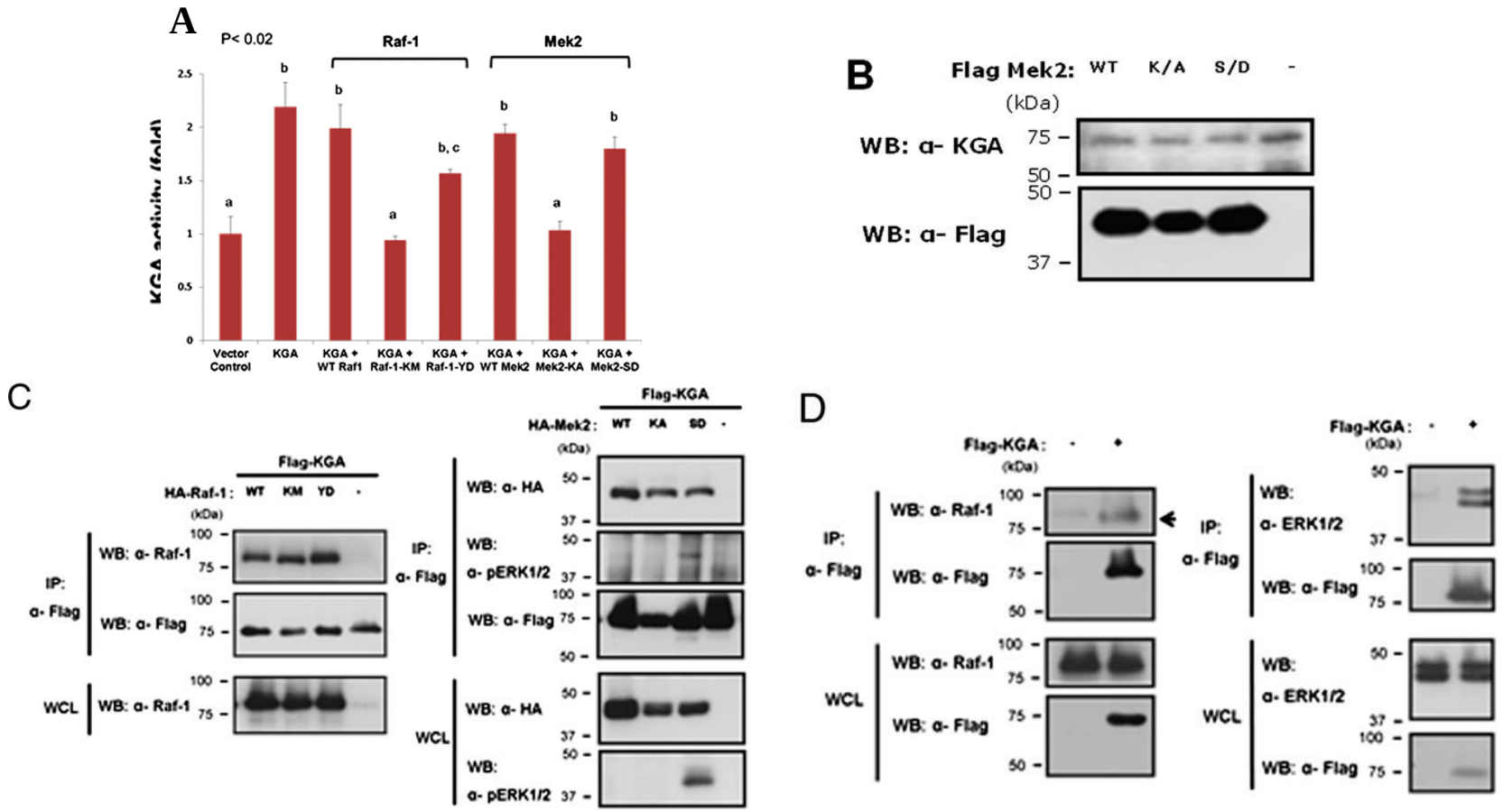

Figure 37: EGFR-Raf-Mek-Erk signaling stimulates KGA activity (*ii*). (**A**) Cells expressing Flag-tagged KGA with or without the HA-tagged wild-type, dominant negative mutants (Raf-1-K375M; Mek2-K101A) or constitutive active mutants (Raf-1-Y340D; Mek2-S222, 226D) were lysed and assayed for glutaminase activity. (**B**) Ectopic expression of the Mek2 mutants does not affect the endogenous levels of KGA. 293T cells expressing wild-type and mutants of Mek2 (Mek2-K101A; Mek2-S222, 226D) were lysed, and the endogenous levels of KGA of these samples were analyzed by Western blot. (**C**) Same batch of cell lysates prepared for the glutaminase assay in A were subjected to immunoprecipitation (IP) with anti-Flag M2 beads. Bound proteins and their expression in whole-cell lysates (WCL) were analyzed with Western blot. (**D**) Cells expressing Flag-tagged KGA were lysed for immunoprecipitation using anti-Flag M2 beads and analyzed for the presence of endogenous Raf-1 or Erk1/2 by Western blot analyses. Arrow denotes band for Raf-1. Values are means ± SD of three independent experiments, each with multiple replicates. Data sharing different letters are statistically significant at P values as indicated, as tested by ANOVA.

To further show that Mek2-enhanced KGA activity requires both the kinase activity of Mek2 and the core residues for KGA catalysis, wild-type or triple mutant (Leu321Ala/Phe322Ala/ Leu323Ala) of KGA was coexpressed with dominant negative Mek2-KA or the constitutive active Mek2-SD and their KGA activities measured. The result shows that the presence of Mek2- KA blocks KGA activity, whereas the triple mutant still remains inert even in the presence of the constitutively active Mek2 (Figure 48A), and despite Mek2 binding to the KGA triple mutant (Figure 48B). Consequently, expressing triple mutant did not support cell proliferation as well as the wild-type control (Figure 48C).

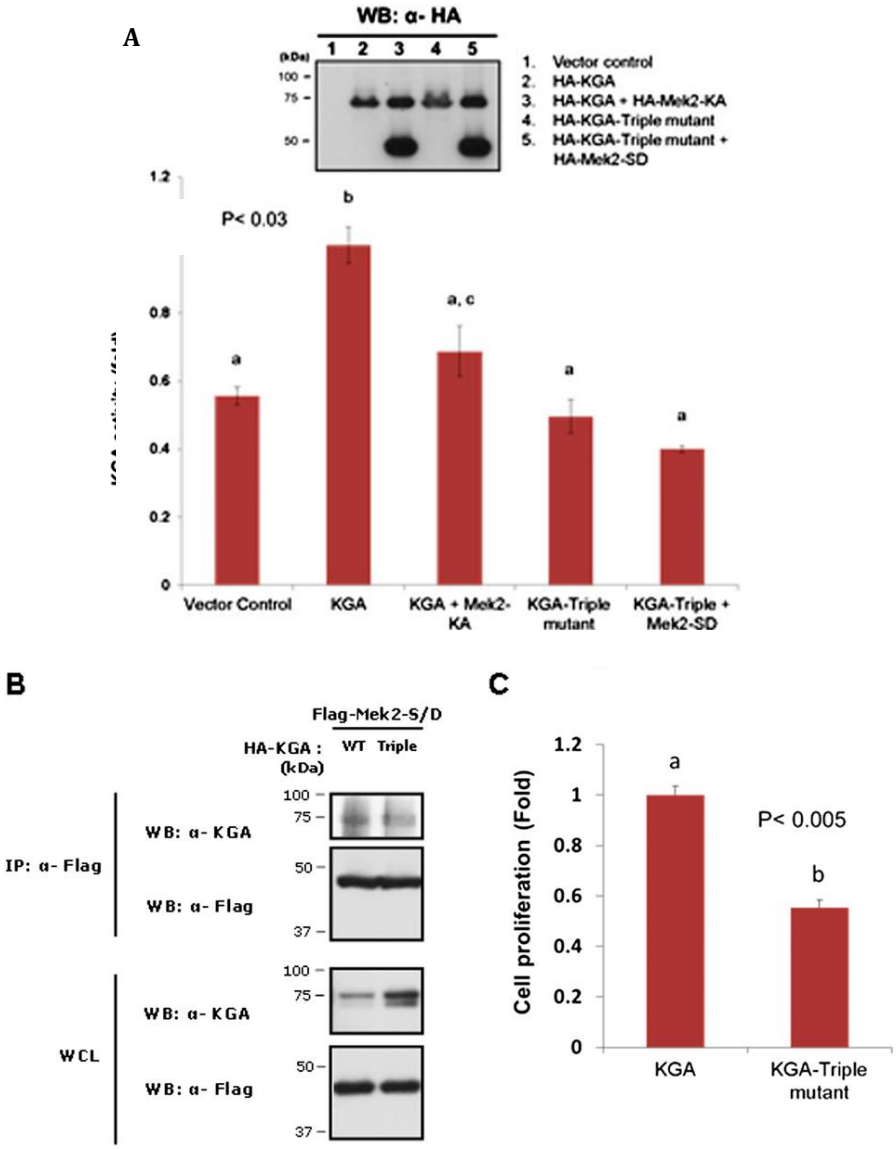

Figure 38: EGFR-Raf-Mek-Erk signaling stimulates KGA activity (*iii*). (**A**) 293T cells were transfected with vector control or plasmids expressing wild-type KGA or the KGA triple mutant (L321A/F322A/L323A), in the absence or presence of Mek2-K101A or Mek2-S222,226D for 24 h before lysates were prepared for glutaminase assays. Expression levels of these proteins were verified by Western blot analyses. (**B**) 293T cells transfected with wild-type and triple mutant of HA-tagged KGA in the presence of Flag-tagged Mek2-SD were lysed for immunoprecipitation with anti-Flag M2 beads and analyzed for their interaction with Western blot analyses. (**C**) 293T cells were transfected with plasmids expressing wild-type KGA, or the triple-mutant for 24 h, and reseeded with equal number into 96-well plates for another 48 h before being assayed for cell proliferation. All values for glutaminase and proliferation assays are means ± SD of three independent experiments, each with multiple replicates. Data sharing different letters are statistically significant at P values as indicated, tested by ANOVA or t test.

We have demonstrated that the KGA activity is dependent on the regulation of Raf-Mek2 signaling and core residues for KGA catalysis. To determine its physiological relevance, we tested whether blocking Raf-Mek2 signaling by the dominant negative mutant of Mek2, and inhibiting KGA by BPTES, could lead to any synergistic effect on cell proliferation. Cells were made to overexpress KGA or/ and Mek2-K101A, and then treated with 20 μM of BPTES for the next 24 h. Figure 49 shows that transient expression of Mek2-K101A alone did not affect cell proliferation. However, it reduced the level of cell proliferation by 10% when cells were treated with a subthreshold dose of BPTES which by itself did not lead to any loss of cell proliferation over this period of treatment. Interestingly, when cells expressing both KGA and Mek2-K101A were treated with subthreshold levels of BPTES, there was a further reduction in cell proliferation by 30% ($p < 0.02$).

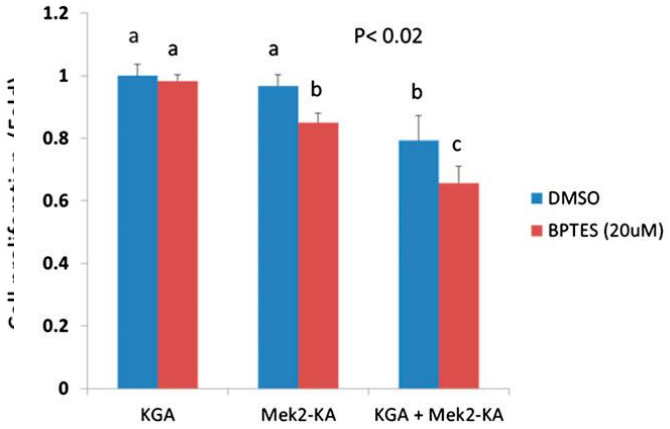

Figure 39: Dominant negative form of Mek2 potentiates BPTES inhibition on cell proliferation. Cell expressing KGA and/or the Mek2-K101A for 24 h were re-seeded with equal numbers into 96-well plates, followed by treatment with suboptimal concentration of BPTES (20 μM) for a further 24 h before being assayed for cell proliferation. Values are means ± SD of three independent experiments, each with multiple replicates. Data sharing different letters are statistically significant at $P < 0.02$, as tested by ANOVA.

Lastly, to determine whether regulation of KGA by Raf- Mek-Erk depends on its phosphorylation status, cells were transfected with KGA with or without the protein phosphatase PP2A and assayed for the KGA activity. PP2A is a ubiquitous and conserved serine/threonine phosphatase with broad substrate specificity. The results indicate that KGA activity was reduced down to the basal level in the presence of PP2A (Figure 50 A). Coimmunoprecipitation study also revealed that KGA interacts with PP2A (Figure 50B), suggesting a negative feedback regulation by this protein phosphatase. Furthermore, treatment of immunoprecipitated and purified KGA with calf-intestine alkaline phosphatase (CIAP) almost completely abolished the KGA activity *in vitro* (Figure 50C). Taken together, these results indicate that KGA activity is regulated by Raf-Mek2 signaling, and KGA activation by EGF could be part of the EGF-stimulated Raf-Mek-Erk signaling program in controlling cell growth and proliferation (Figure 51).

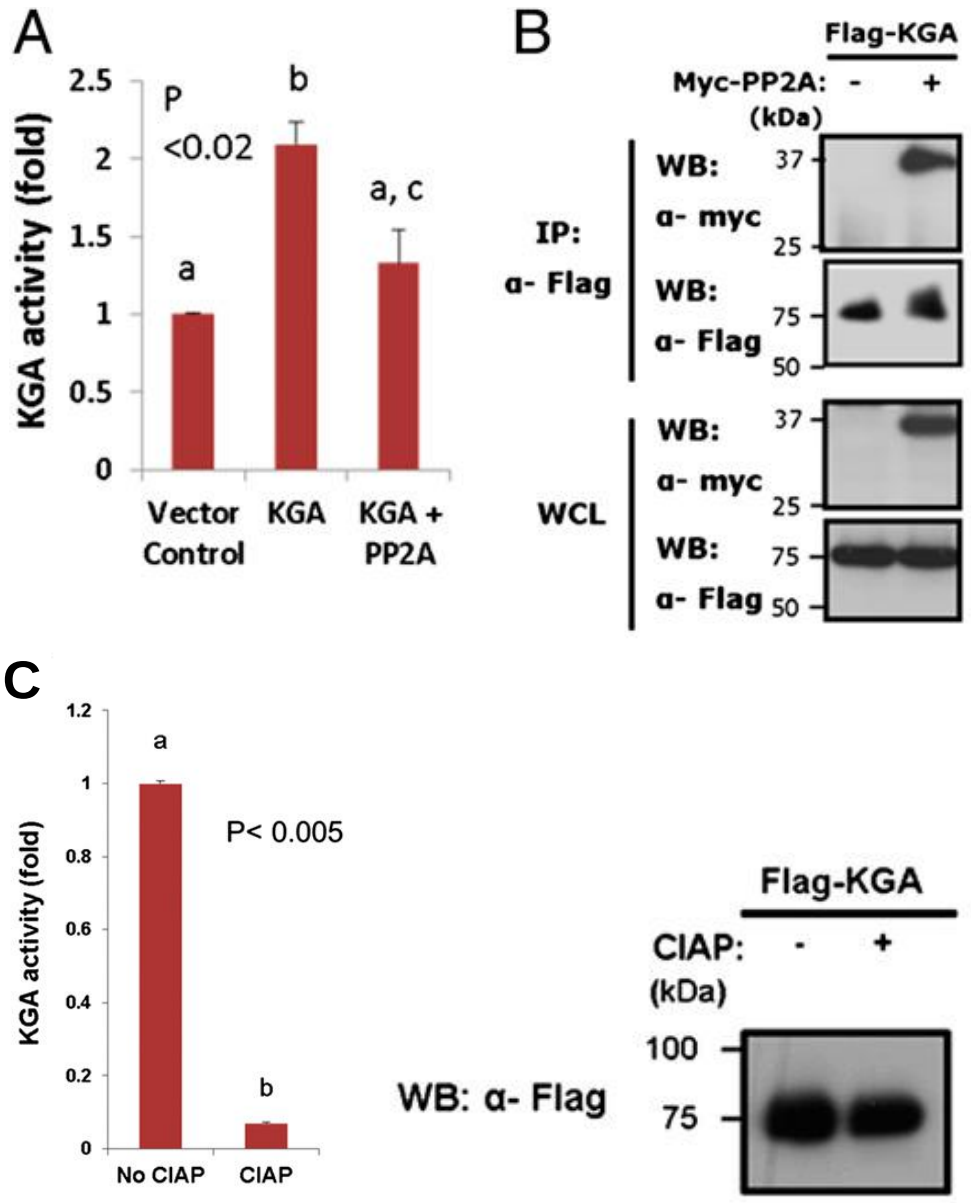

Figure 40: KGA activity is regulated by phosphorylation. (**A**) Lysates were prepared from cells expressing Flag-tagged KGA in the presence or absence of myc-tagged catalytic subunit of the protein phosphatase PP2A and assayed for the glutaminase activity. Values are means ± SD of three independent experiments. Data sharing different letters are statistically significant at $P < 0.02$, as tested by ANOVA. (**B**) Separate aliquots from the same batch of cell lysates prepared for the glutaminase assay in A were subjected to immunoprecipitation (IP). Bound myc-PP2A and their expression levels in whole-cell lysates (WCL) were analyzed by Western blots. (**C**) Cell lysates containing Flag-tagged KGA were immunoprecipitated with anti-flag M2 beads, washed and then treated with or without the calf intestine alkaline phosphatase CIAP at 37 °C for 3 h before assayed for glutaminase activity. Values are means +/− SD of 3 independent experiments. Data sharing different letters are statistically significant at $P < 0.005$, as tested by ANOVA.

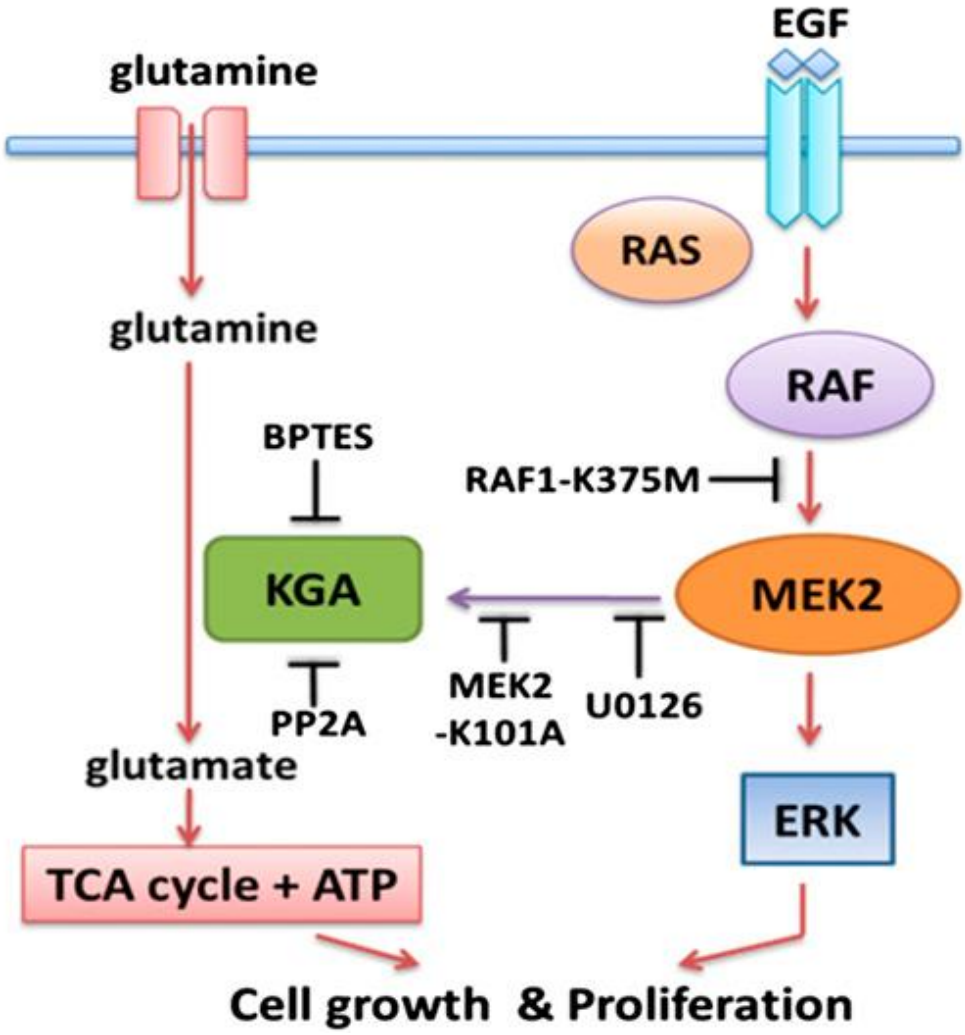

Figure 41: Schematic model depicting the synergistic cross-talk between KGA-mediated glutaminolysis and EGF-activated Raf-Mek-Erk signaling. Exogenous glutamine can be transported across the membrane and converted to glutamate by glutaminase (KGA), thus feeding the metabolite to the ATP-producing tricarboxylic acid (TCA) cycle. This process can be stimulated by EGF receptor mediated Raf-Mek-Erk signaling via their phosphorylation-dependent pathway, as evidenced by the inhibition of KGA activity by the kinase-dead and dominant negative mutants of Raf-1 (Raf-1-K375M) and Mek2 (Mek2- K101A), protein phosphatase PP2A, and Mek-specific inhibitor U0126. Consequently, inhibiting KGA with BPTES and blocking Raf-Mek pathway with Mek2-K101A provide a synergistic inhibition on cell proliferation. Refer to the text for more detail

2.4 Discussion

Small-molecule inhibitors that target glutaminase activity in cancer cells are under development. Earlier efforts targeting glutaminase using glutamine analogs have been unsuccessful owing to their toxicities (DeBerardinis et al., 2008; Ovejera et al., 1979). BPTES has attracted much attention as a selective, non-toxic inhibitor of KGA (Robinson et al., 2007), and preclinical testing of BPTES toward human cancers has just begun (Garber, 2010). BPTES selectively suppresses the growth of glioma cells (Seltzer et al., 2010) and inhibits the growth of lymphoma tumor growth in animal model studies (Le et al., 2012). Wang et al. (Wang et al., 2010) reported a small molecule that targets glutaminase activity and oncogenic transformation. Despite extensive studies, nothing is known about the structural and molecular basis for KGA inhibitory mechanisms and how their function is regulated during normal and cancer cell metabolism. Such limited information impedes our effort in producing better generations of inhibitors for better treatment regimens.

Comparison of the complex structures with *apo* cKGA structure, which has well-defined electron density for the key loop, we provide the atomic view of an allosteric binding pocket for BPTES and elucidate the inhibitory mechanism of KGA by BPTES. The key residues of the loop (Glu312-Pro329) undergo major conformational changes upon binding of BPTES. In addition, structure-based mutagenesis studies suggest that this loop is essential for stabilizing the active site. Therefore, by binding in an allosteric pocket, BPTES inhibits the enzymatic activity of KGA through (*i*) triggering a major conformational change on the key residues that would normally be involved in stabilizing

the active sites and regulating its enzymatic activity; and (*ii*) forming a stable inactive tetrameric KGA form. Our findings are further supported by two very recent reports on KGA isoform (GAC) (Cassago et al., 2012; DeLaBarre et al., 2011) although these studies lack full details owing to limitation of their electron density maps. BPTES is specific to KGA but not to LGA (Robinson et al., 2007). Sequence comparison of KGA with LGA (Figure 52A) reveals two unique residues on KGA, Phe318 and Phe322, which upon mutation to LGA counterparts, become resistant to BPTES. Thus, our study provides the molecular basis of BPTES specificity.

It was recently reported that KGA is up-regulated by Myc and Rho and is subjected to ubiquitination (Colombo et al., 2010; Gao et al., 2009; Wang et al., 2010). However, little is known regarding how the glutaminolytic pathway is functionally linked to growth-promoting signaling pathway(s). Many metabolic enzymes are thought to serve as housekeeping enzymes that control fluxes of metabolites to sustain rather than to primarily regulate cell growth. Here we show that a high level of KGA activity can lead to the increased cell proliferation that is inhibited by BPTES. Most significantly, we show that KGA activity is activated by EGF via the Raf-Mek-Erk signaling module because inhibition of both kinases by their dominant negative mutants or treatment with a specific Mek inhibitor completely abrogates the KGA activity. Consistent with the regulation being phosphorylation-dependent, co-expressing KGA with protein phosphatase PP2A or treatment of purified KGA with alkaline phosphatase all block the elevated KGA activity. When key residues on the loop that stabilizes the catalytic core of

KGA are mutated, such stimulation is lost. These results indicate that Raf-Mek-Erk signaling is linked to reprogramming of growth metabolism.

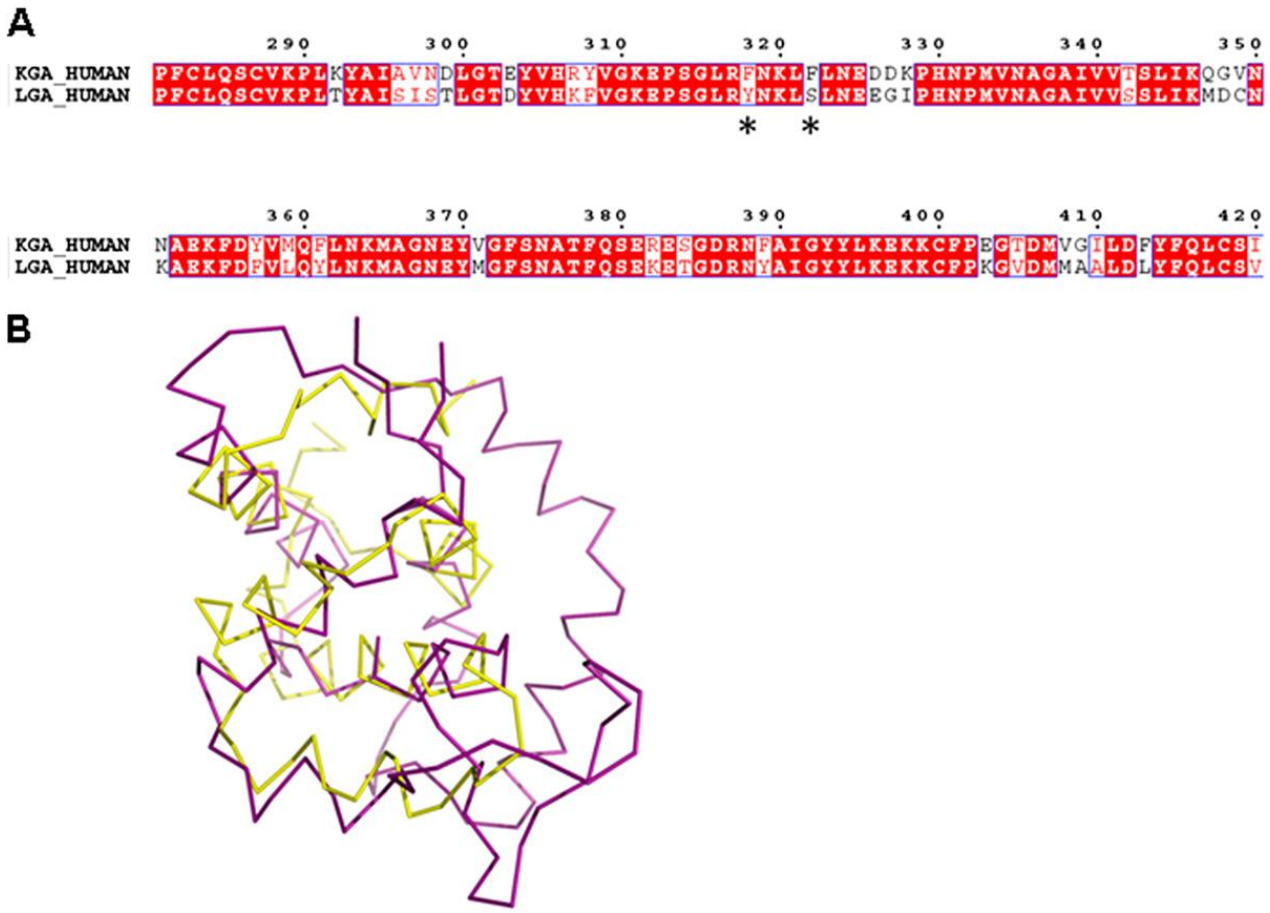

Figure 42: Sequence and structure-based analysis of KGA. (**A**) Sequence alignment between KGA with LGA around the BPTES binding pocket. The residues that form the binding pocket of BPTES are marked with asterisks. The sequence identity between full-length human KGA and full-length LGA is 63%, and their glutaminase domain alone is 81%. Numbering is shown for the KGA sequence. The figure was prepared using Espript2.2 (Gouet et al., 1999). (**B**) Superposition of the domain II of the cKGA with death domain containing protein (PDB code: 2OF5). Cα trace showing the superposition of domain II of the cKGA (magenta) and death domain of the TNF superfamily protein (yellow). These two protein domains superimpose with an rmsd of 2.9 Å for 91 Cα atoms, superposed using the DALI server (Holm and Rosenström, 2010).

We show that the combined inhibitory effect of Mek2 and BPTES on KGA and cell proliferation could offer an exciting regime for multidrug therapy in cancers. Understanding how KGA itself is activated by the Raf-Mek signaling will also provide an alternative approach to further examine whether deregulation of KGA and its hyperactivation can be linked to this pathway. This could be the basis for abnormal cell growth in cancers and possibly other metabolic and neuronal disorders involving glutamate or ammonia as a main metabolite, such as hyperinsulinism/ hyperammonemia/ hepatic encephalopathy and neurotransmission (Kelly and Stanley, 2001; Romero-Gómez et al., 2010). In this regard, we show that KGA forms a complex with Raf-1, Mek2, and Erk1/2, as well as the protein phosphatase PP2A, which can be anchored on a common scaffold protein or present as different subcomplexes. Whether this activation would involve KGA directly as a substrate of Raf-1, Mek2, or/and Erk or whether other immediate substrate(s) of these kinases exist to act as a co-regulator for KGA remains to be further investigated. This is of particular interest because we show that bFGF, despite activating Mek/Erk, does not activate the KGA activity. This result highlights tight regulation of these three-tier kinases that could be spatially coordinated through different scaffolds or by other yet-unknown coregulators. In addition, the domain II of cKGA is homologous to several DEATH domain-containing proteins (Figure 52B), which are known to regulate many signaling pathways, such as NF-κB and apoptosis (Jeong et al., 1999).

In summary, the current structural, biochemical, molecular, and cell-based studies provide detailed insights into allosteric inhibition of human KGA by BPTES, the regulation of KGA activity and cell proliferation by EGF receptor-mediated Raf/ Mek/Erk signaling module, and phosphorylation-dependent regime in cancer cell metabolism. This could pave the way for developing more specific therapeutic inhibitors toward KGA and Mek2-linked pathways and may offer a more effective strategy to tackle glutamine-addicted cancers with greater efficacy.

Chapter III

Structural basis of the active site inhibition mechanism of human kidney type glutaminase (KGA)

3.1 Introduction

The glutamine analogue, 6-Diazo-5-oxo-L-norlucine (DON), was previously shown to inhibit KGA through binding to the active site (Shapiro et al., 1979). DON is an antibiotic that was originally isolated from *Streptomyces*. It is a diazo analogue of L-glutamine and known to interfere with a number of nucleotide and protein synthetic pathways where glutamine primarily act as a nitrogen substrate (Kisner et al., 1980). However, DON lacks selectivity against glutaminase, because it is structurally similar to glutamine that was shown to inhibit many glutamine utilizing enzymes such as amidotransferases, and glutamine synthetase (Ortlund et al., 2000; Pinkus, 1977). The potential anticancer activity of DON has been studied in different animal models; however, it has not progressed to clinical trials due to the toxicity concerns (Ahluwalia et al., 1990; Ovejera et al., 1979), so it warrants the optimization. In addition to DON, the glutamate analogue CK (L-2-amino-4-oxo-5- chloropentanoic acid) was previously reported to act on the active site of KGA. DON is shown to be more effective at high concentrations of phosphate to inhibit KGA (Shapiro et al., 1979) whereas CK effectively inhibits KGA in decreased phosphate concentrations (Shapiro et al., 1978).

Recent crystal structure of glutaminase from *Bacillus subtilis*, with the DON bound form reveals the key role of a serine residue as a catalytic nucleophile (Brown et al., 2008). We recently reported the crystal structure of catalytic domain of kidney type glutaminase (cKGA) in complex with L-glutamine and L-glutamate in active site and proposed the catalytic mechanism of KGA (Thangavelu et al., 2012). The catalytic dyad of KGA consists of Ser286 and Lys289, with the Ser286 acting as a catalytic nucleophile. In addition, we and others have reported the allosteric inhibition mechanism of KGA/ and

GAC isoforms by BPTES (DeLaBarre et al., 2011; Thangavelu et al., 2012). Moreover, we recently have shown that KGA activity can be regulated by Ras\Raf\Mek\Erk signaling in response to growth factor stimulation (Thangavelu et al., 2012). Subsequently, Cassaga et al. have solved the structure of GAC isoform in complex with phosphate, and they proposed the activation mechanism of GAC isoform (Cassago et al., 2012).

So far, there has been no crystal structure reported for any of KGA isoforms in complex with active site inhibitors. Previous kinetic studies have suggested that DON could act on the active site of the glutaminase (Robinson et al., 2007; Shapiro et al., 1979). Nevertheless, the structural basis for the active site inhibition mechanism of DON towards human KGA remains to be elucidated. As a first step towards improving its potency and selectivity with KGA, here we report the crystal structure of cKGA in complex with DON, refined to 2.3 Å resolution. The complex structure revealed the DON binding pocket of KGA. DON makes covalent bond contact with active site residue Ser286 of KGA. Further we performed site-directed mutagenesis to validate the importance of key residues involved in interactions with DON. Based on our studies, currently we are in the process of optimizing the inhibitor.

3.2 Materials and Methods

3.2.1 Expression and Purification of cKGA

Human cKGA was purified following the procedures described in the chapter II. The purified protein (20 mg/mL) was kept in a storage buffer (20 mM Na-Hepes pH 7.5, 200 mM NaCl, 10% glycerol and 3 mM DTT) and used for crystallization experiments. DON (6-diazo-5-oxo-L-norleucine, NSC 7365), azaserine (*O*-diazoacetyl-L-serine, NSC 742), Glufosinate Ammonium, and L-Methionine Sulfoximine were purchased from Sigma.

2.2.3 Glutaminase Assay

Glutaminase assay was performed using a two step assay described previously (Kenny et al., 2003). Briefly, 10 μL of wild-type cKGA or cKGA alanine mutant was incubated separately with 10 μL of first assay mix [20 mM glutamine, 50 mM Tris·acetate (pH 8.6), 100 mM phosphate, and 0.2 mM EDTA] at 37 °C for 10 min, and the reaction was quenched with adding 2 μL of 3 M HCl. Subsequently 200 μL of the second assay mix [2.2 U glutamate dehydrogenase, 80 mM Tris·acetate (pH 9.4), 200 mM hydrazine, 0.25 mM ADP, and 2 mM nicotinamide adenine dinucleotide] was added and incubated for 30 min at room temperature. The absorbance at 340 nm was recorded using a microplate reader (SpectraMax 340; Molecular Devices). Compounds were prepared as a 10-mM stock in water. The IC_{50} values were calculated from the fitted regression equation using the-log plot (Graphpad prism). Each value represents the means ± SD of three independent experiments, each with at least three replicates.

3.2.2 Crystallization and Data Collection

Crystallization screening was carried out by hanging drop vapor diffusion methods at 22ºC. Prior to crystallization the complex was made by incubating 20 mg/mL of cKGA with 10 mM DON (approximately 1:10 molar ratio) for 30 minutes at 4 °C. The crystallization drop consists of 1 µl cKGA: DON complex and 1 µl of the crystallization solution from the reservoir well. The cKGA: DON crystals grew after 2 days in the presence of 0.1 M Bis-Tris Propane pH 7.27 and 1.83 M $LiSO_4$. For the diffraction studies, crystals were cryo-protected with the reservoir solution supplemented with 15% glycerol as a cryoprotectant and flash frozen in liquid nitrogen. Diffraction data were collected at the synchrotron beam line 13B1 (wavelength 1.000 Å) at National Synchrotron Radiation Research Centre (NSRRC, Taiwan). Data sets were processed and scaled resolution using HKL2000 (Otwinowski Z and W., 1993). The crystallographic data collection statistics are provided in Table 7.

3.2.3 Structure Solution and Refinement

The structure of cKGA-DON complex was determined by molecular replacement using the program MolRep (Vagin and Teplyakov, 2010) using the coordinates of *apo* cKGA as the search model (Protein data bank 3VOY, (Thangavelu et al., 2012). One molecule of cKGA: DON complex was observed in the asymmetric unit. The initial R-factor was 39% for cKGA: DON complex from the molecular replacement solution. The model was examined and built in COOT (Emsley and Cowtan, 2004) and subsequent refinement carried out with Phenix-refine (Zwart et al., 2008). Fitting of the inhibitor and refinements were carried out in COOT and Phenix programs respectively. Water

molecules were included at the final stage of the refinement. The final structure was refined up to 2.3 Å resolution with the R-factor and R-free values of 19% and 21% respectively. The overall geometry of final model was analyzed by Ramachandran plot with the program PROCHECK (Laskowski RA et al., 1993). Details of the refinement statistics are provided in Table 7.

3.2.4 Site-Directed Mutagenesis of cKGA

We performed site-directed mutagenesis using the kit from Kapa biosystems to create all structure-guided mutants of cKGA (Table 6). The cKGA cloned into the PET-28 (b) vector was used as a template for mutagenesis. The residues Tyr249, Ser286, Lys289, and Tyr466 of cKGA were mutated to Ala, respectively, as a single-point mutant. All mutations were verified by DNA sequencing. Plasmids containing the point mutations were transformed into the *E. coli* BL21 (DE3) RIL strain and the mutant cKGA proteins were over expressed and purified in the similar manner as the wild-type cKGA.

Table 6: Deoxyoligonucleotides used in this work

Y249A	5'-GGG**A**AAGTTGCGGATGCTATTCCGCAGCTGGCC-3’
	5'-GGCCAGCTGCGGAATAGCATCCGCAACTTTCCC-3’
S286A	5'-TCTGCCTGCAAGCCTGTGTGAAACCGCTGAAAT-3’
	5'-ATTTCAGCGGTTTCACACAGGCTTGCAGGCAGA-3’
K289A	5'-CTGCAAAGCTGTGTGGCACCGCTGAAATACGCG-3’
	5'-CGCGTATTTCAGCGGTGCCACACAGCTTTGCAG-3’
Y466A	5'-CACTCATGCGGGATGGCTGACTTTTCCGGCCAA-3’
	5'-TTGGCCGGAAAAGTCAGCCATCCCGCATGAGTG-3’

3.3 Results and Discussions

3.3.1 Inhibition studies of cKGA by Glutamine and Glutamate analogues

DON and azaserine are glutamine analogs that are known to inactivate several glutamine-utilizing enzymes such as glutaminase, amidotransferases and glutamine synthetase (Barclay and Phillipps, 1966). Besides glutamine analogs, two other glutamate analogs such as glufosinate ammonium and L-methionine sulfoximine were previously shown to inhibit the glutamate dependent enzymes (Gill and Eisenberg, 2001; Liaw and Eisenberg, 1994). We intend to test whether these four inhibitors can inhibit KGA (Figure 53).

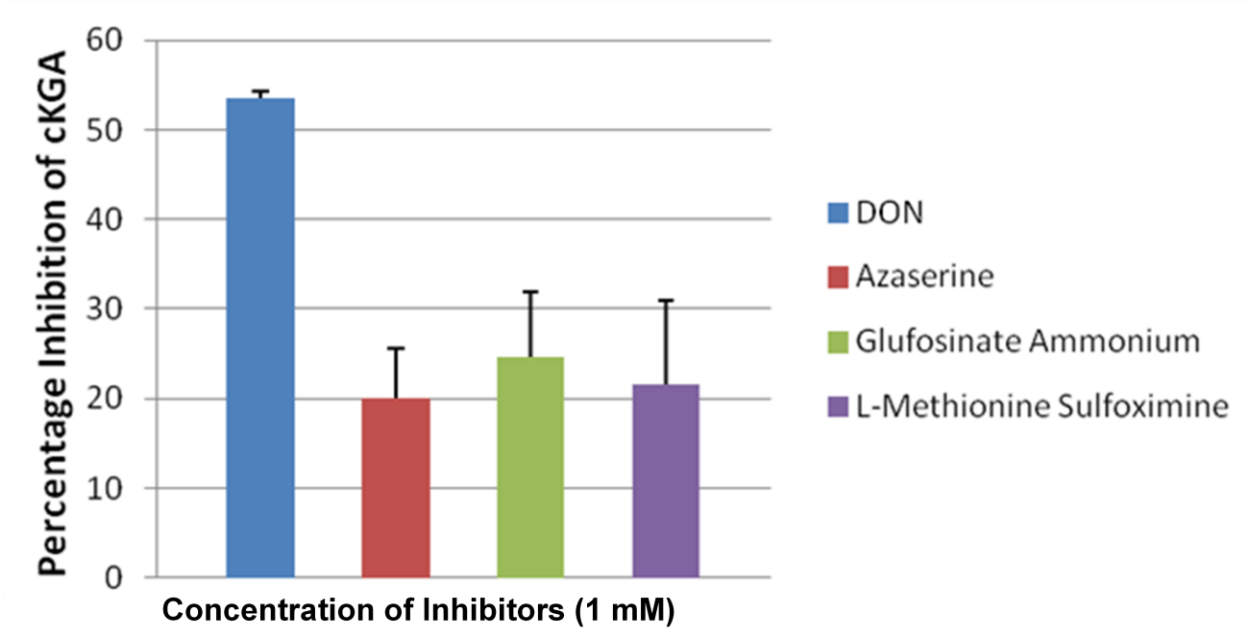

Figure 43: Inhibition studies of cKGA with selected glutamine/glutamate analogs. The relative inhibition percentage of cKGA by selected glutamine/glutamate analog inhibitors at 1 mM concentration (IC_{50} of DON: approximately 0.991 mM) was compared. The assays were performed in triplicates and values are means +/− SD of three independent experiments.

Inhibition assay showed that DON inhibits cKGA with an inhibition value (IC_{50}) of approximately 0.991 mM. However, compared to DON, cKGA activity was not significantly inhibited by other three inhibitors (Figure 53). Thus, DON was taken forward to study KGA's active site based inhibition mechanism. Towards this objective we have determined the complex structure of cKGA and DON.

3.3.2 Crystallization and Data Collection

Single crystals of cKGA: DON complex were obtained after 2 days in hanging drop vapour diffusion method and were grown to full size in 5 days (Figure 54). The crystals were cryo-protected with 15% glycerol and the data was collected at synchrotron source.

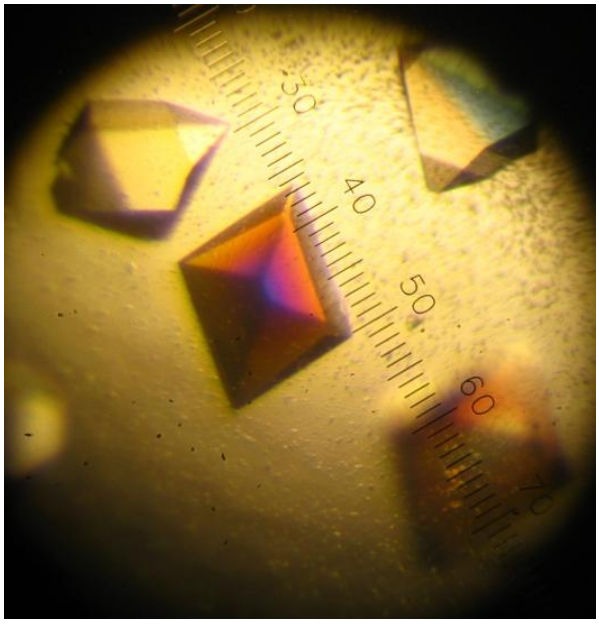

Figure 44: The cKGA: DON complex crystals were obtained with the reservoir solution consists of 0.1 M Bis-Tris Propane pH 7.27 and 1.83 M $LiSO_4$.

Table 7: Crystallographic data and refinement statistics for cKGA: DON complex

	cKGA: DON complex
Space group	$I4_122$
Cell parameters (Å, º)	a= 139.27,b= 139.27,c= 156.50, α= β=γ=90
Resolution range (Å)	30-2.3 (2.34-2.30)
Wavelength (Å)	1.000
Observed *hkl*	392469
Unique *hkl*	34102
Completeness (%)	99.6 (95.7)
Overall $I/\sigma I$	12.7
[a]R_{sym}	0.054 (0.392)
Refinement and quality of the model	
*Resolution range	25.7-2.30
[b]Rwork (%) no. reflections	19.28 (23221)
[c]Rfree (%) no. reflections	21.08 (1722)
Root mean square deviation	
Bond length (Å)	0.007
Bond angle (º)	1.02
Ramachandran plot (%)	
Favored region	88.1
Allowed regions	11.2
Generously allowed region	0.7
Disallowed regions	0
[d]Average B-factors (Å^2)	
Main chain atoms	52.04
Side chain atoms	57.43
Overall protein atoms (no. atoms)	54.63 (2412)
Waters (no. atoms)	54.63 (89)
Ligand (no. atoms)	53.26 (10)

[a] $R_{sym} = |I_i - \langle I \rangle|/|I_i|$ where I_i is the intensity of the i^{th} measurement, and $\langle I \rangle$ is the mean intensity for that reflection.

[b] $R_{work} = |F_{obs} - F_{calc}|/|F_{obs}|$ where F_{calc} and F_{obs} are the calculated and observed structure factor amplitudes respectively.

[c] R_{free} is as for R_{work}, but only for 5.06% of the total reflections chosen at random and omitted from refinement.

[d]Individual B-factor refinement was carried out.

As shown in table, a complete data set was collected up to a resolution of 2.3 Å (Table 7). The data were scaled with $I4_122$ space group with the Rsymm <0.1, suggesting the good quality of the data.

3.3.3 Overall Structure of cKGA: DON complex

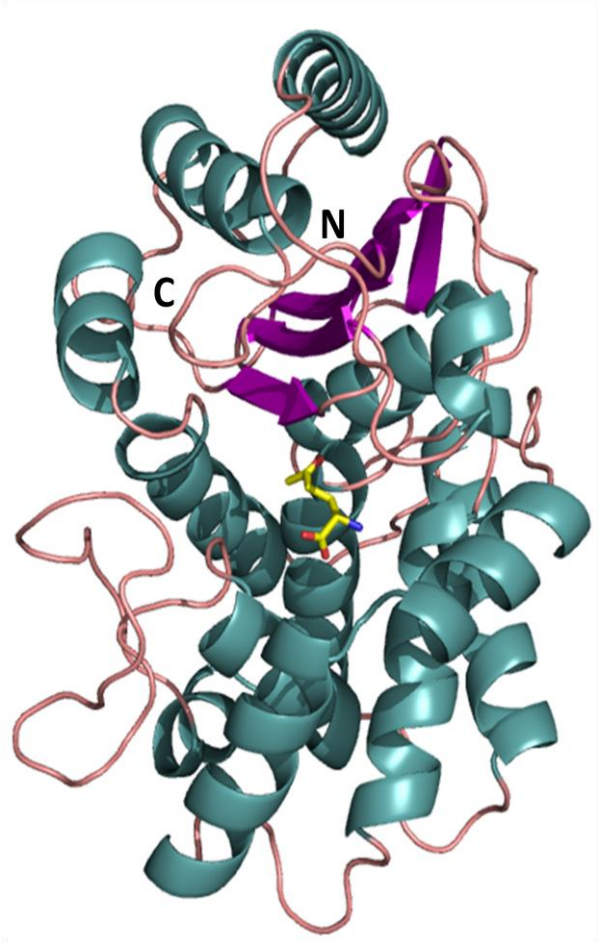

Figure 45: Ribbon representation of the cKGA: DON complex. The secondary structures such as α-helices and β-sheets are shown in cyan and magenta, respectively. The DON is located in the active site cleft and is shown as yellow stick. This figure was prepared using Pymol (DeLano, 2002).

The structure was determined by the molecular replacement method using coordinates derived from *apo* cKGA (PDB code 3voy). The final model has been refined with good stereochemical parameters (Figure 55). The final electron density map *(2Fo-Fc)* for the active site region of cKGA shows the well defined electron density for the DON molecule (Figure 56). The complex structure of cKGA: DON shows that the inhibitor form covalent bond contact with the side chain hydroxyl (OH) group of the catalytic nucleophile Ser286 (1.4 Å) and is conserved among all KGA isoforms. This is clearly evident from the observed continuous electron density from the active-site residue Ser286 with the inhibitor and indicates the possibility of covalent interaction. Based on the structure we reveal that cKGA interacts and remove the diazo group from the 6-Diazo-5-oxo-L-norlucine (cKGA-DON), thereby covalently connecting the enzyme with 5-oxo-l-norleucine (ON), and forms cKGA-ON complex.

The complex structure of cKGA: DON shows that the inhibitor is positioned in the catalytic pocket through several hydrogen bonding, and hydrophobic interactions. The bound inhibitor makes several interactions with Gln285, Ser286, Asn335, Glu381, Asn388, Tyr414, Tyr466, and Val484 (Figure 3.4). The cKGA: DON complex, the carbonyl oxygen of the inhibitor makes two hydrogen bonding interactions with backbone amino (NH) groups of Ser286 (2.9 Å and Val484 (2.8 Å), and forms an oxyanione hole. The α-carboxyl oxygens of the inhibitor makes two hydrogen bonding contacts with the side chains of Asn335 (3.1 Å) and Tyr414 (2.8 Å).

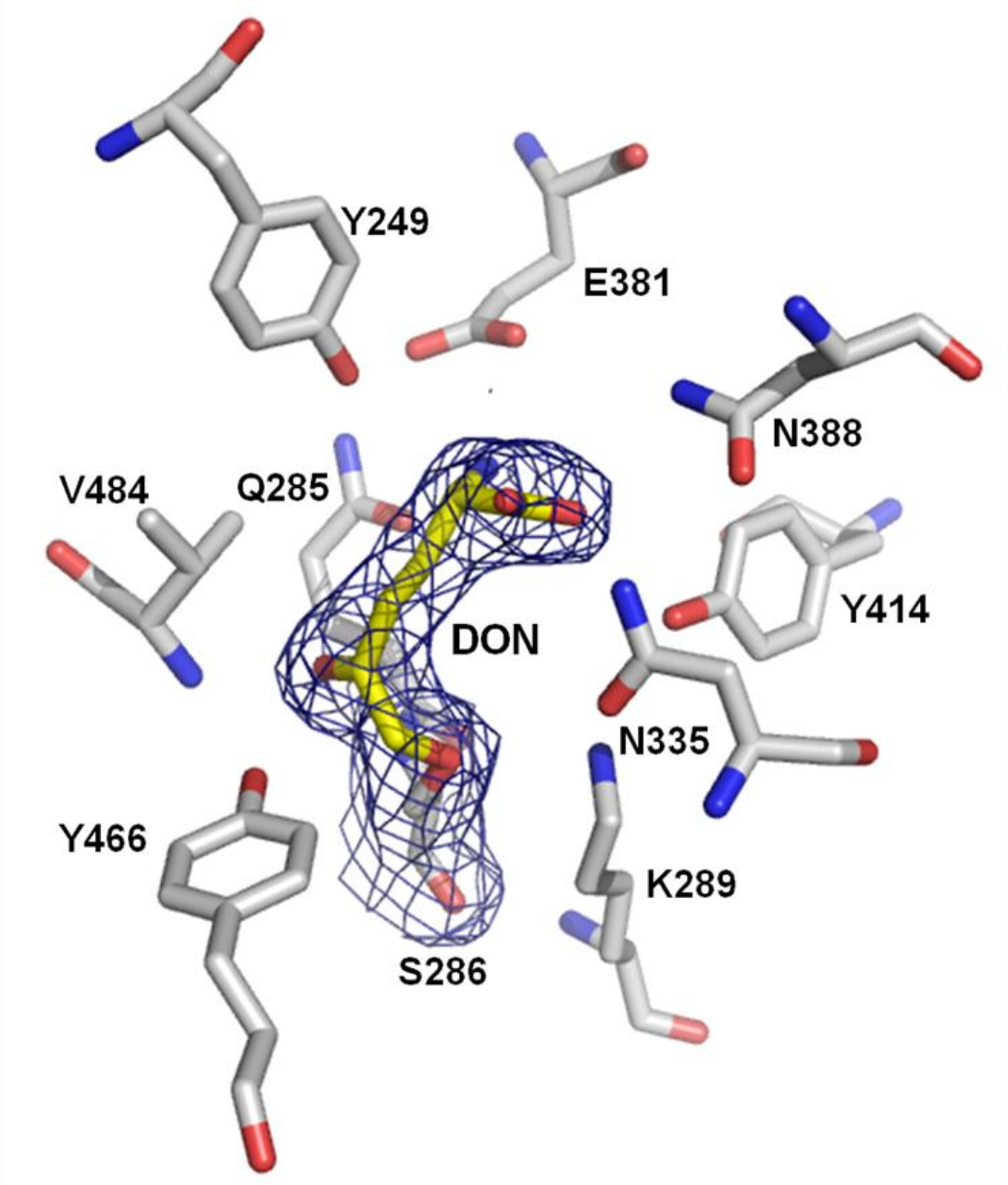

Figure 46: Interactions made by DON in the catalytic pocket of cKGA. DON is shown in yellow and cKGA residues are shown in cyan color. Final *2Fo-Fc* electron density map for the DON and its covalent attachment to Ser286 of cKGA is shown. The map is contoured at σ level of 1.0. This figure was prepared using Pymol (DeLano, 2002).

On the other hand, the backbone NH group of the inhibitor involves in a hydrogen bonding contact with the side chains of Gln285 (2.7 Å) and Glu381 (2.8 Å) (Table 7). Besides, the hydrophobic cluster formed by the side chains of three tyrosine residues such as Tyr249, Tyr414 and Tyr466, which further stabilize the interactions with DON (Figure 56). Notably the Tyr466 is located close to the DON (3.2 Å) and also close to catalytic Ser286 (2.7 Å), which is responsible for the proton transfer during catalysis. Previously we have shown that Tyr466 play key role in catalytic mechanism along with the active site dyad (Ser286 XX Lys289) (Thangavelu et al., 2012). The electrostatic surface potential of the cKGA: DON complex shows a predominantly positively charged active site (Figure 57), which is mainly contributed by the neighboring residues (Lys299 and Lys491) of the active site of KGA.

Table 8: Hydrogen bonds (Å) formed by DON in the active site of cKGA

DON atom	cKGA atom	Distance (Å)
O5	Ser286N	2.98
O5	Val484N	2.82
O1	Asn335ND2	3.13
O5	Tyr466OH	3.25
NH	Gln285OE1	2.79
NH	Glu381OE2	2.85
O5	Tyr249OH	3.24
O1	Tyr414OH	2.84

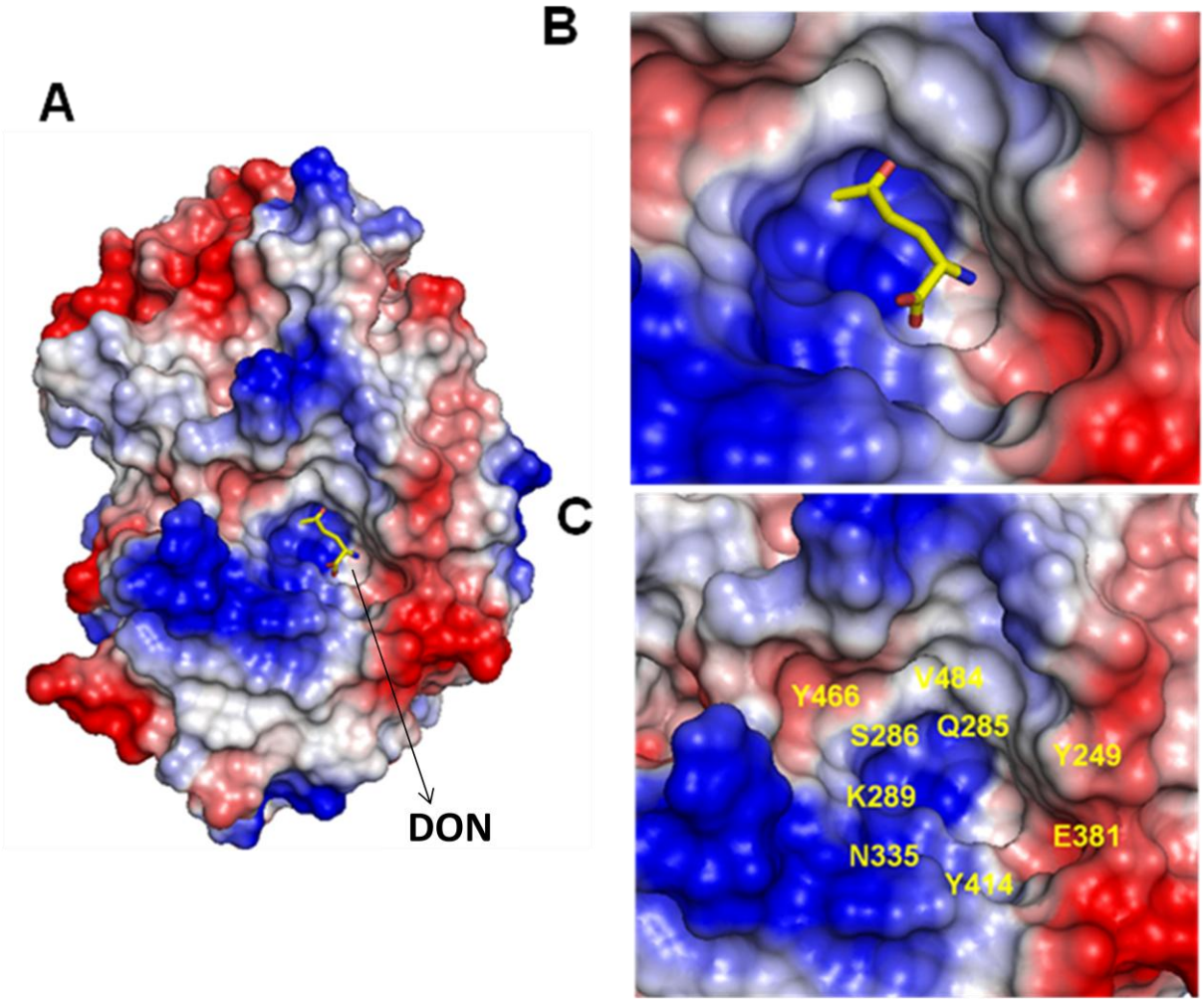

Figure 47: Binding pocket of DON in the active site cleft of cKGA. (A) Electrostatic surface potential representation of cKGA-DON complex, DON is shown as yellow stick. (B) A close view of electrostatic surface potential representation shows that positively charged pocket around DON. (C) The residues interacts with DON in the active site cleft are labeled.

The direct one-to-one comparison (superposition) of cKGA: DON and the *apo*-cKGA revealed no significant structural changes in KGA upon interacting with DON (Figure 58). This superposition yield a root-mean-square deviation (rmsd) of 0.3Å for 315 Cα atoms superimposed.

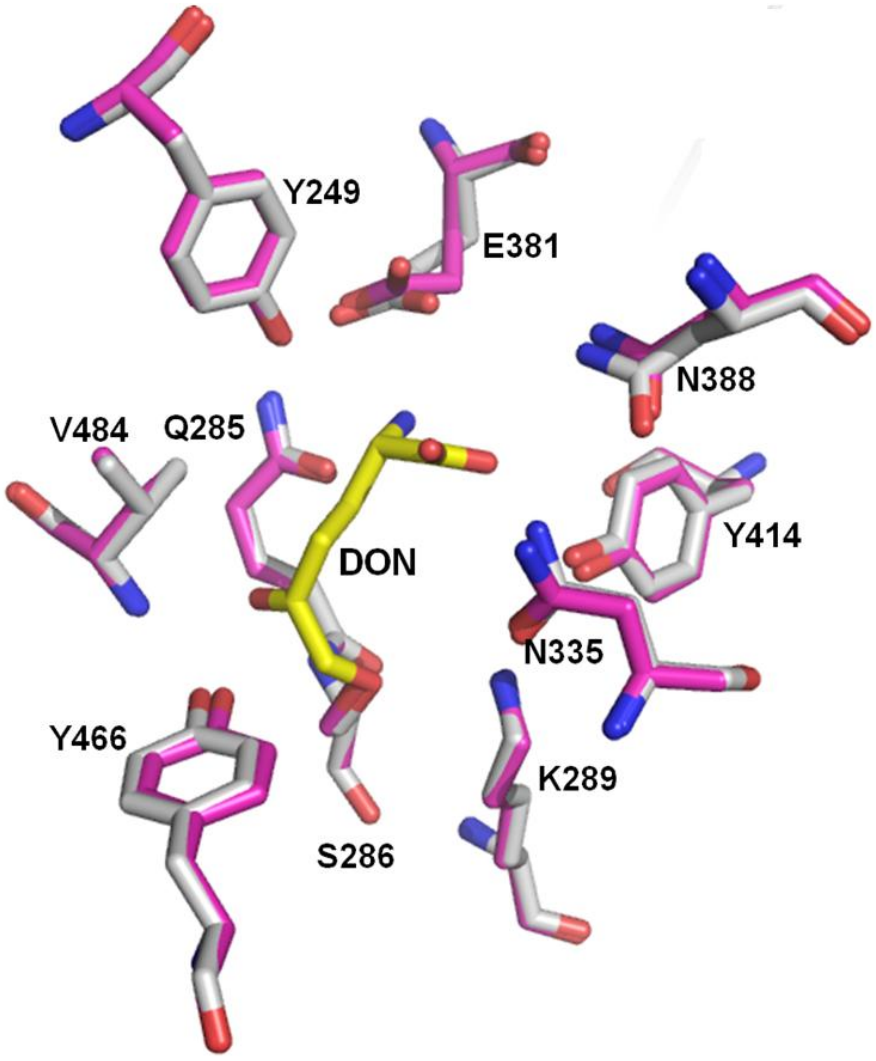

Figure 48: Crystal structure of apo cKGA is superposed with cKGA: DON. The active site residues of *apo* cKGA and cKGA: DON is shown in cyan and magenta respectively.

3.3.4 Mutational Studies of cKGA Residues in the DON Binding Pocket

The complex structure described in this chapter revealed the key residues of KGA that is essential in interactions with DON. To validate the enzymatic activity of DON-interacting residues of KGA, we have generated alanine mutants and measured their activities through the glutaminase assay. Glutaminase activity assay showed that the mutant proteins (Tyr249A, Ser286A, Lys289A, and Tyr466A) significantly reduced the activity when compared to wild type cKGA (Figure 59). The structure-based mutagenesis study indicates that substitution of alanine in the DON-interacting residues greatly affects binding of the substrate. Thus, our study confirms that the putative catalytic dyad (Ser 289 XX Lys289), other residues (Tyr249A and Tyr466A) could play a key role for the activity of KGA.

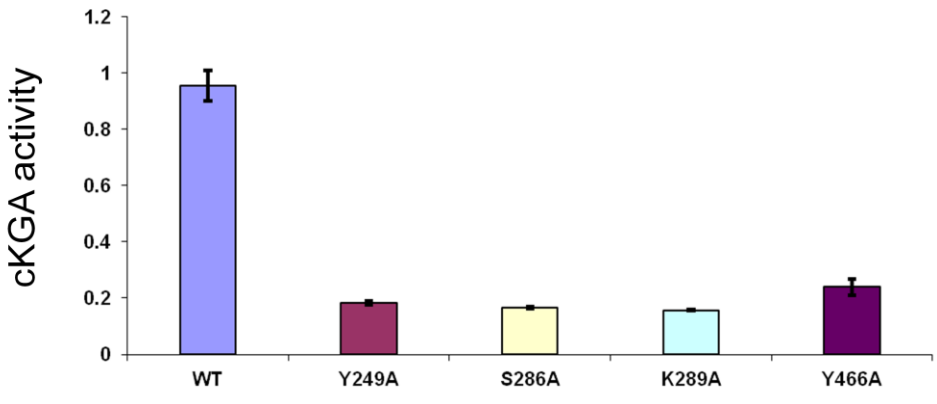

Figure 49: Site directed mutagenesis of cKGA residues in the DON binding pocket. The activities of wild type cKGA were compared with key structure guided-cKGA alanine mutants. Triplicates of data sets were obtained for each of the cKGA constructs, and values are means +/− SD of 3 independent experiments.

3.4. Conclusion

We have solved the crystal structure of cKGA in complex with glutamine analog inhibitor, DON, at resolution of 2.3 Å. On the basis of cKGA: DON complex structure we show that the DON is bound to the active site of KGA through the covalent modification of the residue Ser286, a catalytic nucleophile of the active site. Notably, the sequence and structural homologies between KGA and its homologs proteins suggesting a common mode of the active site inhibition mechanism. Besides, the structure based mutagenesis and kinetic studies were performed to validate the importance of key residues involved in the catalytic function of KGA. Although DON or other glutamine analogs such as acivicin, and azaserine has been widely used for the *in vitro* and *in vivo* studies and shown to have potential antitumor activity against human cancers, they lack selectivity and have toxicity concerns (Ovejera et al., 1979). A recent renewed interest in cancer metabolism raises the possibility that systematic usage of these agents may have effect against human cancers. In our studies, we found DON inhibits the activity of cKGA with an IC_{50} of approximately 1 mM. Hence, it is necessary to improve the affinity and specificity of DON using cKGA: DON complex structure to optimize the design and synthesis of new series of DON analogs towards therapeutic intervention.

Chapter IV

Conclusions and future directions

4.1 Conclusions

Cancer cells exhibit a characteristic metabolism and they use glucose and glutamine as their major energy sources. The kidney-type glutaminase (KGA) is a key enzyme responsible for the process of glutaminolysis that promotes Warburg effect in cancer cells to thrive and become a tumour. KGA is considered to be an attractive and a promising molecular target for human cancer therapies. More importantly, the small molecule inhibitors of KGA are in the early stage of clinical development to treat human cancers. However, the effort to design better inhibitors of KGA and plan for new treatment regimes for cancers is greatly hindered due to the lack of clear understanding on the molecular mechanism of inhibition of KGA and how the function of KGA is controlled by hormones and signaling pathways inside the cells.

In this thesis, we clearly showed that BPTES binds at the dimeric interface of KGA, near the active site. More strikingly, we show that binding of BPTES on the KGA, confers a drastic conformational change of a key loop (Glu312- Pro329), which is essential in stabilizing the catalytic pocket and thus rendering it inactive. Moreover, our site-directed mutagenesis study provides the molecular basis of BPTES specificity to KGA, verified through the mutants that mimic LGA isoform. Besides, the complex structural studies of a few BPTES derived inhibitors with KGA revealed the molecular basis of the potency, selectivity and pharmacophore feature of BPTES. The findings of this study on the BPTES and KGA novel allosteric inhibition mechanism provides valuable information for the optimization and development of improved versions of BPTES derived inhibitors with more selectivity and potency.

Though KGA is a key metabolic enzyme, its regulations and linking to many physiological signaling pathways is not clearly understood. In the chapter II, we demonstrated that the KGA activity can be upregulated by phosphorylation upon stimulation of cells with epidermal growth factor (EGF), a hormone that is linked to cancer growth and metastasis in various tumours. Furthermore we have established that KGA activity is mediated by a key signaling node, the Ras-Raf-Mek2-Erk signaling pathway. Even if BPTES can inhibit KGA activity, but nothing is known about any possible synergism of cancer drug treatments. Interestingly, our studies show that combination of BPTES and U0126, a compound which blocks Mek kinase (a kinase in Ras-Raf-Mek2-Erk signaling pathway) is synergistic and inhibits cancer cell growth and proliferation. These findings open up the possibilities for developing more specific therapeutic agents towards KGA/Mek2-linked pathways and offer a more effective strategy to tackle glutamine-addicted cancers with greater efficacy.

Besides BPTES, DON is a known active site inhibitor of KGA; however there is no structural information available for any of the human glutaminase isoforms in complex with any active site inhibitors. In chapter III, we have reported the structure and structure based studies on cKGA, in complex with DON. The complex structure revealed the DON binding mode on KGA and that form a covalent bond contact with active site. Moreover, we have performed site-directed mutagenesis to validate the importance of a few key residues involved in interactions with DON. This study will lead to design and development of potent and selective active site inhibitors of human glutaminase isoforms.

In conclusion, current structural, biochemical, molecular and cell-based studies provide detailed insights into (i) allosteric inhibition of KGA by BPTES (ii) active site inhibition of KGA by DON (iii) crosstalk and regulation of KGA activities by EGF-mediated Raf-Mek-Erk signaling and (iv) synergism between KGA activity and Mek2 in cancer cell metabolism. These novel findings will help in designing better inhibitors and in development of multi-drug strategies for the treatment of cancers addicted to glutamine metabolism.

4.2 Future directions

The knowledge obtained through the present studies on KGA can be effectively utilized to generate a series of optimized next generation inhibitors of BPTES (allosteric) and DON (active site) analogs. Besides, the current knowledge on KGA: BPTES complex could be systematically expanded to discover small molecule inhibitors for other glutaminase isoform LGA (Liver type glutaminase). This can be achieved by synthesizing a new series of BPTES-modified inhibitors that can specifically interact with LGA isoform.

As a continuation of our studies on KGA: the information of the KGA: BPTES and KGA: DON complex structure will be completely extended to develop chimeric (hybrid) inhibitors to specifically and effectively target KGA. The chimeric (hybrid) inhibitors can be generated using optimized individual allosteric and active-site inhibitors. These chimeric inhibitors will be optimized to have the desirable pharmacological properties of

both inhibitors. By combining these inhibitors, it is expected that DON can help BPTES overcome the problem of water solubility. On the other hand, a reduced dose of DON may be sufficient in the presence of BPTES, thereby lowering its current toxic effects. Hence, compared to single inhibitors, a chimeric of DON and BPTES could offer a greater potent effect on glutaminase.

Following the synthesis of chimeric and optimized inhibitors, kinetic characterizations can be performed for KGA to determine the selectivity and potency of each of the inhibitors. Subsequently, the structures of these optimized individual/chimeric inhibitors will be determined in complex with KGA. Such structural studies will further help to optimize the design and synthesis of these inhibitors. BPTES and DON-derived individual inhibitors or their chimeric compounds can be tested alone and in conjunction with Mek2 inhibitors (dual-hit inhibition) for their efficacy against cancer cell proliferation in culture or any other cancer animal model studies. We therefore believe that the combined chimeric DON and BPTES, along with Mek2 inhibitor (dual-hit), will have greater efficacy, with minimum side-effects. The findings from these studies will result in the identification of potential anti-cancer agents or drug lead inhibitors that will subsequently be developed for clinical trials and applications.

5.1 REFERENCES

Ahluwalia, G.S., Grem, J.L., Hao, Z., and Cooney, D.A. (1990). Metabolism and action of amino acid analog anti-cancer agents. Pharmacol Ther *46*, 243-271.

Aledo, J.C., Gómez-Fabre, P.M., Olalla, L., and Márquez, J. (2000). Identification of two human glutaminase loci and tissue-specific expression of the two related genes. Mamm Genome *11*, 1107-1110.

Altenberg, B., and Greulich, K.O. (2004). Genes of glycolysis are ubiquitously overexpressed in 24 cancer classes. Genomics *84*, 1014-1020.

Anand, P., Kunnumakkara, A.B., Kunnumakara, A.B., Sundaram, C., Harikumar, K.B., Tharakan, S.T., Lai, O.S., Sung, B., and Aggarwal, B.B. (2008). Cancer is a preventable disease that requires major lifestyle changes. Pharm Res *25*, 2097-2116.

Andratsch, M., Feifel, E., Taylor, L., O'Hayre, M., Schramek, H., Curthoys, N.P., and Gstraunthaler, G. (2007). TGF-beta signaling and its effect on glutaminase expression in LLC-PK1-FBPase+ cells. Am J Physiol Renal Physiol *293*, F846-853.

Banerjee, M., Huang, C., Marquez, J., and Mohanty, S. (2008). Probing the structure and function of human glutaminase-interacting protein: a possible target for drug design. Biochemistry *47*, 9208-9219.

Barclay, R.K., and Phillipps, M.A. (1966). Effects of 6-diazo-5-oxol-norleucine and other tumor inhibitors on the biosynthesis of nicotinamide adenine dinucleotide in mice. Cancer Res *26*, 282-286.

Bauer, D.E., Hatzivassiliou, G., Zhao, F., Andreadis, C., and Thompson, C.B. (2005). ATP citrate lyase is an important component of cell growth and transformation. Oncogene *24*, 6314-6322.

Ben-Haim, S., and Ell, P. (2009). 18F-FDG PET and PET/CT in the evaluation of cancer treatment response. J Nucl Med *50*, 88-99.

Bomar, J.M., Benke, P.J., Slattery, E.L., Puttagunta, R., Taylor, L.P., Seong, E., Nystuen, A., Chen, W., Albin, R.L., Patel, P.D., *et al.* (2003). Mutations in a novel gene encoding a CRAL-TRIO domain cause human Cayman ataxia and ataxia/dystonia in the jittery mouse. Nat Genet *35*, 264-269.

Bonnet, S., Archer, S.L., Allalunis-Turner, J., Haromy, A., Beaulieu, C., Thompson, R., Lee, C.T., Lopaschuk, G.D., Puttagunta, L., Harry, G., *et al.* (2007). A mitochondria-K+ channel axis is suppressed in cancer and its normalization promotes apoptosis and inhibits cancer growth. Cancer Cell *11*, 37-51.

Boyle P, L.B. (2008). World Cancer Report Lyon, France: IARC Press; .

Brahimi-Horn, M.C., Chiche, J., and Pouysségur, J. (2007). Hypoxia signalling controls metabolic demand. Curr Opin Cell Biol *19*, 223-229.

Braun, S., Bitton-Worms, K., and LeRoith, D. (2011). The link between the metabolic syndrome and cancer. Int J Biol Sci *7*, 1003-1015.

Brown, G., Singer, A., Proudfoot, M., Skarina, T., Kim, Y., Chang, C., Dementieva, I., Kuznetsova, E., Gonzalez, C.F., Joachimiak, A., *et al.* (2008). Functional and structural characterization of four glutaminases from Escherichia coli and Bacillus subtilis. Biochemistry *47*, 5724-5735.

Brünger, A.T., Adams, P.D., Clore, G.M., DeLano, W.L., Gros, P., Grosse-Kunstleve, R.W., Jiang, J.S., Kuszewski, J., Nilges, M., Pannu, N.S., *et al.* (1998). Crystallography & NMR system: A new software suite for macromolecular structure determination. Acta Crystallogr D Biol Crystallogr *54*, 905-921.

Buschdorf, J.P., Li Chew, L., Zhang, B., Cao, Q., Liang, F.Y., Liou, Y.C., Zhou, Y.T., and Low, B.C. (2006). Brain-specific BNIP-2-homology protein Caytaxin relocalises glutaminase to neurite terminals and reduces glutamate levels. J Cell Sci *119*, 3337-3350.

Cassago, A., Ferreira, A.P., Ferreira, I.M., Fornezari, C., Gomes, E.R., Greene, K.S., Pereira, H.M., Garratt, R.C., Dias, S.M., and Ambrosio, A.L. (2012). Mitochondrial localization and structure-based phosphate activation mechanism of Glutaminase C with implications for cancer metabolism. Proc Natl Acad Sci U S A *109*, 1092-1097.

Choi, D.W., and Rothman, S.M. (1990). The role of glutamate neurotoxicity in hypoxic-ischemic neuronal death. Annu Rev Neurosci *13*, 171-182.

Christofk, H.R., Vander Heiden, M.G., Harris, M.H., Ramanathan, A., Gerszten, R.E., Wei, R., Fleming, M.D., Schreiber, S.L., and Cantley, L.C. (2008a). The M2 splice isoform of pyruvate kinase is important for cancer metabolism and tumour growth. Nature *452*, 230-233.

Christofk, H.R., Vander Heiden, M.G., Wu, N., Asara, J.M., and Cantley, L.C. (2008b). Pyruvate kinase M2 is a phosphotyrosine-binding protein. Nature *452*, 181-186.

Colombo, S.L., Palacios-Callender, M., Frakich, N., Carcamo, S., Kovacs, I., Tudzarova, S., and Moncada, S. (2011). Molecular basis for the differential use of glucose and glutamine in cell proliferation as revealed by synchronized HeLa cells. Proc Natl Acad Sci U S A *108*, 21069-21074.

Colombo, S.L., Palacios-Callender, M., Frakich, N., De Leon, J., Schmitt, C.A., Boorn, L., Davis, N., and Moncada, S. (2010). Anaphase-promoting complex/cyclosome-Cdh1

coordinates glycolysis and glutaminolysis with transition to S phase in human T lymphocytes. Proc Natl Acad Sci U S A *107*, 18868-18873.

Cozzone, A.J. (1988). Protein phosphorylation in prokaryotes. Annu Rev Microbiol *42*, 97-125.

Curthoys, N.P., and Godfrey, S.S. (1976). Properties of rat kidney glutaminase enzymes and their role in renal ammoniagenesis. Curr Probl Clin Biochem *6*, 346-356.

Curthoys, N.P., and Watford, M. (1995). Regulation of glutaminase activity and glutamine metabolism. Annu Rev Nutr *15*, 133-159.

Dang, C.V. (2010a). Glutaminolysis: supplying carbon or nitrogen or both for cancer cells? Cell Cycle *9*, 3884-3886.

Dang, C.V. (2010b). Rethinking the Warburg effect with Myc micromanaging glutamine metabolism. Cancer Res *70*, 859-862.

Dang, L., White, D.W., Gross, S., Bennett, B.D., Bittinger, M.A., Driggers, E.M., Fantin, V.R., Jang, H.G., Jin, S., Keenan, M.C., *et al.* (2010). Cancer-associated IDH1 mutations produce 2-hydroxyglutarate. Nature *465*, 966.

DeBerardinis, R.J., Lum, J.J., Hatzivassiliou, G., and Thompson, C.B. (2008). The biology of cancer: metabolic reprogramming fuels cell growth and proliferation. Cell Metab *7*, 11-20.

DeBerardinis, R.J., Mancuso, A., Daikhin, E., Nissim, I., Yudkoff, M., Wehrli, S., and Thompson, C.B. (2007). Beyond aerobic glycolysis: transformed cells can engage in glutamine metabolism that exceeds the requirement for protein and nucleotide synthesis. Proc Natl Acad Sci U S A *104*, 19345-19350.

DeLaBarre, B., Gross, S., Fang, C., Gao, Y., Jha, A., Jiang, F., Song J, J., Wei, W., and Hurov, J.B. (2011). Full-length human glutaminase in complex with an allosteric inhibitor. Biochemistry *50*, 10764-10770.

DeLano, W.L. (2002). The PyMOL Molecular Graphics System. In Delano Scientific, San Carlos, CA, USA, .

Dhillon, A.S., Hagan, S., Rath, O., and Kolch, W. (2007). MAP kinase signalling pathways in cancer. Oncogene *26*, 3279-3290.

Durán, R.V., Oppliger, W., Robitaille, A.M., Heiserich, L., Skendaj, R., Gottlieb, E., and Hall, M.N. (2012). Glutaminolysis activates Rag-mTORC1 signaling. Mol Cell *47*, 349-358.

Elgadi, K.M., Meguid, R.A., Qian, M., Souba, W.W., and Abcouwer, S.F. (1999). Cloning and analysis of unique human glutaminase isoforms generated by tissue-specific alternative splicing. Physiol Genomics *1*, 51-62.

Emsley, P., and Cowtan, K. (2004). Coot: model-building tools for molecular graphics. Acta Crystallogr D Biol Crystallogr *60*, 2126-2132.

Erdmann, N., Tian, C., Huang, Y., Zhao, J., Herek, S., Curthoys, N., and Zheng, J. (2009). In vitro glutaminase regulation and mechanisms of glutamate generation in HIV-1-infected macrophage. J Neurochem *109*, 551-561.

Erdmann, N.B., Whitney, N.P., and Zheng, J. (2006). Potentiation of Excitotoxicity in HIV-1 Associated Dementia and the Significance of Glutaminase. Clin Neurosci Res *6*, 315-328.

Erickson, J.W., and Cerione, R.A. (2010). Glutaminase: a hot spot for regulation of cancer cell metabolism? Oncotarget *1*, 734-740.

Finn, R.D., Mistry, J., Tate, J., Coggill, P., Heger, A., Pollington, J.E., Gavin, O.L., Gunasekaran, P., Ceric, G., Forslund, K., *et al.* (2010). The Pfam protein families database. Nucleic Acids Res *38*, D211-222.

Fischer, J.E., and Chance, W.T. (1990). Total parenteral nutrition, glutamine, and tumor growth. JPEN J Parenter Enteral Nutr *14*, 86S-89S.

Friday, B.B., and Adjei, A.A. (2008). Advances in targeting the Ras/Raf/MEK/Erk mitogen-activated protein kinase cascade with MEK inhibitors for cancer therapy. Clin Cancer Res *14*, 342-346.

Fritz, G., Just, I., and Kaina, B. (1999). Rho GTPases are over-expressed in human tumors. Int J Cancer *81*, 682-687.

Gao, P., Tchernyshyov, I., Chang, T.C., Lee, Y.S., Kita, K., Ochi, T., Zeller, K.I., De Marzo, A.M., Van Eyk, J.E., Mendell, J.T., *et al.* (2009). c-Myc suppression of miR-23a/b enhances mitochondrial glutaminase expression and glutamine metabolism. Nature *458*, 762-765.

Garber, K. (2010). Oncology's energetic pipeline. Nat Biotechnol *28*, 888-891.

Gatenby, R.A., and Gillies, R.J. (2004). Why do cancers have high aerobic glycolysis? Nat Rev Cancer *4*, 891-899.

Gill, H.S., and Eisenberg, D. (2001). The crystal structure of phosphinothricin in the active site of glutamine synthetase illuminates the mechanism of enzymatic inhibition. Biochemistry *40*, 1903-1912.

Godfrey, S., Kuhlenschmidt, T., and Curthoys, P. (1977). Correlation between activation and dimer formation of rat renal phosphate-dependent glutaminase. J Biol Chem *252*, 1927-1931.

Gómez-Fabre, P.M., Aledo, J.C., Del Castillo-Olivares, A., Alonso, F.J., Núñez De Castro, I., Campos, J.A., and Márquez, J. (2000). Molecular cloning, sequencing and expression studies of the human breast cancer cell glutaminase. Biochem J *345 Pt 2*, 365-375.

Gouet, P., Courcelle, E., Stuart, D.I., and Métoz, F. (1999). ESPript: analysis of multiple sequence alignments in PostScript. Bioinformatics *15*, 305-308.

Hanahan, D., and Weinberg, R.A. (2000). The hallmarks of cancer. Cell *100*, 57-70.

Hanahan, D., and Weinberg, R.A. (2011). Hallmarks of cancer: the next generation. Cell *144*, 646-674.

Hartwick, E.W., and Curthoys, N.P. (2011). BPTES inhibition of hGA(124-551), a truncated form of human kidney-type glutaminase. J Enzyme Inhib Med Chem.

Heery, D.M., Kalkhoven, E., Hoare, S., and Parker, M.G. (1997). A signature motif in transcriptional co-activators mediates binding to nuclear receptors. Nature *387*, 733-736.

Hitosugi, T., Kang, S., Vander Heiden, M.G., Chung, T.W., Elf, S., Lythgoe, K., Dong, S., Lonial, S., Wang, X., Chen, G.Z., *et al.* (2009). Tyrosine phosphorylation inhibits PKM2 to promote the Warburg effect and tumor growth. Sci Signal *2*, ra73.

Holm, L., and Rosenström, P. (2010). Dali server: conservation mapping in 3D. Nucleic Acids Res *38*, W545-549.

Hu, W., Zhang, C., Wu, R., Sun, Y., Levine, A., and Feng, Z. (2010). Glutaminase 2, a novel p53 target gene regulating energy metabolism and antioxidant function. Proc Natl Acad Sci U S A *107*, 7455-7460.

Jeong, E.J., Bang, S., Lee, T.H., Park, Y.I., Sim, W.S., and Kim, K.S. (1999). The solution structure of FADD death domain. Structural basis of death domain interactions of Fas and FADD. J Biol Chem *274*, 16337-16342.

Jones, N.P., and Schulze, A. (2012). Targeting cancer metabolism--aiming at a tumour's sweet-spot. Drug Discov Today *17*, 232-241.

Jones, T.A., Zou, J.Y., Cowan, S.W., and Kjeldgaard, M. (1991). Improved methods for building protein models in electron density maps and the location of errors in these models. Acta Crystallogr A *47 (Pt 2)*, 110-119.

Kabsch, W. (2010). Integration, scaling, space-group assignment and post-refinement. Acta Crystallogr D Biol Crystallogr *66*, 133-144.

Keibler, M.A., Fendt, S.M., and Stephanopoulos, G. (2012). Expanding the concepts and tools of metabolic engineering to elucidate cancer metabolism. Biotechnol Prog.

Kelly, A., and Stanley, C.A. (2001). Disorders of glutamate metabolism. Ment Retard Dev Disabil Res Rev *7*, 287-295.

Kenny, J., Bao, Y., Hamm, B., Taylor, L., Toth, A., Wagers, B., and Curthoys, N.P. (2003). Bacterial expression, purification, and characterization of rat kidney-type mitochondrial glutaminase. Protein Expr Purif *31*, 140-148.

Kim, J.W., Tchernyshyov, I., Semenza, G.L., and Dang, C.V. (2006). HIF-1-mediated expression of pyruvate dehydrogenase kinase: a metabolic switch required for cellular adaptation to hypoxia. Cell Metab *3*, 177-185.

Kinkade, C.W., Castillo-Martin, M., Puzio-Kuter, A., Yan, J., Foster, T.H., Gao, H., Sun, Y., Ouyang, X., Gerald, W.L., Cordon-Cardo, C., *et al.* (2008). Targeting AKT/mTOR and ERK MAPK signaling inhibits hormone-refractory prostate cancer in a preclinical mouse model. J Clin Invest *118*, 3051-3064.

Kisner, D.L., Catane, R., and Muggia, F.M. (1980). The rediscovery of DON (6-diazo-5-oxo-L-norleucine). Recent Results Cancer Res *74*, 258-263.

Kondo, K., Klco, J., Nakamura, E., Lechpammer, M., and Kaelin, W.G. (2002). Inhibition of HIF is necessary for tumor suppression by the von Hippel-Lindau protein. Cancer Cell *1*, 237-246.

Kroemer, G., and Pouyssegur, J. (2008). Tumor cell metabolism: cancer's Achilles' heel. Cancer Cell *13*, 472-482.

Kvamme, E., and Torgner, I.A. (1974). The effect of acetyl-coenzyme A on phosphate-activated glutaminase from pig kidney and brain. Biochem J *137*, 525-530.

Laskowski RA, McArthur MW, Moss DS, and JM., T. (1993). PROCHECK: a program to check the stereochemical quality of protein structures. . J Appl Crystallog *26*, 282-291.

Le, A., Lane, A.N., Hamaker, M., Bose, S., Gouw, A., Barbi, J., Tsukamoto, T., Rojas, C.J., Slusher, B.S., Zhang, H., *et al.* (2012). Glucose-independent glutamine metabolism via TCA cycling for proliferation and survival in B cells. Cell Metab *15*, 110-121.

Lehninger, A.L. (1945). Fatty acid oxidation and the Krebs trocarboxylic acid cycle. J Biol Chem *161*.

Li, J., Mahajan, A., and Tsai, M.D. (2006). Ankyrin repeat: a unique motif mediating protein-protein interactions. Biochemistry *45*, 15168-15178.

Liaw, S.H., and Eisenberg, D. (1994). Structural model for the reaction mechanism of glutamine synthetase, based on five crystal structures of enzyme-substrate complexes. Biochemistry *33*, 675-681.

Lobo, C., Ruiz-Bellido, M.A., Aledo, J.C., Márquez, J., Núñez De Castro, I., and Alonso, F.J. (2000). Inhibition of glutaminase expression by antisense mRNA decreases growth and tumourigenicity of tumour cells. Biochem J *348 Pt 2*, 257-261.

Locasale, J.W., and Cantley, L.C. (2010). Altered metabolism in cancer. BMC Biol *8*, 88.
López-Ríos, F., Sánchez-Aragó, M., García-García, E., Ortega, A.D., Berrendero, J.R., Pozo-Rodríguez, F., López-Encuentra, A., Ballestín, C., and Cuezva, J.M. (2007). Loss of the mitochondrial bioenergetic capacity underlies the glucose avidity of carcinomas. Cancer Res *67*, 9013-9017.

Lora, J., Alonso, F.J., Segura, J.A., Lobo, C., Márquez, J., and Matés, J.M. (2004). Antisense glutaminase inhibition decreases glutathione antioxidant capacity and increases apoptosis in Ehrlich ascitic tumour cells. Eur J Biochem *271*, 4298-4306.

Low, B.C., Seow, K.T., and Guy, G.R. (2000). The BNIP-2 and Cdc42GAP homology domain of BNIP-2 mediates its homophilic association and heterophilic interaction with Cdc42GAP. J Biol Chem *275*, 37742-37751.

Lu, W., Pelicano, H., and Huang, P. (2010). Cancer metabolism: is glutamine sweeter than glucose? Cancer Cell *18*, 199-200.

Lua, B.L., and Low, B.C. (2004). BPGAP1 interacts with cortactin and facilitates its translocation to cell periphery for enhanced cell migration. Mol Biol Cell *15*, 2873-2883.

Lua, B.L., and Low, B.C. (2005). Activation of EGF receptor endocytosis and ERK1/2 signaling by BPGAP1 requires direct interaction with EEN/endophilin II and a functional RhoGAP domain. J Cell Sci *118*, 2707-2721.

Lupianez, J.A., Hortelano, P., Sanchez-Medina, F., Sanchez-Pogo, A., McFarlane-Anderson, N., Barnswell, J., and Alleyne, G.A. (1981). The mechanism of the increase in renal ammoniagenesis in the rat with acute metabolic acidosis. FEBS Lett *128*, 361-363.

Mankoff, D.A., Eary, J.F., Link, J.M., Muzi, M., Rajendran, J.G., Spence, A.M., and Krohn, K.A. (2007). Tumor-specific positron emission tomography imaging in patients: [18F] fluorodeoxyglucose and beyond. Clin Cancer Res *13*, 3460-3469.

Márquez, J., de la Oliva, A.R., Matés, J.M., Segura, J.A., and Alonso, F.J. (2006). Glutaminase: a multifaceted protein not only involved in generating glutamate. Neurochem Int *48*, 465-471.

Masola, B., and Ngubane, N.P. (2010). The activity of phosphate-dependent glutaminase from the rat small intestine is modulated by ADP and is dependent on integrity of mitochondria. Arch Biochem Biophys *504*, 197-203.

Masson, J., Darmon, M., Conjard, A., Chuhma, N., Ropert, N., Thoby-Brisson, M., Foutz, A.S., Parrot, S., Miller, G.M., Jorisch, R., *et al.* (2006). Mice lacking brain/kidney phosphate-activated glutaminase have impaired glutamatergic synaptic transmission, altered breathing, disorganized goal-directed behavior and die shortly after birth. J Neurosci *26*, 4660-4671.

Mazurek, S., Boschek, C.B., Hugo, F., and Eigenbrodt, E. (2005). Pyruvate kinase type M2 and its role in tumor growth and spreading. Semin Cancer Biol *15*, 300-308.

Meng, J., Dai, B., Fang, B., Bekele, B.N., Bornmann, W.G., Sun, D., Peng, Z., Herbst, R.S., Papadimitrakopoulou, V., Minna, J.D., *et al.* (2010). Combination treatment with MEK and AKT inhibitors is more effective than each drug alone in human non-small cell lung cancer in vitro and in vivo. PLoS One *5*, e14124.

Michelakis, E.D., Sutendra, G., Dromparis, P., Webster, L., Haromy, A., Niven, E., Maguire, C., Gammer, T.L., Mackey, J.R., Fulton, D., *et al.* (2010). Metabolic modulation of glioblastoma with dichloroacetate. Sci Transl Med *2*, 31ra34.

Morehouse, R.F., and Curthoys, N.P. (1981). Properties of rat renal phosphate-dependent glutaminase coupled to Sepharose. Evidence that dimerization is essential for activation. Biochem J *193*, 709-716.

Murshudov, G.N., Vagin, A.A., and Dodson, E.J. (1997). Refinement of macromolecular structures by the maximum-likelihood method. Acta Crystallogr D Biol Crystallogr *53*, 240-255.

Nau, M.M., Brooks, B.J., Battey, J., Sausville, E., Gazdar, A.F., Kirsch, I.R., McBride, O.W., Bertness, V., Hollis, G.F., and Minna, J.D. (1985). L-myc, a new myc-related gene amplified and expressed in human small cell lung cancer. Nature *318*, 69-73.

Newcomb, R. (2002). Selective inhibition of glutaminase by bis-thiadiazoles. . US Patent *6*, 828 B821.

Newcomb, R., Sun, X., Taylor, L., Curthoys, N., and Giffard, R.G. (1997). Increased production of extracellular glutamate by the mitochondrial glutaminase following neuronal death. J Biol Chem *272*, 11276-11282.

Olalla, L., Gutiérrez, A., Campos, J.A., Khan, Z.U., Alonso, F.J., Segura, J.A., Márquez, J., and Aledo, J.C. (2002). Nuclear localization of L-type glutaminase in mammalian brain. J Biol Chem *277*, 38939-38944.

Olalla, L., Gutiérrez, A., Jiménez, A.J., López-Téllez, J.F., Khan, Z.U., Pérez, J., Alonso, F.J., de la Rosa, V., Campos-Sandoval, J.A., Segura, J.A., *et al.* (2008). Expression of the scaffolding PDZ protein glutaminase-interacting protein in mammalian brain. J Neurosci Res *86*, 281-292.

Ortega, A.D., Sánchez-Aragó, M., Giner-Sánchez, D., Sánchez-Cenizo, L., Willers, I., and Cuezva, J.M. (2009). Glucose avidity of carcinomas. Cancer Lett *276*, 125-135.

Ortlund, E., Lacount, M.W., Lewinski, K., and Lebioda, L. (2000). Reactions of Pseudomonas 7A glutaminase-asparaginase with diazo analogues of glutamine and asparagine result in unexpected covalent inhibitions and suggests an unusual catalytic triad Thr-Tyr-Glu. Biochemistry *39*, 1199-1204.

Osthus, R.C., Shim, H., Kim, S., Li, Q., Reddy, R., Mukherjee, M., Xu, Y., Wonsey, D., Lee, L.A., and Dang, C.V. (2000). Deregulation of glucose transporter 1 and glycolytic gene expression by c-Myc. J Biol Chem *275*, 21797-21800.

Otwinowski Z, and W., M. (1993). Processing of X-ray diffraction data collected in oscillation mode. Methods Enzymol *276*, 307–326.

Ovejera, A.A., Houchens, D.P., Catane, R., Sheridan, M.A., and Muggia, F.M. (1979). Efficacy of 6-diazo-5-oxo-L-norleucine and N-[N-gamma-glutamyl-6-diazo-5-oxo-norleucinyl]-6-diazo-5-oxo-norleucine against experimental tumors in conventional and nude mice. Cancer Res *39*, 3220-3224.

Pan, C.Q., Liou, Y.C., and Low, B.C. (2010). Active Mek2 as a regulatory scaffold that promotes Pin1 binding to BPGAP1 to suppress BPGAP1-induced acute Erk activation and cell migration. J Cell Sci *123*, 903-916.

Pearson, G., Robinson, F., Beers Gibson, T., Xu, B.E., Karandikar, M., Berman, K., and Cobb, M.H. (2001). Mitogen-activated protein (MAP) kinase pathways: regulation and physiological functions. Endocr Rev *22*, 153-183.

Pérez-Gómez, C., Campos-Sandoval, J.A., Alonso, F.J., Segura, J.A., Manzanares, E., Ruiz-Sánchez, P., González, M.E., Márquez, J., and Matés, J.M. (2005). Co-expression of glutaminase K and L isoenzymes in human tumour cells. Biochem J *386*, 535-542.

Pinkus, L.M. (1977). Glutamine binding sites. Methods Enzymol *46*, 414-427.

Porter, L.D., Ibrahim, H., Taylor, L., and Curthoys, N.P. (2002). Complexity and species variation of the kidney-type glutaminase gene. Physiol Genomics *9*, 157-166.

Reitzer, L.J., Wice, B.M., and Kennell, D. (1979). Evidence that glutamine, not sugar, is the major energy source for cultured HeLa cells. J Biol Chem *254*, 2669-2676.

Roberts, P.J., and Der, C.J. (2007). Targeting the Raf-MEK-ERK mitogen-activated protein kinase cascade for the treatment of cancer. Oncogene *26*, 3291-3310.

Robinson, M.M., McBryant, S.J., Tsukamoto, T., Rojas, C., Ferraris, D.V., Hamilton, S.K., Hansen, J.C., and Curthoys, N.P. (2007). Novel mechanism of inhibition of rat kidney-type glutaminase by bis-2-(5-phenylacetamido-1,2,4-thiadiazol-2-yl)ethyl sulfide (BPTES). Biochem J *406*, 407-414.

Romero-Gómez, M., Jover, M., Del Campo, J.A., Royo, J.L., Hoyas, E., Galán, J.J., Montoliu, C., Baccaro, E., Guevara, M., Córdoba, J., *et al.* (2010). Variations in the promoter region of the glutaminase gene and the development of hepatic encephalopathy in patients with cirrhosis: a cohort study. Ann Intern Med *153*, 281-288.

Sancak, Y., Peterson, T.R., Shaul, Y.D., Lindquist, R.A., Thoreen, C.C., Bar-Peled, L., and Sabatini, D.M. (2008). The Rag GTPases bind raptor and mediate amino acid signaling to mTORC1. Science *320*, 1496-1501.

Schnelzer, A., Prechtel, D., Knaus, U., Dehne, K., Gerhard, M., Graeff, H., Harbeck, N., Schmitt, M., and Lengyel, E. (2000). Rac1 in human breast cancer: overexpression, mutation analysis, and characterization of a new isoform, Rac1b. Oncogene *19*, 3013-3020.

Seltzer, M.J., Bennett, B.D., Joshi, A.D., Gao, P., Thomas, A.G., Ferraris, D.V., Tsukamoto, T., Rojas, C.J., Slusher, B.S., Rabinowitz, J.D., *et al.* (2010). Inhibition of glutaminase preferentially slows growth of glioma cells with mutant IDH1. Cancer Res *70*, 8981-8987.

Seyfried, T.N., Kiebish, M., Mukherjee, P., and Marsh, J. (2008). Targeting energy metabolism in brain cancer with calorically restricted ketogenic diets. Epilepsia *49 Suppl 8*, 114-116.

Seyfried, T.N., and Shelton, L.M. (2010). Cancer as a metabolic disease. Nutr Metab (Lond) *7*, 7.

Shapiro, R.A., Clark, V.M., and Curthoys, N.P. (1978). Covalent interaction of L-2-amino-4-oxo-5-chloropentanoic acid with rat renal phosphate-dependent glutaminase. Evidence for a specific glutamate binding site and of subunit heterogeneity. J Biol Chem *253*, 7086-7090.

Shapiro, R.A., Clark, V.M., and Curthoys, N.P. (1979). Inactivation of rat renal phosphate-dependent glutaminase with 6-diazo-5-oxo-L-norleucine. Evidence for interaction at the glutamine binding site. J Biol Chem *254*, 2835-2838.

Shapiro, R.A., Haser, W.G., and Curthoys, N.P. (1985). The orientation of phosphate-dependent glutaminase on the inner membrane of rat renal mitochondria. Arch Biochem Biophys *243*, 1-7.

Shaw, R.J., and Cantley, L.C. (2012). Decoding key nodes in the metabolism of cancer cells: sugar & spice and all things nice. F1000 Biol Rep *4*, 2.

Shijie, J., Takeuchi, H., Yawata, I., Harada, Y., Sonobe, Y., Doi, Y., Liang, J., Hua, L., Yasuoka, S., Zhou, Y., *et al.* (2009). Blockade of glutamate release from microglia attenuates experimental autoimmune encephalomyelitis in mice. Tohoku J Exp Med *217*, 87-92.

Souba, W.W. (1993). Glutamine and cancer. Ann Surg *218*, 715-728.

Suwa, H., Ohshio, G., Imamura, T., Watanabe, G., Arii, S., Imamura, M., Narumiya, S., Hiai, H., and Fukumoto, M. (1998). Overexpression of the rhoC gene correlates with progression of ductal adenocarcinoma of the pancreas. Br J Cancer *77*, 147-152.

Suzuki, S., Tanaka, T., Poyurovsky, M.V., Nagano, H., Mayama, T., Ohkubo, S., Lokshin, M., Hosokawa, H., Nakayama, T., Suzuki, Y., *et al.* (2010). Phosphate-activated glutaminase (GLS2), a p53-inducible regulator of glutamine metabolism and reactive oxygen species. Proc Natl Acad Sci U S A *107*, 7461-7466.

Taub, R., Kirsch, I., Morton, C., Lenoir, G., Swan, D., Tronick, S., Aaronson, S., and Leder, P. (1982). Translocation of the c-myc gene into the immunoglobulin heavy chain locus in human Burkitt lymphoma and murine plasmacytoma cells. Proc Natl Acad Sci U S A *79*, 7837-7841.

Teicher, B.A., Linehan, W.M., and Helman, L.J. (2012). Targeting cancer metabolism. Clin Cancer Res *18*, 5537-5545.

Tennant, D.A., Durán, R.V., and Gottlieb, E. (2010). Targeting metabolic transformation for cancer therapy. Nat Rev Cancer *10*, 267-277.

Thangavelu, K., Pan, C.Q., Karlberg, T., Balaji, G., Uttamchandani, M., Suresh, V., Schüler, H., Low, B.C., and Sivaraman, J. (2012). Structural basis for the allosteric inhibitory mechanism of human kidney-type glutaminase (KGA) and its regulation by Raf-Mek-Erk signaling in cancer cell metabolism. Proc Natl Acad Sci U S A *109*, 7705-7710.

Thompson, J.D., Higgins, D.G., and Gibson, T.J. (1994). CLUSTAL W: improving the sensitivity of progressive multiple sequence alignment through sequence weighting, position-specific gap penalties and weight matrix choice. Nucleic Acids Res *22*, 4673-4680.

Turner, A., and McGivan, J.D. (2003). Glutaminase isoform expression in cell lines derived from human colorectal adenomas and carcinomas. Biochem J *370*, 403-408.

Vagin, A., and Teplyakov, A. (2010). Molecular replacement with MOLREP. Acta Crystallogr D Biol Crystallogr *66*, 22-25.

Vander Heiden, M.G. (2011). Targeting cancer metabolism: a therapeutic window opens. Nat Rev Drug Discov *10*, 671-684.

Vander Heiden, M.G., Cantley, L.C., and Thompson, C.B. (2009). Understanding the Warburg effect: the metabolic requirements of cell proliferation. Science *324*, 1029-1033.
Vogelstein, B., and Kinzler, K.W. (2004). Cancer genes and the pathways they control. Nat Med *10*, 789-799.

Wallace, A.C., Laskowski, R.A., and Thornton, J.M. (1995). LIGPLOT: a program to generate schematic diagrams of protein-ligand interactions. Protein Eng *8*, 127-134.

Wang, J.B., Erickson, J.W., Fuji, R., Ramachandran, S., Gao, P., Dinavahi, R., Wilson, K.F., Ambrosio, A.L., Dias, S.M., Dang, C.V., *et al.* (2010). Targeting mitochondrial glutaminase activity inhibits oncogenic transformation. Cancer Cell *18*, 207-219.

WARBURG, O. (1956a). On the origin of cancer cells. Science *123*, 309-314.

Warburg, O. (1956b). On the origin of cancer cells. . Science *123*, 309-314.

Warburg, O., Gawehn, K., and Geissler, A.W. (1960a). The transformation of embryonal metabolism in cancer metabolism. Z Naturforsch B *15B*, .

WARBURG, O., GAWEHN, K., and GEISSLER, A.W. (1960b). [The transformation of embryonal metabolism in cancer metabolism]. Z Naturforsch B *15B*, 378-379.

Warburg, O., Wind, F., and Negelein, E. (1927). THE METABOLISM OF TUMORS IN THE BODY. J Gen Physiol *8*, 519-530.

Wise, D.R., DeBerardinis, R.J., Mancuso, A., Sayed, N., Zhang, X.Y., Pfeiffer, H.K., Nissim, I., Daikhin, E., Yudkoff, M., McMahon, S.B., *et al.* (2008). Myc regulates a transcriptional program that stimulates mitochondrial glutaminolysis and leads to glutamine addiction. Proc Natl Acad Sci U S A *105*, 18782-18787.

Wise, D.R., and Thompson, C.B. (2010). Glutamine addiction: a new therapeutic target in cancer. Trends Biochem Sci *35*, 427-433.

Yoshimune, K., Shirakihara, Y., Wakayama, M., and Yumoto, I. (2010). Crystal structure of salt-tolerant glutaminase from Micrococcus luteus K-3 in the presence and absence of its product L-glutamate and its activator Tris. FEBS J *277*, 738-748.

Yu, A.C., Fisher, T.E., Hertz, E., Tildon, J.T., Schousboe, A., and Hertz, L. (1984). Metabolic fate of [14C]-glutamine in mouse cerebral neurons in primary cultures. J Neurosci Res *11*, 351-357.

Zwart, P.H., Afonine, P.V., Grosse-Kunstleve, R.W., Hung, L.W., Ioerger, T.R., McCoy, A.J., McKee, E., Moriarty, N.W., Read, R.J., Sacchettini, J.C., *et al.* (2008). Automated structure solution with the PHENIX suite. Methods Mol Biol *426*, 419-435.

Zwick, E., Bange, J., and Ullrich, A. (2001). Receptor tyrosine kinase signalling as a target for cancer intervention strategies. Endocr Relat Cancer *8*, 161-173.

Structural basis for the allosteric inhibitory mechanism of human kidney-type glutaminase (KGA) and its regulation by Raf-Mek-Erk signaling in cancer cell metabolism

K. Thangavelu[a,1], Catherine Qiurong Pan[a,b,1], Tobias Karlberg[c], Ganapathy Balaji[d], Mahesh Uttamchandani[a,d,e], Valiyaveettil Suresh[d], Herwig Schüler[c], Boon Chuan Low[a,b,2], and J. Sivaraman[a,2]

Departments of [a]Biological Sciences and [d]Chemistry, National University of Singapore, Singapore 117543; [b]Mechanobiology Institute Singapore, National University of Singapore, Singapore 117411; [c]Structural Genomics Consortium, Department of Medical Biochemistry and Biophysics, Karolinska Institutet, Stockholm SE-17177, Sweden; and [e]Defence Medical and Environmental Research Institute, DSO National Laboratories, Singapore 117510

Edited by John Kuriyan, University of California, Berkeley, CA, and approved March 22, 2012 (received for review October 11, 2011)

Besides thriving on altered glucose metabolism, cancer cells undergo glutaminolysis to meet their energy demands. As the first enzyme in catalyzing glutaminolysis, human kidney-type glutaminase isoform (KGA) is becoming an attractive target for small molecules such as BPTES [bis-2-(5 phenylacetamido-1, 2, 4-thiadiazol-2-yl) ethyl sulfide], although the regulatory mechanism of KGA remains unknown. On the basis of crystal structures, we reveal that BPTES binds to an allosteric pocket at the dimer interface of KGA, triggering a dramatic conformational change of the key loop (Glu312-Pro329) near the catalytic site and rendering it inactive. The binding mode of BPTES on the hydrophobic pocket explains its specificity to KGA. Interestingly, KGA activity in cells is stimulated by EGF, and KGA associates with all three kinase components of the Raf-1/Mek2/Erk signaling module. However, the enhanced activity is abrogated by kinase-dead, dominant negative mutants of Raf-1 (Raf-1-K375M) and Mek2 (Mek2-K101A), protein phosphatase PP2A, and Mek-inhibitor U0126, indicative of phosphorylation-dependent regulation. Furthermore, treating cells that coexpressed Mek2-K101A and KGA with suboptimal level of BPTES leads to synergistic inhibition on cell proliferation. Consequently, mutating the crucial hydrophobic residues at this key loop abrogates KGA activity and cell proliferation, despite the binding of constitutive active Mek2-S222/226D. These studies therefore offer insights into (*i*) allosteric inhibition of KGA by BPTES, revealing the dynamic nature of KGA's active and inhibitory sites, and (*ii*) cross-talk and regulation of KGA activities by EGF-mediated Raf-Mek-Erk signaling. These findings will help in the design of better inhibitors and strategies for the treatment of cancers addicted with glutamine metabolism.

Warburg effect | RAS/MAPK | crystallography

The Warburg effect in cancer biology describes the tendency of cancer cells to take up more glucose than most normal cells, despite the availability of oxygen (1, 2). In addition to altered glucose metabolism, glutaminolysis (catabolism of glutamine to ATP and lactate) is another hallmark of cancer cells (2, 3). In glutaminolysis, mitochondrial glutaminase catalyzes the conversion of glutamine to glutamate (4), which is further catabolized in the Krebs cycle for the production of ATP, nucleotides, certain amino acids, lipids, and glutathione (2, 5).

Humans express two glutaminase isoforms: KGA (kidney-type) and LGA (liver-type) from two closely related genes (6). Although KGA is important for promoting growth, nothing is known about the precise mechanism of its activation or inhibition and how its functions are regulated under physiological or pathophysiological conditions. Inhibition of rat KGA activity by antisense mRNA results in decreased growth and tumorigenicity of Ehrlich ascites tumor cells (7), reduced level of glutathione, and induced apoptosis (8), whereas Myc, an oncogenic transcription factor, stimulates KGA expression and glutamine metabolism (5). Interestingly, direct suppression of miR23a and miR23b (9) or activation of TGF-β (10) enhances KGA expression. Similarly, Rho GTPase that controls cytoskeleton and cell division also up-regulates KGA expression in an NF-κB–dependent manner (11). In addition, KGA is a substrate for the ubiquitin ligase anaphase-promoting complex/cyclosome (APC/C)-Cdh1, linking glutaminolysis to cell cycle progression (12). In comparison, function and regulation of LGA is not well studied, although it was recently shown to be linked to p53 pathway (13, 14). Although intense efforts are being made to develop a specific KGA inhibitor such as BPTES [bis-2-(5-phenylacetamido-1, 2, 4-thiadiazol-2-yl) ethyl sulfide] (15), its mechanism of inhibition and selectivity is not yet understood. Equally important is to understand how KGA function is regulated in normal and cancer cells so that a better treatment strategy can be considered.

The previous crystal structures of microbial (Mglu) and *Escherichia coli* glutaminases show a conserved catalytic domain of KGA (16, 17). However, detailed structural information and regulation are not available for human glutaminases especially the KGA, and this has hindered our strategies to develop inhibitors. Here we report the crystal structure of the catalytic domain of human *apo* KGA and its complexes with substrate L-glutamine), product (L-glutamate), BPTES, and its derived inhibitors. Further, Raf-Mek-Erk module is identified as the regulator of KGA activity. Although BPTES is not recognized in the active site, its binding confers a drastic conformational change of a key loop (Glu312-Pro329), which is essential in stabilizing the catalytic pocket. Significantly, EGF activates KGA activity, which can be abolished by the kinase-dead, dominant negative mutants of Mek2 (Mek2-K101A) or its upstream activator Raf-1 (Raf-1-K375M), which are the kinase components of the growth-promoting Raf-Mek2-Erk signaling node. Furthermore, coexpression of phosphatase PP2A and treatment with Mek-specific inhibitor or alkaline phosphatase all abolished enhanced KGA activity inside the cells and in vitro, indicating that stimulation of KGA is phosphorylation dependent. Our results therefore provide mechanistic insights into KGA inhibition by BPTES and its regulation by EGF-mediated Raf-Mek-Erk module in cell growth and possibly cancer manifestation.

Results

Structures of cKGA and Its Complexes with L-Glutamine and L-Glutamate. The human KGA consists of 669 amino acids. We refer to Ile221-Leu533 as the catalytic domain of KGA (cKGA) (Fig. 1*A*). The crystal structures of the *apo* cKGA and in complex

Author contributions: K.T., C.Q.P., B.C.L., and J.S. designed research; K.T., C.Q.P., T.K., and G.B. performed research; K.T., C.Q.P., V.S., H.S., B.C.L., and J.S. contributed new reagents/analytic tools; K.T., C.Q.P., M.U., B.C.L., and J.S. analyzed data; and K.T., C.Q.P., B.C.L., and J.S. wrote the paper.

The authors declare no conflict of interest.

This article is a PNAS Direct Submission.

Freely available online through the PNAS open access option.

Data deposition: Crystallography, atomic coordinates, and structure factors reported in this paper have been deposited in the Protein Data Bank, www.pdb.org (PDB ID codes 3VOY, 3VP0, 3CZD, 3VOZ, 3VP1, 3VP2, 3VP3, and 3VP4).

[1]K.T. and C.Q.P. contributed equally to this work.

[2]To whom correspondence may be addressed. E-mail: dbsjayar@nus.edu.sg or dbslowbc@nus.edu.sg.

This article contains supporting information online at www.pnas.org/lookup/suppl/doi:10.1073/pnas.1116573109/-/DCSupplemental.